

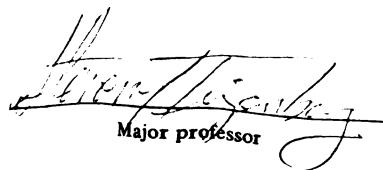
This is to certify that the
thesis entitled
VP16 localization during herpes simplex-1
infection

presented by

Dawn Renee Greensides

has been accepted towards fulfillment
of the requirements for

M. S. degree in Cell and Molecular
Biology


Major professor

Date

8/16/00

**LIBRARY
Michigan State
University**

PLACE IN RETURN BOX to remove this checkout from your record.
TO AVOID FINES return on or before date due.
MAY BE RECALLED with earlier due date if requested.

DATE DUE	DATE DUE	DATE DUE

VP16 LOCALIZATION DURING HERPES SIMPLEX-1 INFECTION

By

Dawn Renee Greensides

A THESIS

**Submitted to
Michigan State University
in partial fulfillment of the requirements
for the degree of**

MASTER OF SCIENCE

Cell and Molecular Biology Program

2000

ABSTRACT

VP16 LOCALIZATION DURING HERPES SIMPLEX VIRUS-1 INFECTION

Dawn Renee Greensides

VP16 is an essential structural component of Herpes simplex virus-1 (HSV-1) and activates transcription of the viral immediate early genes. Both of these roles rely on the localization of the protein to specific locations in the cell at certain times. This thesis demonstrates the patterns of VP16 localization during an HSV-1 infection.

A recombinant HSV-1 virus, DG1, contains a gene fusing the VP16 open reading frame with that encoding the enhanced green fluorescent protein (EGFP). The fusion protein could be visualized within live infected cells by fluorescence microscopy. At early times, newly synthesized VP16-EGFP was localized to the nucleus within uniform nuclear dots. As infection progressed the dots grew and filled the infected cell nucleus, and VP16-EGFP began accumulating within the cytoplasm perinuclearly and in cytoplasmic speckles. At late times, intense expression of VP16-EGFP was observed throughout the infected cells. The localization of the viral capsid protein, VP26, was also observed as a GFP fusion protein. VP26-GFP localized in the nucleus in intense, punctate dots organized along the inner membrane of the infected cell nucleus, presumably sites of capsid assembly. At later times, cytoplasmic accumulation of VP26-GFP occurred. The nuclear localization of virion VP16, and subsequent initiation of infection requires the interaction of VP16 with the cellular protein HCF-1. This interaction was studied by using temperature sensitive tsBN67 cells, which contain a single amino acid substitution within HCF-1 that disrupts the interaction with VP16.

ACKNOWLEDGMENTS

I would first like to thank Steve for being a great advisor and for being very understanding and supportive when I realized that I needed to change the path I was on. I have learned a great deal about what it means to be a good scientist in his lab and I hope to apply what I've learned here to all my next adventures. I would like to thank my committee members, Dr. Bill Henry, Dr. Donna Koslowsky, Dr. Suzanne Thiem, and Dr. John Wang. I would also like to thank Dr. Mel Schindler and Pete Davidson for helping me with the laser microscope.

To the members of the Triezenberg lab, Kostas, Mao, Billy, Ryann, John, Yuri, and especially Søren (the Grump) and Francisco (Narigon), you guys have all been great and a lot of fun to work with. I wish each of you great success in your futures.

For all my other friends that I have made here especially, Kirsten F, Nikki, Heather, Kirsten JO, Sheldon, as well as Søren and Francisco again, thank you so much for encouraging me and for keeping me sane while going through this whole life change thing!

To my parents thank you for supporting me and my decisions, even though I know sometimes you don't understand them. You don't know what it means to me to have your full support and encouragement, thank you! Who knows, maybe someday you will have a doctor for a daughter.

“All those who wander are not lost” – J.R.R.Tolkien

TABLE OF CONTENTS

List of Figures	vi
List of Abbreviations	viii
Chapter One: Introduction and Literature Review	
Herpesviruses	1
HSV-1 virion structure	2
HSV-1 infection	6
HSV-1 transcriptional cascade	8
Nuclear structure	9
VP16	12
Models of Herpesvirus egress	15
HSV-1 protein localization	21
Nuclear import	23
Chapter Two: Materials and Methods	
Cells and viral strains	26
Plaque Assays	27
Virion purification	28
Viral DNA extraction and purification	28
Green Fluorescent Protein (EGFP) fusion plasmids	29
Generating recombinant virus DG1	32
Southern Blot	33
Western Blot	34
DG1 growth curve	34
Microscopy and live cell imaging	34
Chapter Three: VP16 and VP26 Localization throughout a time course of HSV-1 infection	
Introduction	36
Experimental Results	
Isolation and identification of recombinant HSV-1 expressing VP16-EGFP	40
Growth characteristics of recombinant DG1	44
Detection of fluorescent VP16-EGFP	44
Time Course analysis of VP16-EGFP during a viral infection	
High multiplicity infection	47
Low multiplicity infection	74
Time course analysis of VP26-GFP during a viral infection	90
Discussion	
VP16-EGFP localization	103

VP26-GFP localization	1 18
Chapter Four: HCF-1 dependent nuclear localization of VP16	
Introduction	122
Experimental Results	124
Discussion	132
Chapter Five: Conclusion and future directions	139
Appendices	
List of Appendix Figures	145
List of References	196

LIST OF FIGURES

Figure 1. Schematic representation of an HSV-1 KOS virion	3
Figure 2. Plasmid map of pDRG24-2	31
Figure 3. Schematic representation of the two models of viral egress	39
Figure 4. HSV-1 genomic structure and the fragment that contains the VP16 gene in different viruses	42
Figure 5. Southern blot analysis of recombinant viral DNA confirms the presence of VP16-EGFP	43
Figure 6. Western blot analysis of recombinant virions confirms the presence of a VP16-EGFP gene product	45
Figure 7. Recombinant virus DG1 grows with wild type kinetics	46
Figure 8. VP16-EGFP in the context of infection shows a different localization than transfected VP16-EGFP	49
Figure 9. DG1 time course 10 MOI, VP16-EGFP localization at 2 hpi and 4 hpi	52
Figure 10. DG1 time course 10 MOI, VP16-EGFP localization at 6 hpi	55
Figure 11. DG1 time course 10 MOI, VP16-EGFP localization at 8 hpi	58
Figure 12. DG1 time course 10 MOI, VP16-EGFP localization at 10 hpi	61
Figure 13. DG1 time course 10 MOI, VP16-EGFP localization at 12 hpi	63
Figure 14. DG1 time course 10 MOI, VP16-EGFP localization at 14 hpi	66
Figure 15. DG1 time course 10 MOI, VP16-EGFP localization at 16 hpi	69
Figure 16. DG1 time course 10 MOI, VP16-EGFP localization at 20 hpi	71
Figure 17. DG1 time course 10 MOI, VP16-EGFP localization at 24 hpi	73
Figure 18. DG1 time course 1 MOI, VP16-EGFP localization at 2 hpi and 4 hpi	76
Figure 19. DG1 time course 1 MOI, VP16-EGFP localization at 6 hpi	78
Figure 20. DG1 time course 1 MOI, VP16-EGFP localization at 8 hpi	81

Figure 21. DG1 time course 1 MOI, VP16-EGFP localization at 10 hpi	83
Figure 22. DG1 time course 1 MOI, VP16-EGFP localization at 14 hpi	86
Figure 23. DG1 time course 1 MOI, VP16-EGFP localization at 16 hpi	88
Figure 24. DG1 time course 1 MOI, VP16-EGFP localization at 20 hpi	92
Figure 25. DG1 time course 1 MOI, VP16-EGFP localization at 24 hpi	94
Figure 26. Summary of VP16-EGFP localization during a complete time course of infection with DG1	96
Figure 27. K26GFP time course, VP26-GFP localization at 2 hpi and 4 hpi	99
Figure 28. K26GFP time course, VP26-GFP localization at 6 hpi, 8 hpi and 10 hpi	101
Figure 29. K26GFP time course, VP26-GFP localization at 12 hpi and 16 hpi	105
Figure 30. K26GFP time course, VP26-GFP localization at 20 hpi	107
Figure 31. Summary of VP26-GFP localization during a complete time course of infection with K26GFP	109
Figure 32. DG1 infection of BHK cells at 33°C and 39°C, localization of VP16-EGFP	126
Figure 33. DG1 infection of tsBN67 cells at 33°C and 39°C, localization of VP16-EGFP at 2 hpi	129
Figure 34. DG1 infection of tsBN67 cells at 33°C and 39°C, localization of VP16-EGFP at 6 hpi	131
Figure 35. DG1 infection of tsBN67 cells at 33°C and 39°C, localization of VP16-EGFP at 9 hpi	134
Figure 36. DG1 infection of tsBN67 cells at 33°C and 39°C, localization of VP16-EGFP at 24 hpi	136

LIST OF ABBREVIATIONS

DE	delayed early
DMEM	Dulbecco's modified minimal essential medium
E	early
EGFP	enhanced green fluorescent protein
FCS	fetal calf serum
GFP	green fluorescent protein
HSV	herpes simplex virus
hpi	hours post infection
IE	immediate early
L	late
MOI	multiplicity of infection
MSV	Maloney sarcoma virus
PAGE	polyacrylamide gel electrophoresis
PBS	phosphate buffered saline
pfu	plaque forming unit
SDS	sodium dodecyl sulfate
VIC	VP16 induced complex
VP16	virion protein 16
VP22	virion protein 22
VP26	virion protein 26

Chapter 1

INTRODUCTION

Herpesviruses

Herpes simplex virus infections in humans have been recognized since ancient times. Scholars of Greek civilization defined the word *herpes* as “to creep or crawl” in reference to the spreading nature of the skin lesions formed by the viral infection. Not until the early nineteenth century was the vesicular nature of the lesions associated with herpes infections characterized, and in 1893 the human-to-human transmission of HSV was recognized [1]. Today herpes simplex infections are reported worldwide and more than 80% of the American population is infected with HSV-1 (CDC reports).

Over the past few decades the application of molecular biology to the disease has made significant advances. One discovery has been the detection of antigenic differences between HSV types 1 and 2. HSV-1 is commonly associated with the oral form of the disease, whereas HSV-2 is associated with the genital form. The most common diseases caused by these viruses are recurrent oral and genital lesions, but more serious and life-threatening diseases can also occur. These illnesses include neonatal herpesvirus infection, herpes infection of the eye, and herpes encephalitis, a very dangerous infection of the brain. Successful antiviral therapies have been established for HSV genital infections and systemic HSV infections in an immunocompromised host. Differences between strains of HSV have also been established, and this knowledge has become an important epidemiological tool.

The family *Herpesviridae* comprises three subfamilies of herpes viruses, α , β and γ . The viruses in these families make up the largest and most complex of all DNA viruses. Alpha herpesviruses, which include HSV-1, HSV-2, varicella-zoster virus (VZV), pseudorabies virus (PrV), bovine herpesvirus type 1 (BHV-1), equine herpesviruses types 1 and 4 (EHV-1/-4), and the simian B virus, have a wide and variable host range. Viruses in this subfamily have short lytic reproductive cycles, spread rapidly in culture, efficiently destroy infected cells, and can establish latent infections in sensory ganglia. Beta herpesviruses include all forms of the cytomegalovirus (CMV), as well as human herpesviruses 6 and 7 (HHV-6/-7). Viruses in this subfamily have a restricted host range, a long reproductive cycle, and a slowly progressing infection in culture. These viruses can also be maintained in the latent form in secretory glands, kidneys and other tissues. Gamma herpesviruses, including the Epstein-Barr virus (EBV), have a very limited host range. Viruses in this subfamily are specific for either T or B lymphocytes and latent virus is usually found in lymphoid tissue (reviewed in [2]).

HSV-1 virion structure

Herpes simplex virus-1 (HSV-1) is one of the most studied of the herpesviruses. The HSV-1 virion is made up of four compartments: the envelope, tegument, capsid and core (Fig. 1). The core contains 152 Kb of linear double stranded viral DNA, packaged with the polyamine spermine to neutralize the negative charge. The DNA has been reported to adopt a spooled organization within the capsid [3], [4]. According to the spool model, DNA passes into the capsid through an entry port and then wraps around the inner

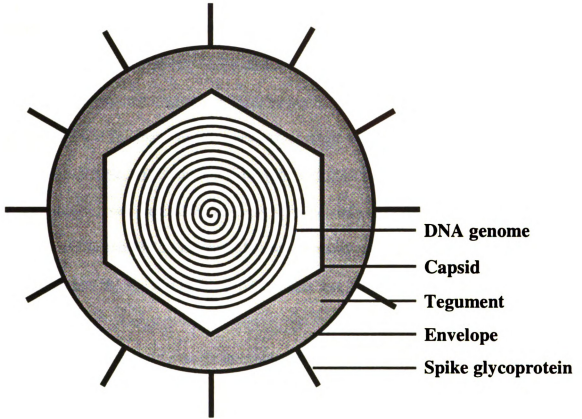


Figure 1. Schematic representation of an HSV-1 KOS virion

surface of the capsid shell accumulating one layer at a time, with the layers *becoming less* well ordered as their distance from the shell increases.

The capsid, which protects the viral genome, forms an icosahedral structure approximately 15 nm thick and 100 nm in diameter. Its major structural features are 162 capsomers (150 hexons and 12 pentons) that lie on a T=16 icosahedral lattice. The capsomers are connected in groups of three by asymmetric structures called triplexes (reviewed in [5]). The major components of the capsid shell are the virally encoded proteins VP5, VP19c, VP23, and VP26 [6] [7]. VP5 (149 KDa; 960 copies) forms the basic icosahedral matrix with distinct forms at the penton and hexon sites [8]. VP19c (50 KDa; 350 copies) and VP23 (35 KDa; 550 copies) make up the triplex structures with a 1:2 configuration [8]. VP26 (12 KDa; 1000 copies) sits at the tip of each copy of VP5 in the hexons [6].

Three different forms of capsids accumulate in infected cell nuclei. A-capsids lack both DNA and scaffolding proteins, B-capsids lack the viral genome but contain scaffolding proteins, and C-capsids contain the viral genome and are the precursors to the enveloped, infectious viral particles [3] [9]. A, B, and C capsids arise from the maturation of a short-lived unstable capsid precursor, termed the procapsid or large-cored B capsid [10]. Shortly after its formation, the spherical procapsid angularizes into the polyhedral form of the B and C capsids. Angularization is accompanied by the formation of the mature VP5 hexons and pentons to which VP26 binds [11]. The new polyhedral *shell* is more stable than the procapsid.

The capsid is surrounded by the tegument, a proteinaceous layer comprised of *approximately* 12 viral proteins including the major structural proteins; VP1/2, VP13/14,

VP16, VP22, as well as the virion host shut off protein (vhs) [1] [12]. These *proteins* have been hypothesized to play several roles during HSV-1 infection and latency. *VP1/2* is thought to be important in the transfer of the viral genome from the capsid to the cell nucleus at the nuclear pore [13]. VP16 is a powerful transcriptional activator of viral immediate early (IE) genes [14], and is also an essential protein for the production of infectious virions [15]. VP13/14 is thought to be a modulator of VP16-mediated induction of the IE genes [16]. The exact role of VP22 during virus infection remains unclear. This protein is subjected to a range of post-translational modifications [17] [18] and has been shown to interact with VP16 [19]. The vhs protein is an mRNAse responsible for the degradation of the cellular mRNAs during the IE and delayed early (DE) stages of infection [20]. The vhs protein has also been shown to interact with VP16 [21]. All of these proteins provide important functions to the life cycle of the virus, and yet little is known about the fate of these proteins in infected cells.

The entire structure is enclosed within the envelope, a lipid membrane of host origin containing at least 11 viral glycoproteins; gB, gC, gD, gE, gG, gH, gI, gJ, gK, gL, and gM. The envelope also contains at least two, possibly more, nonglycosylated intrinsic membrane proteins [1]. The total diameter of the virion particle is approximately 200nm.

A second type of particle, designated light (L) particles, has also been discovered [22]. These particles are non-infectious and are produced in similar quantities as virions *in culture*. Velocity gradient purification separates the L-particles from the typical HSV-1 virions. These L-particles resemble virions in appearance; they contain all the envelope *and tegument* proteins, but lack the nucleocapsid (capsid proteins and viral DNA). In *addition*, L-particles include four or five phosphoproteins which are not detected in

mature virions [22] [23]. When the envelope from the L-particles is removed, *the remaining tegument material retains its structural integrity*. This indicates that the structure of the tegument does not depend on the presence of the capsid or envelope and can exist as a defined structure on its own. The production of L-particles is not restricted to HSV-1, but is also a feature of other α herpesviruses that have been tested [23].

HSV-1 infection

Infection occurs when the virus gains entrance through the mucous membrane of an epithelial tissue. If the virus then enters the axon of a neuron it is transported to the neuronal cell body where it will become latent. The virus can remain latent in the human host indefinitely or it can be reactivated when the host experiences local stresses (reviewed in [1]). Reactivation of the virus can lead to either symptomatic disease or asymptomatic shedding.

HSV-1 initiates infection of an epithelial cell by binding to heparan sulfate receptors on the cell surface via spike glycoproteins gB and/or gC. After this initial attachment, gD interacts with its own cell surface receptors, and the virion envelope rapidly fuses with the cell membrane [24]. In a study by Sodiek et al., electron micrograph images and protease protection experiments showed that the internalization rate of HSV-1 was very rapid and efficient, with a half-time of 8 minutes [25]. The same study, as well as others showed that after envelope fusion, the capsid separates from the bulk of the tegument, which largely remains associated with the cytoplasmic surface of the plasma membrane [25] [12]. Comparable results were also observed in a similar study of incoming pseudorabies virus [26].

The de-enveloped capsids are then transported from the cell periphery *through the* cytoplasm to the nuclear pores. Movement of the viral particles through the cell is not likely to occur through free diffusion. The capsid likely uses the cell's motile functions for transport. Most of the evidence for the interaction of viral capsids with microtubules has been determined by studying the transport of reactivated virus through the axon of a neuron. In both retrograde and anterograde transport through the axon terminal, HSV-1 capsids have been visualized in close proximity to microtubules (>95% were within 100 nm) [27] [28]. Association of nucleocapsids with axonal microtubules was also strongly suggested by the rapid velocity of transport (2-4 mm/h) [27]. Incubation of infected neuronal cultures with nocodazole (a microtubule depolymerizer) also inhibited the axonal anterograde transport of capsids [29].

The evidence from neuronal cells, and transport of the capsid after the reactivation from latent infection, cannot be directly applied to the lytic infection in epidermal cells. Sensory neurons have a unique anatomy, in that the virion must be transported over distances from 10-100 cm. The transport of virions in epidermal cells, which are much more compact, may involve modifications of this transport pathway. Nevertheless, evidence for capsid interaction with microtubules has been observed in epidermal cells. Vero cells (monkey kidney cells) were utilized to observe the transport of incoming HSV-1 capsids by immunofluorescence and electron microscopy in the presence and absence of microtubule depolymerizing agents. Microtubule assisted transport was not essential for infection but did accelerate both the transfer of the capsids to the nucleus and the onset of viral protein synthesis. In addition, dynein was found associated with

many of the capsids, suggesting that the microtubule dependent motor mediates the transport of the capsid along the microtubule [25].

When the capsids reach the nucleus they accumulate at the cytosolic face of the nuclear pore complexes (NPCs), oriented with a penton toward the nuclear pore [30] [26]. The viral genome is then rapidly and efficiently released into the cell's nucleus where it will be transcribed and replicated. Within an hour or two after HSV penetration into a cell, viral proteins begin to be synthesized and host cell protein synthesis is dramatically inhibited [20].

HSV-1 transcriptional cascade

The HSV genes fall into three main transcriptionally regulated classes; immediate early (IE or α), delayed early (DE or β), and late (L or γ). The production of viral gene products occurs in a regulated and sequential fashion using the host cell's RNA polymerase II and ribosomes. The first genes to be transcribed are the IE genes. The products of these genes are ICP0, ICP4, ICP22, ICP27, and ICP47. The synthesis of these proteins reaches peak rates approximately 2 to 4 hours post infection and they continue to accumulate at nonuniform rates throughout infection. All the IE gene products are believed to have regulatory functions. ICP4 and ICP0 are essential to the virus in that they are responsible for the expression of the DE and L gene products. ICP27 is also an essential gene product that plays numerous roles, such as stimulation of DNA synthesis and inhibition of RNA splicing. ICP22 and ICP47 are dispensable gene products in the virus, and their regulatory roles have not yet been defined (reviewed in [31] [1]). DE gene transcription begins before any viral DNA replication, reaching peak

synthesis about 5 to 7 hours post infection. The DE genes encode for *the seven proteins* essential for viral DNA replication. The appearance of the DE gene products *signals the* onset of viral DNA synthesis. The L genes consist of two groups, dependent upon *their* timing of expression. The “leaky late” genes, including VP16, are initially expressed before the onset of viral DNA replication, whereas the true late genes are expressed only after DNA synthesis has begun (for review see [1]).

Nuclear structure

Upon HSV-1 infection, significant reorganization occurs in the nucleus of the cell. The mammalian cell nucleus is comprised of a highly organized three-dimensional framework, within which functional domains and factor storage sites are arranged. The nucleolus, the site of rRNA synthesis and processing, is the only nuclear structure visible in light microscopy. However, many other domains have been identified using more advanced methods such as immunolabeling and electron microscopy.

Studies of uninfected mammalian nuclei have demonstrated that mRNA transcription occurs in hundreds to thousands of discrete foci [32] [33] [34] [35]. RNA polymerase II is distributed widely throughout the nucleus, usually concentrated in these discrete transcription foci [32] [33] [34] [36] [37]. The core proteins of heterogeneous and small ribonucleoprotein complexes (hnRNPs and snRNPs) are also seen to colocalize at intranuclear sites of RNA synthesis [38] [39] [40]. Introduction of new transcription sites by virus infection results in the relocalization of RNAPII and host splicing factors to new sites of RNA synthesis [41] [42] [43].

Upon infection of a cell with HSV-1, antigens associated with the *mRNA processing* complexes reorganize from a widespread diffuse “speckled” pattern to a pronounced punctate pattern within the periphery of the cell nucleus [44] [43]. This redistribution of snRNP proteins occurs within 1.5 hours post infection (hpi) and has been demonstrated to be under the control of the viral IE gene products, specifically ICP27 [43]. Only four genes in the HSV-1 genome contain intron sequences so there is a limited requirement for the cellular splicing machinery. The HSV-1 specific inactivation of the splicing machinery may be a defense mechanism that helps reduce cellular gene expression and processing without affecting the expression of the HSV-1 genes.

Sites of HSV-1 transcription and replication in infected cell nuclei have been visualized by fluorescent immunodetection of Br-UTP and biotin-11-dUTP incorporation [42]. These sites have been identified as discrete compartments within the infected cell nucleus. The number of viral transcription sites was shown to approximately double over the course of infection (4-16 hpi, with an upper limit of approximately 20 foci) [42]. The increase in transcription foci at early times is consistent with an early amplification of input virus DNA that then becomes transcriptionally active [45]. Double labeling of both transcription and replication foci in the same nucleus demonstrates that the two processes colocalize [42]. Consistent with this evidence is the data that RNAPII is localized to viral replication compartments early in infection [41]. This indicates that input viral genomes are transcribed and replicated simultaneously within the same domains.

Nuclear domains (ND10s), also called PML oncogenic domains (PODs) or nuclear bodies (NBs), were first recognized using autoantibodies from patients with primary biliary cirrhosis [46] [47]. ND10s are present in most cell types at varying frequencies

(2-10), yet they are absent in germ cells and cells from neural crest origin. Thus, **ND10s** are not ubiquitous and cells can live without them (reviewed in [48]). **Sp100** and **PML** (Pro-Myelocytic Leukemia) were the first proteins to be characterized from these domains [47] [49]. Since then several other proteins have been localized to ND10s, including **ISG20** (interferon-stimulated gene product) [50], **HAUSP** (herpesvirus associated ubiquitin-specific protease) [51], and **PIC-1/SUMO-1** (small ubiquitin-related modifier) [52]. Both the **PML** and **Sp100** genes, like **ISG20**, contain functional interferon (IFN) α/β stimulated response elements and IFN γ activation sites [53] [54]. The direct induction of these three proteins by IFN suggests a role for this nuclear structure in cell growth suppression in response to viral infection.

Several groups have shown that **PML** is dispersed from ND10s upon infection by any of several DNA viruses (reviewed in [55]). Upon infection with **HSV-1**, the viral genome localizes to the periphery of these structures. Within 2 hours of infection a complete loss of ND10 occurs. The loss of ND10 structures is due to **PML** and **Sp100** protein redistribution throughout the nucleus. The IE protein **ICP0** was shown to associate with ND10s early in infection and to induce the disruption of the structure [56] [57]. **ICP0** is a potent activator of gene expression and plays a role both in the lytic and latent cycle of the virus. The structure of **ICP0** is similar to **PML** in that it contains a RING finger zinc-binding motif. In the case of **PML**, the RING motif is required for its localization at the ND10. **ICP0** mutants lacking the RING motif localize to the ND10, but are incapable of disrupting them [57].

ICP0 has also been shown to interact with **HAUSP**, and both proteins are seen to colocalize with **PML** [51] [58] and the ubiquitin-like protein, **PIC-1/SUMO-1**, at ND10s

[52] [59]. This interaction led to the discovery that the ability of ICP0 to *disrupt ND10s* is mediated by a proteasome mediated pathway [60]. HAUSP might normally *protect the* PML protein, but either inhibition of its activity or its sequestration by ICP0 allows the induction of a process that leads to the ubiquitination and proteasome-dependant degradation of PML isoforms.

HSV-1 replication begins in the nucleus at a limited number of sites. An increased amount of infectious virus does not increase the initial number of replication sites. The ability of HSV-1 to disperse ND10 proteins via an IE gene product early in infection made it difficult to associate viral replication sites with ND10s. However, in experiments with ICP0-deficient viruses the HSV-1 genome preferentially localized adjacent to ND10s as one of the earliest events in the HSV-1 nuclear replication cycle [61] [62]. HSV-1 encodes seven viral gene products that are essential for viral replication, including the HSV DNA polymerase and the DNA binding protein, ICP8. During productive viral replication ICP8 colocalized with the viral DNA in large, globular compartments [63] [64]. This localization was later determined to be the association of ICP8 with replicating HSV-1 DNA associated with ND10 structures [61].

VP16

HSV-1 regulated cascade of gene expression is initially stimulated by the HSV-1 virion phosphoprotein VP16. This “leaky” late, 65 KDa protein is the major trans-activator for IE gene expression. Along with being a powerful transcriptional activator, VP16 is an abundant and essential structural protein, packaged in the virion tegument [1]. The VP16 protein enters the host cell with the infecting virion (at approximately 1000

copies/virion [65]). After transport to the cell nucleus, VP16 activates *transcription* through at least two cis-acting DNA sequences in the IE gene promoters, the TAATGARAT sequence [66] [67] and the GA-rich element [68]. VP16 itself does not contain a DNA binding domain, therefore its ability to activate transcription is dependent upon its interaction with other factors.

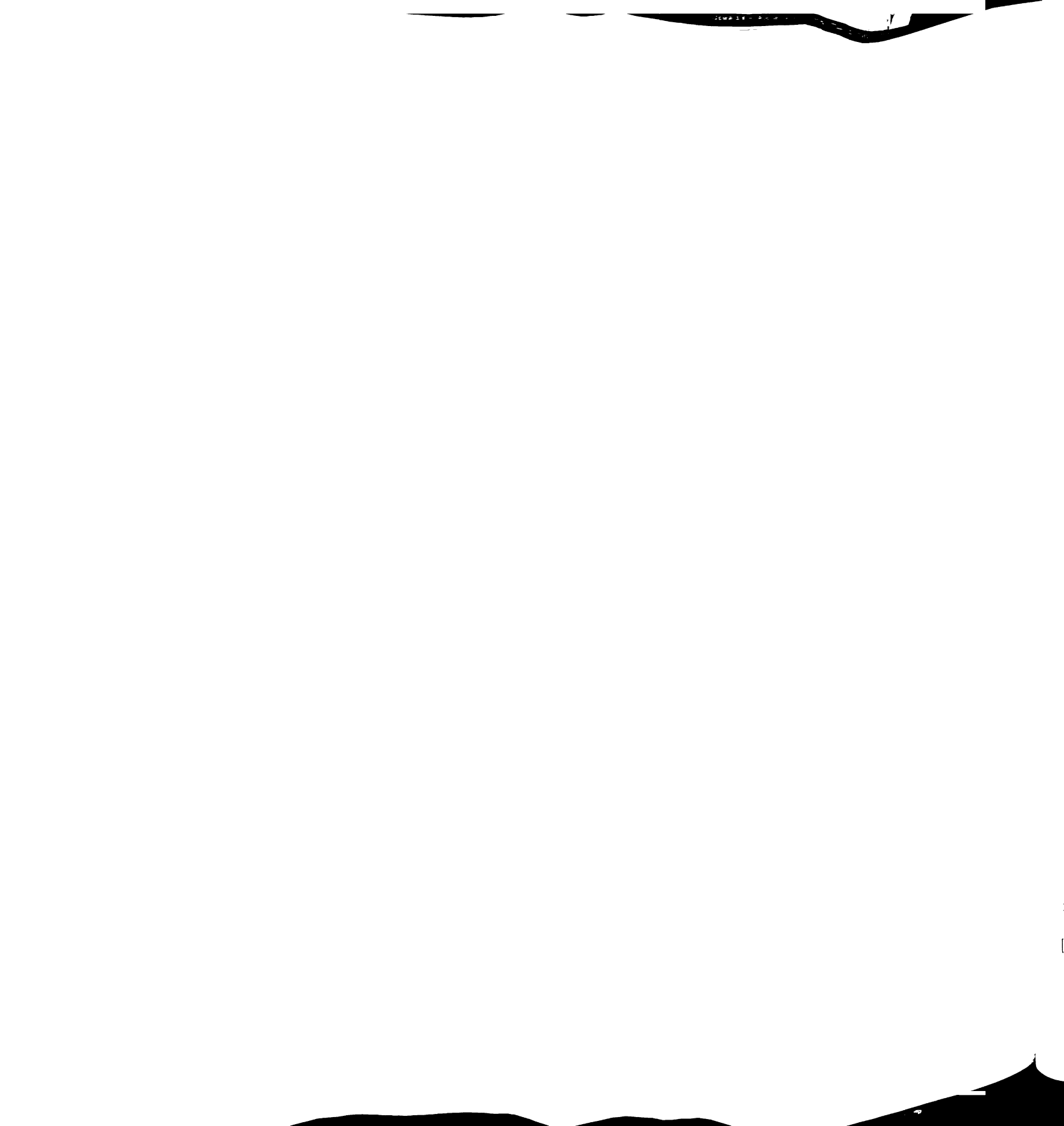
Oct-1, a ubiquitous cellular protein, is a member of the POU domain family of transcription factors [69]. Members of this family of proteins frequently function in multi-protein complexes, and bind to specific DNA octamer sequences within promoters and enhancers of several cellular genes. The POU domain of these proteins can be subdivided into the POU-specific domain and a POU homeo domain. Collectively these two domains are responsible for the high affinity, sequence specific binding to the octamer element [69]. Homologues of the octamer elements, containing the “core” TAATGARAT sequence, are found in the promoter regulatory domains of HSV-1 IE genes. Oct-1 is capable of binding these promoter elements, but is not sufficient to induce transcription [70] [71]. Rather, VP16 and Oct-1 assemble into a specific protein-DNA complex that is required for IE gene expression (reviewed in [72]). The ability of VP16 and Oct-1 to assemble into this VP16 induced complex (VIC) requires another cellular factor, HCF-1 [71] [73]. The first step in assembly of this complex is the association of VP16 with HCF-1, which subsequently associates with Oct-1 already bound to the TAATGARAT motif [74], [75].

HCF-1, a putative cell cycle control protein, is synthesized as a large, 2035 amino acid (300 KDa), precursor protein that is processed by cleavage at a number of specific sites. These sites, called HCF_{PRO} repeats, are highly conserved 26 amino acid sequences

repeated six times toward the middle of the precursor protein. Cleavage gives rise to a range of polypeptides from 110 to 150 KDa in size. After cleavage the majority of the amino and carboxy-terminal regions of the protein remain tightly but noncovalently bound together [76]. The N-terminal domain includes the region of HCF-1 that associates with VP16 for assembly of VIC on IE genes [77]. This domain, consisting of amino acids 1-380, contains six copies of a repeated motif, termed kelch repeats, which fold into a six-bladed β -propeller structure [77]. The β propeller structure itself is sufficient for VIC assembly and transcriptional activation by VP16 [77] [78].

VP16, a 490 amino acid protein, is comprised of two different structural and functional domains. The first 400 amino acids contain regions of interaction with HCF-1 (residues 355-370), Oct-1 (residues 370-390), and vhs (residues 1-400) [79]. The C-terminal 80 amino acids (410-490) make up the transcriptional activation domain (AD) [80]. Without this domain VP16 can still interact with HCF-1 and Oct-1 at IE promoters, but can not activate transcription.

Another interaction of VP16 has been observed with the virion host shutoff protein (vhs) [21]. After HSV-1 infection, one or more proteins act to suppress host protein synthesis and induce turnover of cellular mRNAs (reviewed in [1]). One such protein is believed to be vhs. Immunoprecipitation of vhs from infected cell lysates resulted in coprecipitation of VP16. Mutational analysis of both proteins revealed a small contiguous region of vhs (residues 238-341) that is necessary and sufficient for binding VP16, while in VP16 multiple non-overlapping segments, not including the activation domain, were required for complex assembly with vhs. Vhs also suppressed VIC formation *in vitro*.



These results suggest a regulatory link between the two proteins [21], in which VP16 keeps vhs from degrading the newly synthesized viral mRNAs [81].

Models of Herpesvirus egress

Currently there are two models of herpesvirus egress and maturation. Included in both models is the general agreement that viral capsids containing DNA are assembled in the nucleus, and that they acquire an initial envelope by budding through the inner nuclear membrane into the perinuclear space (reviewed in [1]). This is where the two models diverge. The first model, suggested by Johnson and Spear in 1982, implies that after the capsid gains an immature form of the envelope at the inner nuclear membrane, it is moved via the secretory pathway through the endoplasmic reticulum (ER) into the Golgi network, ultimately being released through the plasma membrane [82]. This model implies that the virion acquires a full complement of transmembrane glycoproteins at the inner nuclear membrane and that those immature glycoproteins are processed during transport through the Golgi complex. The second model was initially suggested by Stackpole et. al in 1969. This model implies that after the initial envelopment at the inner nuclear membrane there is a subsequent de-envelopment at the outer nuclear membrane and naked nucleocapsids are released into the cytosol. These naked capsids acquire their envelopes by budding into cytoplasmic vacuoles that are part of the trans-Golgi network [83].

Ample evidence exists for both models. The model of “nuclear envelopment” receives support from electron microscopic studies [84] [85] [86] [87], drug treatments [82], and glycoprotein processing (reviewed in [1]). In the initial observation of nuclear

envelopment, Johnson and Spear reported that treatment of infected cells with monensin, a drug that blocks the budding of vesicles from the Golgi, led to the accumulation of enveloped particles in what are believed to be Golgi-derived vesicles [82]. These virions contained immature forms of the viral envelope suggesting that the late stages of viral glycoprotein processing were blocked. This suggests that the virions acquired their envelope from the inner nuclear membrane and were transported to the Golgi through a pathway that involves the processing of the envelope glycoproteins.

Electron microscopy has been one of the main techniques used to visualize virions throughout infection. In a study performed by Torrisi et al., the HSV glycoproteins B (gB) and D (gD) were labeled with antibodies and lectins that distinguished the immature from mature forms. The immature forms of the glycoproteins were present on the envelopes of virions within the perinuclear space as well as on the inner nuclear membrane, whereas the mature glycoproteins were seen on the envelopes of virions within membrane bound vesicles [84].

In a similar study, Stannard et al. localized gB and gD within the nucleus and at the nucleoplasmic side of the inner nuclear membrane [85]. This localization, using immunogold labeling, was mainly at sites of virus assembly. This evidence led to the hypothesis that precursor gB and gD proteins are first transported into the nucleus, and then, together with maturing capsids, are targeted to the inner nuclear membrane, and later into viral envelopes at the site of budding [85].

Electron micrographs of infected cells have produced great images of what is occurring throughout HSV-1 infection, but how those images are interpreted is important. One of the main controversies over the path of HSV-1 virion envelopment and egress is



the observance of a limited number of unenveloped, naked capsids in the cytoplasm. For supporters of nuclear envelopment, the existence of the naked capsids in the cytoplasm is believed to result from fusion of the cytoplasmic membranes with viruses in transport. This fusion is believed to be a terminal deenvelopment, since the morphology of the capsids suggest they are undergoing degradation [88]. These capsids are presumably not caused by superinfection of the cell, because gD prevents superinfection by hindering fusion between virion envelopes and the membranes of the transport structures [89]. In a mutant virus carrying a deletion of the gD gene, a large number of naked capsids accumulated in the cytoplasm and demonstrated a degraded morphology [88].

Contrary to the “nuclear envelopment” model is the “cytoplasmic envelopment” model. This model gains support from studies with HSV-1 as well as the other herpes viruses [90], [91], [92], [93], [94], [95], [96], [97], [26]. According to this model, the naked capsids in the cytoplasm represent one step in the multi-budding process of virion envelopment and egress. In a study performed by Genderen et al., the phospholipid composition of extracellular herpes was compared to that of the nuclear membranes of infected cells. The viral envelope had a 3-fold enrichment in sphingomyelin (SM) and phosphatidylserine (PS), and decreased levels of phosphatidylcholine (PC) and phosphatidylinositol (PI), when compared to the infected nuclear membranes [98]. They report that these differences are very similar to the differences reported to exist between the Golgi membranes and the nuclear membranes/ER.

A genetic approach to investigate virion envelopment was performed by Browne et al. in 1996. This group constructed recombinant viruses in which the essential gH is retained in the membranes of the ER, by means of an ER retention signal. The resulting

virions pro

extension o

in either th

Golgi allo

gD from th

somewher

performed

in the me

and extra

cisternae.

Utiliz

proteins.

subseque

examine

proximit

VPS, a n

or gB ur

associat

also sug

cytoplas

Wha

where t

tegume

virions produced contained no detectable amounts of gH in their envelopes [99]. An extension of the above study was performed by Whiteley et al. in which gD was retained in either the ER or the trans-Golgi network. They report that the retention of gD in the Golgi allows incorporation into the viral envelope, whereas retention in the ER excludes gD from the virion [100]. These results imply a mechanism of envelopment that occurs somewhere other than the nuclear membrane/ER. In an electron microscopic study performed by Komuro et al., the localization of mature gD was found to be accumulated in the membranes of the trans Golgi cisternae, as well as on the envelopes of cytoplasmic and extracellular virions [101]. Numerous naked capsids were also found in proximity to cisternae, frequently seen surrounded by a double membrane of short Golgi cisternae.

Utilizing a different approach, Holland et al. studied the axonal transport of HSV proteins. A system that allows selective virus inoculation of dorsal root ganglia and subsequent observation of viral transport along the axons to epidermal cells was examined under immunoelectron microscopy. Not only were capsids seen in close proximity to microtubules (MTs), but VP16 was generally localized within 150 nm of VP5, a major capsid protein. In contrast, VP16 and VP5 did not co-localize with gC, gD or gB until the capsid reached the axon terminal [28]. Overall, these findings suggest an association of tegument, nucleocapsid and MTs during transport through the axon. They also suggest that tegument assembly and envelopment of the virion occurs in the cytoplasm.

While both models are backed up by good evidence, it is still inconclusive as to where the virion is attaining its envelope. If we knew where the virion acquired its tegument, the structural layer between the capsid and envelope, we would have a better

view on the egress of HSV-1. If the nuclear envelopment route is correct, then all the tegument proteins must accumulate and assemble in the nucleus. If the cytoplasmic envelopment route is correct, then the tegument proteins can accumulate in the nucleus and undergo multiple envelopments, or accumulate and assemble in a late cytoplasmic compartment. In an electron micrograph of a virion, the tegument appears as an electron-dense, opaque substance. In electron micrographs of infected cells, cytoplasmic capsids are sometimes seen associated with a dense “protein coat” [83], or are usually seen associated with or budding into Golgi derived membranes that show a thick and electron-dense region in the inner membrane facing the viral particle [101].

Most electron micrograph evidence of tegument location and assembly comes from studies of the herpes viruses other than HSV-1. In an ultrastructural study of the α herpesvirus, PrV, nucleocapsids were observed budding into the perinuclear space acquiring an initial tegument that was sharp bordered, homogenous, and very electron dense [26]. Following this initial envelopment, capsids were seen to deenvelope through the outer nuclear membrane, releasing naked capsids into the cytoplasm. Secondary envelopment was observed at Golgi derived membranes, where there was an addition of an enlarged tegument material of less electron density than after the initial envelopment. Therefore, there were visible differences in virion morphology after primary and secondary envelopment, yet tegument was seen both in the nucleus and in the cytoplasm.

In another α herpesvirus study, images of VZV capsids budding through the inner nuclear membrane were captured, yet these virions did not contain any discernable tegument [91]. Analogous to the PrV studies, the VZV cytoplasmic capsids were seen budding into Golgi derived membranes. The convex surface of these membranes had

tegument-like material adherent to them. In light of this evidence, the following model has been proposed by Gershon et al. to account for the envelopment of VZV and PrV. Envelope glycoproteins are transported from the rough ER to the Golgi apparatus, where they are processed to mature forms, and are ultimately delivered to the trans Golgi network (TGN), where they accumulate in specialized sacs. Tegument is transported to these sacs, either complexed with glycoproteins or independently. One side of the TGN concentrates glycoproteins and tegument in the immediately adjacent cytoplasm. These TGN-derived sacs then wrap around capsids, which have been attracted to the tegument. The process of envelopment then proceeds, trapping tegument between the TGN-derived envelope and the nucleocapsid.

Ultrastructural analysis of members of the β herpesvirus family shows a different pattern of tegumentation. In cells infected with either HHV-6 or HHV-7, all unenveloped cytoplasmic capsids were observed to be tegument-coated. This suggests that the capsids are acquiring their tegument within the nucleus. In the cells infected with HHV-6, intranuclear compartments associated with the inner nuclear membrane, contain capsids that have tegument of variable thickness [94]. These tegumented capsids subsequently cross the nuclear envelope and are present as unenveloped capsids in the cytoplasm where they associate with a cytoplasmic vacuole and acquire an envelope. Cells infected with HHV-7, were not found to contain the intranuclear compartments of tegumented capsids, yet all unenveloped cytoplasmic capsids were coated with mature tegument [93]. The model for β herpes virus egress closely resembles that for PrV and VZV, with the difference being where the virus acquires its tegument, namely as it exits from the nucleus into the cytoplasm.

HSV-1 protein localization

A study by Morrison et al. compared the differences in the intracellular localization and fate of different HSV tegument proteins [12]. The tegument proteins were observed using immunofluorescence. Incoming tegument proteins were visualized at 30 minutes post infection of cells infected with 100 plaque forming units (pfu) per cell. VP1/2 was not observed in the nucleus, but was found to have a strong perinuclear staining pattern with a weak speckled pattern in the cytoplasm. VP13/14 and VP16 displayed similar patterns of weak speckled cytoplasmic staining, but also displayed a strong nuclear localization, with nucleolar exclusion. The patterns of localization of newly synthesized tegument proteins were observed at three hours post infection in cells infected with 10 pfu per cell. These patterns were strikingly different than those observed for the input tegument proteins. VP1/2 was observed primarily in the perinuclear region of the cell. VP13/14 also demonstrated a perinuclear staining pattern, with some concentrations at small distinct structures at the edge of the nucleus. VP16 displayed a diffuse cytoplasmic localization, though not in the perinuclear region, and was also observed in specific globular spots within the nucleus [12].

This nuclear staining of VP16 was characterized further by double staining with ICP-8 (HSV-1 DNA binding protein) and VP22a (capsid scaffolding protein). VP16 and ICP-8 were observed to co-localize within the nucleus, and the globular compartments of localization were observed to increase in size over time. VP16 was also seen to localize with VP22a, suggesting association with capsid assembly sites. The tegument protein VP22, which could not be observed at early times, was found to be at distinct intranuclear

sites around six hours post infection. These sites were not specifically localized with the VP16 sites, but were directly adjacent to them [12].

In a separate study [19], the *in vivo* protein-protein interaction between VP22 and VP16 was examined in both infected cells and coexpressing cells. A direct interaction between the two proteins in infected cells was demonstrated by affinity chromatography and colocalization. Within the infected cells, VP22 and VP16 were observed to colocalize at the edge of the nucleus and the edge of the cell. In coexpressing cells there was a dramatic relocation of VP22 to novel spherical structures (“tegument bodies”) located right outside the nucleus. Some VP16 also appeared in this structure. The ability of this relocation was dependent upon the presence of the VP16 activation domain [19].

Recently Elliot et al. constructed an HSV-1 virus that expresses a VP22 green fluorescent protein (GFP) fusion. This fusion allows for the visualization of VP22 in a live cell throughout infection. The VP22-GFP fusion was detected in live cells as early as three hours post infection. In time-lapse analysis, the *de novo* synthesized VP22 initially appeared as a diffuse cytoplasmic pattern which progressed into a more distinctive pattern, concentrated in particles to one side of the nucleus [102]. This pattern is believed to be localized with the Golgi apparatus. The fluorescence was then observed to travel towards the cell periphery, eventually appearing extracellularly as individual fluorescent particles.

In light of the current evidence, the specific location at which the virion acquires its tegument is still controversial. One other piece of evidence to consider is the existence of L-particles (discussed above). McLauchlan et al. demonstrated that the removal of the

envelope from L particles did not alter the size or shape of the tegument material. This demonstration that the tegument can exist as a defined structure in the absence of capsid and envelope suggests that the proteins that make up this structural matrix, can self-assemble [23]. If tegument assembly were to be occurring in the nucleus, all of the structural proteins would need to be actively transported from the cytosol where they are synthesized, into the nucleus.

Nuclear Import

Eukaryotic cells regulate a number of cellular processes at the level of nucleocytoplasmic transport. The fate of any protein depends on its amino acid sequence which can contain sorting signals that direct its delivery to many locations within the cell. Most proteins do not have sorting signals and therefore remain in the cytosol as permanent residents. Proteins that do have specific sorting signals will be directed from the cytosol into the nucleus, ER, mitochondria, or peroxisomes (reviewed in [103]).

Proteins that need to move between the nucleus and cytoplasm in order to perform their normal cellular functions identify themselves with nuclear localization signals (NLS) and nuclear export signals (NES). The classical basic NLS is a lysine rich sequence typically from four to eight amino acids in length [103]. These signals are recognized by members of the nuclear transport receptor family, at the NPC [104].

One of the HSV proteins that plays a key role in the infected cell nucleus is VP16. This tegument protein must get into the nucleus to activate the viral IE gene expression. VP16 does not possess its own NLS signal, and is found to be largely cytoplasmic in transfection assays [105]. It is likely that VP16 relies on the interaction with an NLS-

bearing protein for its nuclear import. One such possibility is the cell cycle factor, HCF-1. As discussed above, HCF-1 is the mediating protein required for formation of the transcriptionally active VP16 induced complex (VIC) [71].

Within the past year, La Boissiere et al. have found, by deletion analysis, a putative NLS near the carboxy terminus of HCF-1 (between residues 2015 and 2031). In cells cotransfected with expression vectors for full length VP16 and full length HCF-1 or HCF-1 with just the N and C terminal domains, VP16 relocalized from a diffuse to a mainly nuclear pattern. Deletion of the NLS in HCF-1, while not affecting the ability to form VIC *in vitro*, resulted in no nuclear localization of VP16. The candidate NLS was also fused to a reporter gene that is normally localized in both the cytoplasm and nucleus resulting in induced nuclear accumulation of that gene product. These results indicate that HCF-1 contains an NLS and may be acting as a nuclear import factor for VP16 [105].

The interaction of VP16 with HCF-1 is believed to be through VP16s' REHAYS motif (residues 360-365) [106] [79]. This small motif is also seen in the ubiquitous basic leucine zipper transcription factor, LZIP or Luman [107] [108]. This cellular protein is the only other known target of HCF-1. Mutations affecting the REHAYS motif of VP16 abolished its interaction with HCF-1 *in vitro*, and VP16 was not shown to localize to the nucleus [105]. These results indicate that one role of HCF-1 is as a chaperone for the nuclear entry of VP16.

HSV-1 is the most studied of the herpesvirus family, yet many aspects of infection by HSV-1 remain poorly understood. The functions of about half of the HSV coded proteins have been shown to be absolutely necessary for successful host invasion, genome

transcription, replication, particle assembly, maturation, egress and pathogenicity [109].

Following infection by HSV-1, the cell nucleus is converted into a factory for the expression and replication of the viral genome, as well as an assembly area for progeny virus. Currently there are two contrasting models of virion maturation and egress. These models stem from studies done in the absence of viral infection or by using techniques that involve a lot of processing of the sample before the actual observation is documented. A useful study would be to observe HSV-1 proteins in a live cell in the context of a viral infection.

Specific Aims:

1. To observe the localization of VP16, throughout a course of HSV-1 infection in live cells.
2. To compare the localization of a tegument protein (VP16) and a capsid protein (VP26) throughout a course of HSV-1 infection in live cells.
3. To determine if HCF-1 is required for VP16 localization into the cell nucleus.

Chapter 2

MATERIALS AND METHODS

Cell lines and viral strains

Vero cells (ATCC) and 16-8 cells [15] were maintained in Dulbecco's modified minimal essential medium (DMEM; GibcoBRL) containing 10% fetal calf serum (FCS; Atlanta Biologicals) at 37°C in a 10% CO₂ environment. The Vero cell line was originally derived from the kidney of an African green monkey. 16-8 cells are derivatives of Vero cells with an integrated VP16 gene [15]. BHK cells (ATCC) and tsBN67 cells [110] were maintained in DMEM/10% FCS at 33°C in 7.5% CO₂, the permissive environment for the temperature sensitive cells. The BHK cell line was originally derived from the kidney of a 1-day old hamster. tsBN67 cells are a temperature sensitive derivative of BHK cells with a mutation in the gene encoding the Host Cell Factor (HCF-1) [110]. The tsBN67 cells were provided by W. Herr and by the RIKEN cell bank (Japan).

The parental wildtype virus used in this study was HSV-1 KOS. A mutant virus lacking the VP16 gene, designated 8MA, was used for producing recombinant viruses [15]. The K26GFP virus, containing a VP26-GFP fusion gene, was kindly provided by P. Desai [111].

High titer stocks of virions were purified from infected cells. In a T150 tissue culture flask (Nalgene) approximately 1.5×10^7 cells (Vero cells for production of KOS, 16-8 cells for production of 8MA) were infected at a multiplicity of infection (MOI) of 0.01 in 1.5 ml serum free DMEM. The virus was incubated with the cells for 1 hour at

37°C/10% CO₂ under intermittent agitation. After 1 hour, the cells were washed with serum-free DMEM and fed with 25 ml DMEM/2% FCS. The infected cells were incubated for 3-5 days until abundant cytopathic effect was seen. The virus was then harvested by scraping the cells off the TC flask surface into the media. The collected cells were transferred to a sterile conical tube (Nalgene) and pelleted in a Beckmann tabletop centrifuge at 1000 rpm for 5 minutes. Fourteen milliliters of the supernatant were removed and aliquoted as low titer stocks. The cell pellet was resuspended in the remaining 10-11 ml media and transferred to a 25 ml TC flask (Nalgene). Virion particles were released from the cell debris by sonication in a cup horn (Heat Systems - Ultrasonics). Sonication occurred in three 30 second stages consisting of 1-second pulses at 90% duty cycle and the output control set between 9 and 10. The solution was transferred to a 15 ml conical tube and the cellular debris was spun down in the tabletop centrifuge at 4000 rpm for 10 minutes. The supernatant was aliquoted as high titer stocks and stored at -80°C. Titer was determined by plaque assay of a thawed aliquot.

Plaque Assays

Cells were seeded onto a P60 tissue culture plate (Nalgene) at 5×10^5 cells per plate in DMEM/10% FCS and grown overnight. Dilutions of the virus stocks to be titered were made in triplicate. The final dilution sets were 10^{-3} , 10^{-4} , and 10^{-5} for low titer stocks and 10^{-4} , 10^{-5} and 10^{-6} for high titer stocks. The cells were washed in serum free DMEM and then inoculated with 100 µl of the diluted virus. The cells were incubated with the virus for 1 hour at 37°C/10% CO₂ with intermittent agitation. After 1 hour the cells were washed with serum free DMEM and overlaid with an equal part mix

of 2X DMEM/10% FCS and 1.8% Sea-Plaque™ (FMC) agarose (pre-melted at 65°C).

The agarose overlay was allowed to solidify at room temperature for 15 minutes, then the overlaid cells were incubated at 37°C/10% CO₂ until plaque formation was evident (approximately 4-5 days). The agarose was removed from the cellular monolayer without disrupting the plaques. The plates were then stained for approximately 5 minutes with 1% methylene blue in 70% isopropanol. The stain was removed and the plates were washed with distilled water and allowed to dry before plaques were counted.

Virion Purification

To purify virions from the cell lysate, Vero cells (for wild type viral strains) or 16-8 cells (for VP16 mutant viral strains) were infected and harvested from T150 culture flasks as described above. The supernatant, which contains the virion particles, was placed on top of 10 ml of 20% glycerol in PBS (137 mM NaCl, 10 mM Na₂HP0₄, 1.5 mM KH₂PO₄, and 2.7 mM KCl) and centrifuged at 28K rpm in a SW28 rotor (Beckman), at 4° C for 90 minutes. The supernatant was discarded and the virion pellet was resuspended in phenol red free DMEM. The virion suspension was then aliquoted and frozen at -80° C as purified viral stock.

Viral DNA extraction and purification

To purify viral DNA from strain 8MA for generating recombinant viruses, virions from 16-8 cells were purified from T150 tissue culture flasks as described above. The pelleted virus was resuspended in 2 ml of virion lysis buffer (100 mM NaCl, 10 mM EDTA, 50 mM Tris-HCl pH 8.0, and 0.5% lauryl sarconisate), treated with proteinase K

(final concentration 0.2 mg/ml) and incubated for 1 hour at 37° C, two times. The DNA was isolated by ultracentrifugation by combining with a 1:1 mix of PBS: cesium trifluoroacetate (2 g/ml, CsTFA™, Amersham Pharmacia) and ethidium bromide (stock concentration 10 mg/ml). The sample was transferred to a 35 ml ultracentrifuge tube (Beckman) and spun at 45K rpm in a Vti50 rotor (Beckman), at 4°C overnight. The ethidium bromide labeled DNA band was removed from the tube through a 22-gauge needle. Extraction with pentanol removed the ethidium bromide, and repeated dialysis against TE (10 mM Tris-HCl, 1 mM EDTA) removed the CsTFA. The DNA concentration was determined by absorbance at 260 nm.

Green Fluorescent Protein (EGFP) fusion plasmids

The enhanced GFP gene (pEGFP-N3,) was subcloned into pKOS-VP16-GFP (constructed by E. Chung 2/96). The pKOS-VP16-GFP plasmid contains an older version of GFP fused to VP16 at an inserted *Bam*HI site 19 base pairs upstream of the stop codon. This plasmid was digested with restriction endonuclease *Xba*I. The methylated *Xba*I site in the GFP gene remained uncut, while the unmethylated *Xba*I site, located in the polylinker of the 5' flanking sequence, was cut. The 5' vector overhangs were filled in using Klenow enzyme (GibcoBRL), and blunt end re-ligated using T4-DNA ligase (GibcoBRL). This plasmid, designated pDRG24-1, was amplified and purified from electrocompetent *E.coli* GM48 cells (*dam*-) so that the *Xba*I site in the GFP gene would be unmethylated. Plasmid pDRG24-1 was then digested with *Bam*HI and *Xba*I to remove the unenhanced GFP gene. Plasmid pEGFP-N3 was also digested with *Bam*HI and *Xba*I to release the enhanced GFP gene. The pDRG24-1 vector and EGFP-

N3 fragment were purified from an agarose gel (Qiagen) and ligated using T4- DNA ligase. The ligation product was transformed into *E.coli* GM48 cells, and DNAs from resulting colonies were screened by digestion with restriction endonucleases to identify the correct clone. The resulting construct, designated pDRG24-2 (Fig. 2), contains a VP16-EGFP fusion flanked with 5' and 3' viral DNA and was used in the production of recombinant viruses.

To obtain a plasmid that would express the VP16-EGFP fusion in transfected cells, a strong mammalian promoter was needed to replace the native VP16 promoter. Plasmid pMSVP16 Δ C +119 [80] contains a VP16 gene driven by the mammalian Maloney sarcoma virus (MSV) promoter. This plasmid also contains a unique *KpnI* site within the VP16 open reading frame. Restriction digestion with *KpnI* yielded a linear vector. Plasmid pDRG24-2 contains a *KpnI* site in the same position within VP16 as pMSVP16 Δ C +119, and a second *KpnI* site within the 3' flanking sequence. When this plasmid was digested with *KpnI*, a linear vector fragment and a VP16-EGFP-3' fragment were produced. Plasmid pMSVP16 Δ C +119 vector DNA was extracted with phenol: chloroform: isoamyl alcohol (25:24:1 v/v, Boehringer Mannheim) and VP16-EGFP-3' DNA was agarose gel purified. The vector and fragment DNAs were ligated with T4 DNA ligase and transformed into *E.coli* DH5 α electrocompetent cells. DNA from resulting colonies were screened by digestion with restriction endonucleases to verify the correct orientation of the inserted fragment. The resulting construct, designated pDRG31-1, contains a VP16-EGFP fusion protein expressed from a MSV promoter.

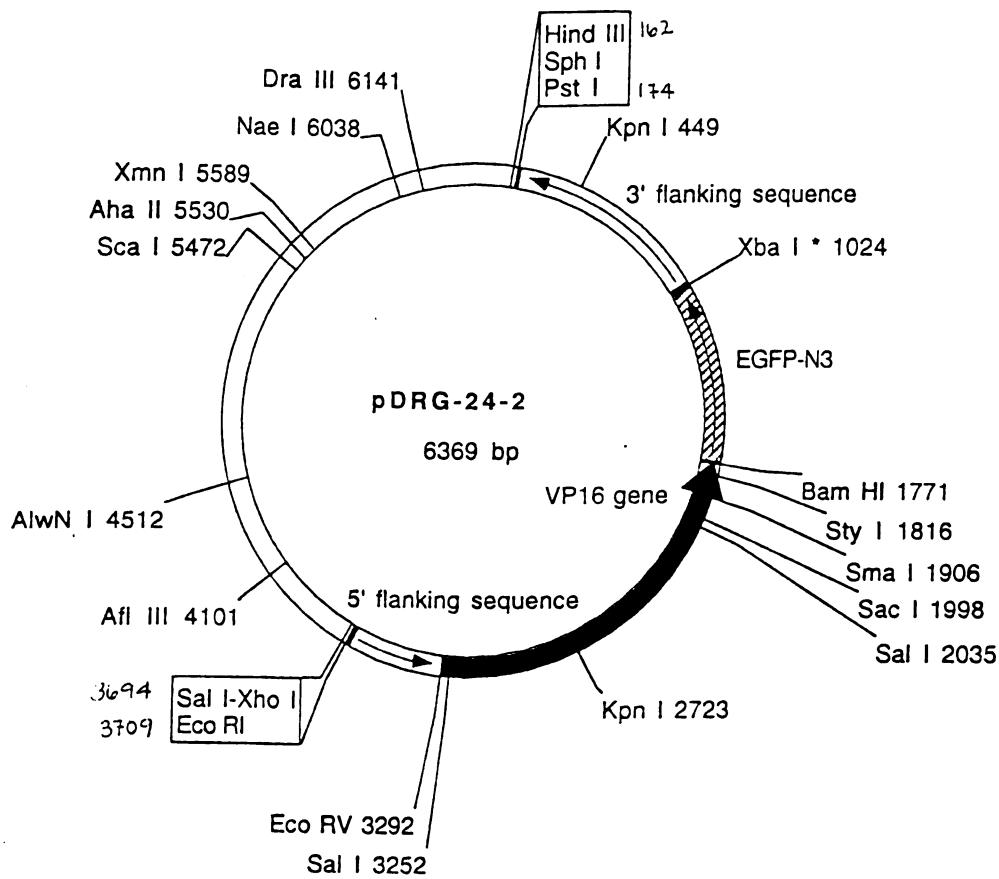


Figure 2. Plasmid map of pDRG24-2. The pKOS-VP16-GFP (E. Chung) contained an old version of GFP inserted at a *Bam*HI site 19 bp upstream of the stop codon within the VP16 gene. Removal of the old GFP gene and insertion of a new enhanced GFP gene resulted in this construct which was used to produce recombinant virus DG1 (described in detail in the methods section).

Generating Recombinant Virus DG1

Plasmid pDRG24-2 was digested with *EcoRI* and *PstI* to release the VP16-EGFP fragment with the 5' and 3' flanking sequences. Vero cells were seeded in P60 tissue culture plates at 2×10^5 cells per plate and incubated overnight in DMEM/10% FCS. Cells were treated with 60 µg/ml of chloroquine for one to three hours. Prior to transfection the chloroquine media was replaced with serum free DMEM. Each plate was transfected with a mixture of 5 µg of 8MA viral genomic DNA, 5 µg of VP16-EGFP fragment, and 20 µg of carrier DNA (sheared salmon sperm DNA, Boehringer Mannheim). The DNA mixture was prepared in 2X HEPES-buffered saline (HBS; 280 mM NaCl, 10 mM KCl, 1.5 mM Na₂HPO₄, 12 mM dextrose, 50 mM HEPES) and precipitated with 1/20th volume of 2.5 M CaCl₂. The precipitate was added directly to the media. After 5 hours of incubation with the DNA transfection mixture, the medium was removed and the cells were shocked for three minutes with 2 ml of 10% glycerol in PBS. The glycerol was removed with two washes of 5 ml of DMEM/2% FCS. The cells were then overlaid with 5 ml of an equal part mix of 2X DMEM/10% FCS and 1.8% Sea PlaqueTM agarose, and incubated at 37° C/10% CO₂ for 6 days. Eight plaques were picked and stored in 1 ml DMEM at -80° C.

The primary candidates were plaque purified twice more to obtain clonal stocks of recombinant viruses. The tertiary plaque purified candidates were used to make larger viral stocks. DNA and protein preparations of each were analyzed by Southern blot and Western blot, respectively, to verify that the isolated viruses contain the proper VP16 insert. The stocks were titered by plaque assay.

Southern Blot

To isolate viral DNAs for Southern blot analysis, 0.5 ml of viral stock was treated with 10% sodium dodecyl sulfate (SDS) and proteinase K (final concentration 0.2 mg/ml) for 1 hour at 37° C. The DNA was then extracted once with phenol and once with phenol: chloroform: isoamyl alcohol, followed by isopropanol precipitation and dilution in double distilled H₂O (diH₂O). The recombinant viral DNA was digested to completion with *Kpn*I and separated by gel electrophoresis in a 1% agarose gel. The gel was then prepared for DNA transfer by treatment with 0.25 M HCl for 20 minutes, then rinsed with diH₂O. The DNA was denatured by soaking the gel in denaturation solution (1.5 M NaCl and 0.5 M NaOH) for 20 minutes. The gel was then rinsed in diH₂O and soaked in neutralization solution (1.5 M NaCl and 0.5 M Tris-HCl pH 7.0) for 20 minutes. After an additional rinse in diH₂O, the DNA was transferred to a nitrocellulose membrane using standard methods [112].

After transfer was complete the membrane was dried under vacuum at 80° to bind the DNA to the nitrocellulose. The blot was then pre-hybridized for three hours in aqueous prehybridization solution (APH; 5X Denhardt's solution (Sambrook, et. al., 1989), 6X SSC (Sambrook et. al., 1989), and 0.5% SDS) with 100 µg salmon sperm DNA at 65°C. A VP16 specific ³²P-labelled DNA probe was made by random primed DNA labeling of a *Sal*I fragment of the VP16 gene. The synthesized probe was denatured by boiling for 10 minutes and added to new APH solution which was incubated with the blot overnight in a hybridization oven at 65°C. The blot was subsequently washed twice with 2X SSC/0.1% SDS, twice with 0.2X SSC/0.1% SDS, and once in 2X SSC, all washes carried out at room temperature. The blot was then exposed to X-ray

film (X-OMAT AR, Kodak) for 2 days, and the film was developed using an automatic film processor.

Western Blot

Protein samples were prepared by mixing 10 µl virion stock with 10 µl of 2X SDS sample loading buffer and heating to 100°C for 10 minutes. The proteins were separated in a 12% SDS polyacrylamide gel. The proteins were then transferred to a nitrocellulose membrane using standard methods [112]. Western Blot analysis was performed using the anti-VP16 polyclonal antibody LA2-3 at a dilution of 1:100,000 and a goat anti rabbit antibody (BioRad) at a dilution of 1:40,000. The antibodies were visualized using the Lumi Light chemiluminescence detection system (Roche).

DG1 Growth Curve

Vero cells were seeded at 2×10^5 cells/well on a six well tissue culture dish and incubated overnight in DMEM/10% FCS. Cells were infected in triplicate with DG1 and KOS at 5 pfu/cell. Infected cell extracts were collected at 4, 8, 12, 16, 20, and 24 hours post infection. Plaque assays were performed in triplicate as described above.

Microscopy and Live Cell Imaging

Images were obtained using a Meridian Insight confocal laser scanning microscope with a 60X oil immersion objective. Images were analyzed using L View Pro Image Processor, Version 2.6 and 2.8.

Vero cells were seeded at 1×10^5 cells/chamber onto 2 well , chambered coverslides (Nalgene Nunc) and grown overnight in DMEM/10% FCS. All visualization experiments were conducted in serum free DMEM without phenol red, to avoid excess fluorescence. The cells were washed, and 100 μ l inoculum of either 1 or 10 pfu/cell of purified DG1 and K26GFP viruses were prepared. The inoculum was incubated with the cells for one hour, and then the cells were washed to remove any excess virions. One milliliter of serum free DMEM without phenol red was added to each chamber. The infections were allowed to progress and images were collected at various times after infection.

BHK and tsBN67 cells were seeded in chambered coverslides at 2×10^4 and 2.5×10^4 respectively, and maintained either at the permissive temperature (33°) or the nonpermissive temperature (39°) for 2 days. Infection with DG1 was carried out as stated above, at either 1, 10, 50 or 100 pfu/cell in the presence or absence of 100 μ g/ml cycloheximide. Images were collected at varying times post infection.

Chapter 3

VP16 AND VP26 LOCALIZATION THROUGHOUT A TIME COURSE OF HSV-1 INFECTION

Introduction

Herpes simplex virus-1 (HSV-1) infects and proliferates in epithelial cells. Upon infection the lipid envelope fuses with the cell membrane releasing the icosahedral capsid and the proteinaceous tegument into the cytosol of the cell (reviewed in [24]). The capsid is then transported to the nuclear pore complex for the release of the viral genome into the nucleus. The tegument proteins, including VP16, VP22, and the virion host shutoff (vhs) protein, are also relocalized throughout the cell, but little is known about their fate during infection. It is well known that viral capsids are assembled in the nucleus, and that they acquire an initial envelope by budding through the inner nuclear membrane [1]. Yet, the remaining steps of herpesvirus egress and maturation are controversial.

The first model of herpesvirus egress implies that after the virion acquires an immature form of the envelope at the inner nuclear membrane, it is transported through the secretory pathway where the maturation of the envelope glycoproteins occurs [82]. This model is clouded by the observance of unenveloped, naked capsids in the cytoplasm of infected cells. Supporters of the above "nuclear envelopment" model suggest that such capsids represent a "dead end" pathway, or terminal deenvelopment [88].

The second model of herpesvirus egress incorporates the cytoplasmic naked capsids into the process of viral maturation and egress. The "cytoplasmic envelopment" model implies a multi-step budding process, where the virion gains the initial envelope

by budding through the inner nuclear membrane followed by development at the outer nuclear membrane, releasing naked capsids into the cytoplasm. These capsids then acquire their final envelope by budding into cytoplasmic vacuoles that are part of the Golgi network [83]. A schematic representation of the two models of HSV-1 egress is shown in figure 3.

The HSV-1 protein VP16 is an essential component of the viral tegument [1]. Along with being a structural element of the virion it is also a powerful transcriptional activator of the viral IE genes. VP16 enters the host cell with the infecting virion and is then transported to the nucleus for activation of viral transcription. It is unknown if VP16 is transported alone or still bound to the capsid. Once in the nucleus, VP16 forms a complex with cellular factors Oct-1 and HCF-1 at the TAATGARAT sequences within the promoter of IE genes.

Recently, two groups have produced recombinant viruses expressing green fluorescent protein (GFP) fusion proteins. Elliot et al. constructed an HSV-1 virus that expresses and incorporates VP22-GFP into the virion tegument [102] Desai et al. constructed an HSV-1 virus expressing and incorporating VP26-GFP into the viral capsid [111].

The isolation and cloning of the green fluorescent protein from the jellyfish *Aequorea victoria*, has had a major impact on our ability to observe events within living cells. The GFP chromophore requires no other *Aequorea* proteins, substrates, or

Figure 3. Schematic representation of the lytic cycle of HSV-1 infection. (1) Viral entry by fusion of envelope with plasma membrane. (2) The viral capsid containing the DNA and VP16 are transported to the nucleus. (3) The viral DNA is released in the nucleus and it circularizes. (4) Transcription of the IE genes is induced by VP16, IE gene are translated and transported back into the nucleus. (5) Presence of the IE gene products induces expression of the DE genes. (6) The DE gene products initiate the replication of the viral DNA as well as the expression of the L genes. (7) L gene products, which consist of the viral structural proteins, may be transported back into the nucleus or to a cytoplasmic compartment (perinuclear or associated with a cytoplasmic vesicle). (8) Capsid assembly and viral DNA packaging occurs within crystalline arrays along the inner nuclear membrane. (9) Tegumentation could occur within the nucleus. The tegumented virion may bud through the inner nuclear membrane acquiring an immature envelope that gets processed as the virion travels through the ER/Golgi secretory pathway. (10) Alternatively the virion may bud through the inner and outer nuclear envelopes resulting in naked capsids within the cytosol of the infected cell. The capsid may acquire the tegument from the perinuclear area. (11) Capsids travel through the cytoplasm and bud into a golgi derived vesicle acquiring a mature envelope and possibly some tegument proteins. (12) Mature virions are released from the cell by exocytosis.

cofactors to fluoresce. GFP absorbs UV or blue light and emits a *green fluorescence* that occurs even when fused with other proteins (reviewed in [113]). The original GFP chromophore has been modified through codon optimization for use in mammalian systems. Furthermore, the 238 amino acid enhanced green fluorescent protein (EGFP) has a serine to threonine replacement at position 65. This modification shifts the excitation peak from UV to 489 nm resulting in an 18-fold increase in fluorescence intensity [114]. This increase in fluorescence has allowed EGFP to be easily visualized by fluorescence microscopy and flow cytometry.

To observe the localization of the viral tegument protein VP16, I constructed a recombinant virus expressing a VP16-EGFP fusion protein. This virus was determined to be fully viable and exhibits growth kinetics similar to those of the parental wild type virus. Infection of Vero cells with this virus allows us to visualize newly synthesized VP16-EGFP within live cells as early as 4 hours post infection. Because of the ease of visualization of VP16-EGFP within the cell, I used confocal microscopy to monitor the localization of VP16-EGFP within individual cells throughout a course of infection.

Experimental Results

Isolation and identification of recombinant HSV-1 expressing VP16-EGFP

To construct a recombinant virus that contained a VP16-EGFP fusion gene within the viral genome, I utilized a homologous recombination strategy. I prepared a plasmid, pDRG24-2 (Figure 2 from materials and methods) that contained a VP16-EGFP fusion gene surrounded by 5' and 3' viral DNA flanking regions, as described in Materials and Methods. This 5'-VP16-EGFP-3' fragment of DNA was cotransfected with purified viral

genomic DNA from the HSV-1 8MA strain onto a monolayer of Vero cells. The HSV-1 8MA strain is a mutant virus lacking the essential VP16 gene and can only grow on complementing cells that express VP16. The 8MA genome carries a *lacZ* gene in the place of VP16 and it is therefore nonviable when grown on non-complementing cells. Vero cells are non-complementing cells for the defect in 8MA, and therefore only recombinant virus would be capable of propagating within these cells. The resulting virus was named DG1. The genomic structure of the viruses used in this study is shown in figure 4.

Virus that was carried through plaque purification three times was characterized by Southern blot to determine the correct placement of VP16 within the genome. Wild type VP16 carries a *KpnI* site within the middle of the gene; this site is 1523 bp from the *KpnI* site within the 3' viral flanking sequences. As seen in figure 5, in both the wild type HSV-1 KOS parental strain, and in plasmid DNA containing the wild type VP16 with surrounding flanking sequences (pKOS-VP16-2), a band corresponding to this size is observed. Also seen in the wild type HSV-1 KOS DNA is the fragment that contains the remaining piece of VP16 and upstream sequences. This larger band is also observed in the recombinant viral DNA isolated from DG1. The second band, with a size of 2274 bp, from the DG1 viral DNA corresponds to the same 1523 bp fragment as seen in wild type, with the addition of the EGFP fusion gene of 751 bp.

To confirm that this recombinant virus expresses and packages the VP16-EGFP fusion product, purified DG1 virion was subjected to Western blot analysis. Polyclonal antibody against VP16 was used as the probe. As seen in figure 6, an approximately 65 kDa protein was detected in wild type HSV-1 KOS. This corresponds to the full length

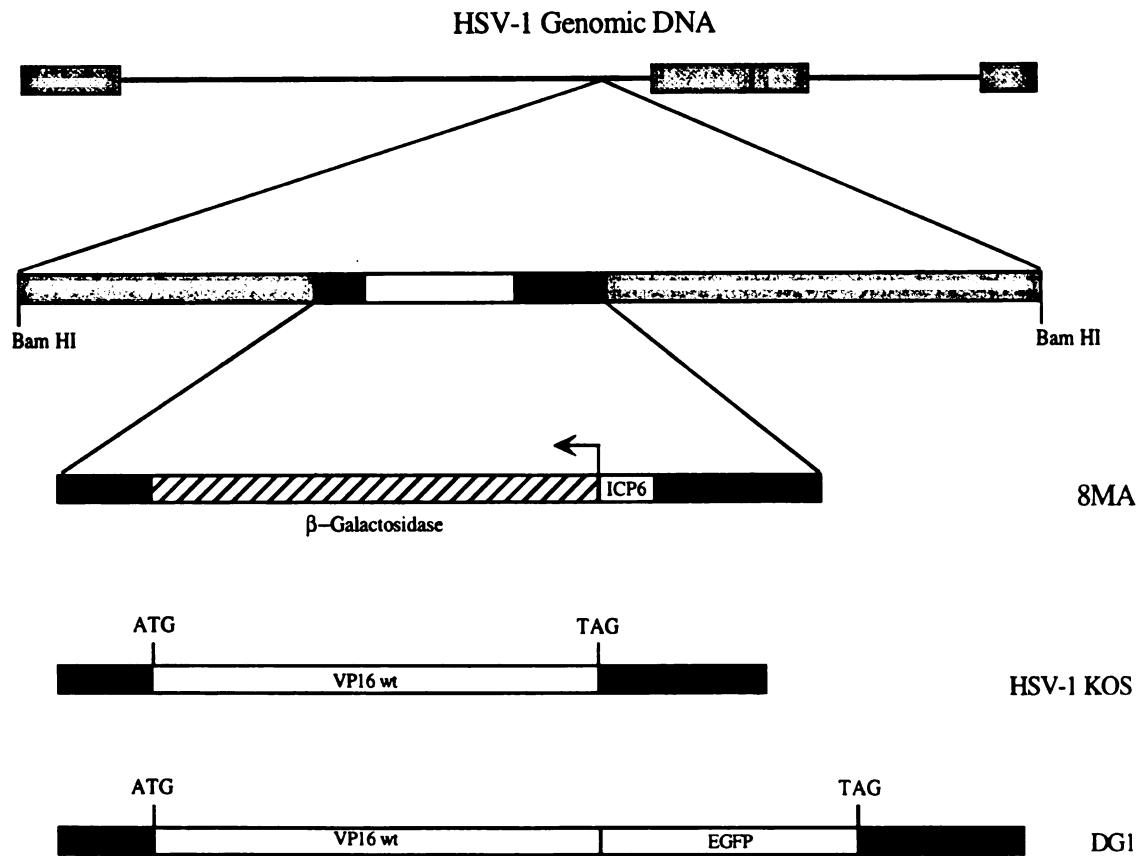


Figure 4. HSV-1 genomic structure and the fragment that contains the VP16 gene in different viruses. The HSV-1 KOS viral strain containing wild type VP16 gene. The HSV-1 8MA viral strain and the fragment used for the construction of recombinant virus DG1. The fragment consisting of the 5'-VP16-EGFP-3' fusion gene came from plasmid pDRG24-2.

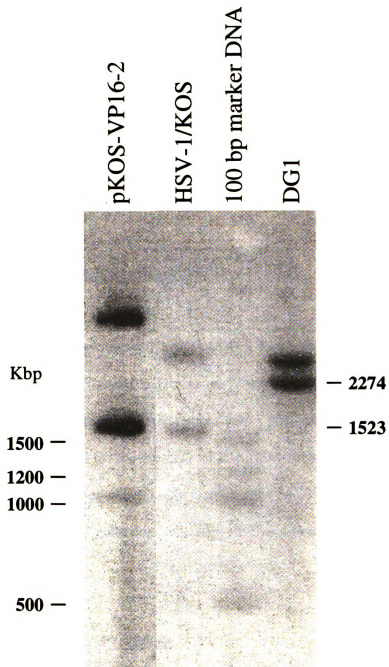


Figure 5. Southern blot analysis of recombinant viral DNA confirms the presence of VP16-EGFP. Viral DNA purified from Vero cells infected with either wild type HSV-1 KOS or recombinant DG1 was digested to completion with *KpnI* and electrophoresed in a 1% agarose gel. The DNA was then transferred to a nitrocellulose membrane and hybridized with a probe specific for the VP16 gene.

VP16 protein. DG1 contains a slower migrating polypeptide at approximately 92 KDa in size. This corresponds to the VP16-EGFP fusion protein (65 KDa VP16 + 27 KDa GFP).

Southern and Western blot analyses confirm that recombinant virus DG1 contains and expresses a VP16-EGFP fusion gene. These results indicate that isolation of a recombinant virus with the fusion of a large protein to the C-terminal activation domain of VP16 is possible.

Growth characteristics of recombinant DG1

To establish the growth properties of DG1, a growth curve was carried out for both wild type HSV-1 KOS and DG1 viruses. Vero cells were infected at a multiplicity of infection (MOI) of 5 and harvested every 4 hours post infection up to 24 hours. Total cell lysates were assayed for the presence of infectious virus by plaque assay. Figure 7 demonstrates that DG1 grows with wild type kinetics, indicating that the fusion of EGFP to the VP16 activation domain does not affect viral replication, assembly, or egress from the cell.

Detection of fluorescent VP16-EGFP

Vero cells were seeded in chambered cover slips and either transfected with 1 μ g pEGFP-N3 or pDRG31-1, or infected with DG1 at an MOI of 1. Cells were imaged in brightfield (Fig. 8A, B, C) and fluorescence (Fig. 8B, D, F) 24 hours after transfection or

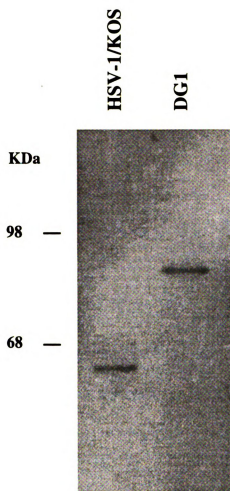


Figure 6. Western blot analysis of recombinant virions confirms the presence of a VP16-EGFP gene product. Purified virions were analyzed by SDS-PAGE on a 10% acrylamide gel followed by Western blotting with a polyclonal antibody against VP16.



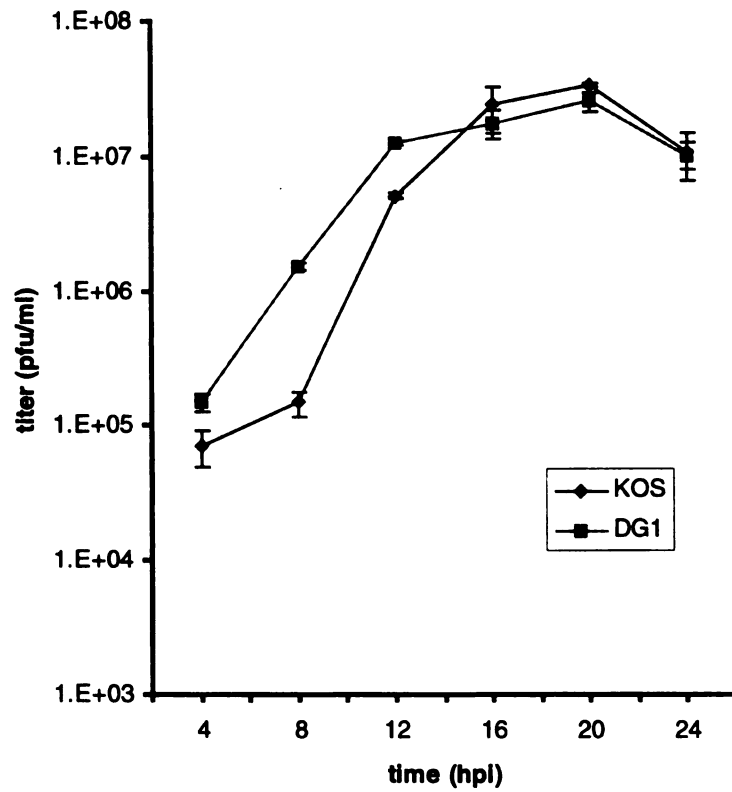


Figure 7. Recombinant virus DG1 grows with type kinetics. Single step growth curves for wild type HSV-1 KOS and recombinant DG1 viruses. Vero cells infected with either KOS or DG1 at 5 pfu/cell were harvested every 4 hours post infection up to 24 hours and were assayed for the presence of infectious virus via plaque assay.

6 hours post infection. Cells transfected with pEGFP-N3 (Fig. 8A, B) display a diffuse, homogenous expression throughout both the cytoplasm and nucleus. This same expression pattern is seen with the transfected plasmid expressing the VP16-EGFP fusion protein (Fig. 8C, D). In contrast to the diffuse expression observed in transfection, cells infected with a virus that contains VP16-EGFP show distinct compartments of localization (Fig. 8E, F). This localization is mostly nuclear, with a faint background of diffuse expression. Nucleolar exclusion is observed in both the transfection and infection data.

Time course analysis of VP16-EGFP during a viral infection

High multiplicity infection

To further analyze the localization of VP16-EGFP throughout a full viral reproductive cycle, I examined infected cells at 2,4,6,8,10,12,14,16,20, and 24 hours post infection as explained in Materials and Methods. Due to the amount of time it takes for one time point to be documented, the time course was set up in a number of different chambered cover slips. This allowed for one chamber of cells to be used for one time point and a different chamber of cells to be used for the next. Each chamber of infected cells was imaged for only one time point within 4 hours.

Vero cells were infected with DG1 at an MOI of 10. The inoculum was removed after one hour and the cells were washed and phenol red free and serum free DMEM was added to the infected cells. The chambers were incubated at 37°C/10% CO₂ throughout the time course. The infected cells are a population in logarithmic growth. They are not synchronized and therefore the timing of infection is variable. Throughout these

Figure 8. VP16-EGFP in the context of infection shows a different localization than transfected VP16-EGFP. Live cell analysis of EGFP, and VP16-EGFP plasmid expression, as well as VP16-EGFP from infection with DG1. (A, B) Cell transfected with plasmid pEGFP-N3. (C, D) Cell transfected with plasmid pDGR31-1, expressing the VP16-EGFP fusion. (E, F) Cells infected with 1 MOI of purified DG1, visualized 6 hours post infection. (A, C, and E) brightfield images, (B, D, and F) fluorescent images.

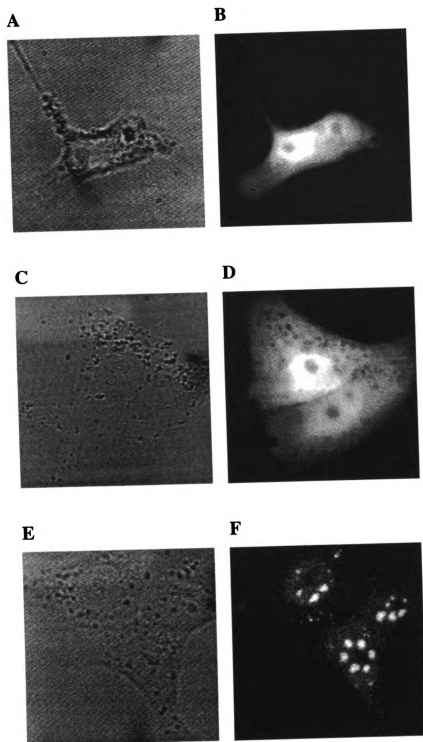


Figure 8

experiments there was one pattern of VP16-EGFP expression and localization that was developed. This pattern was observed in over 50% of the infected cells for that specific time point. Some cells displayed a delayed manifestation of this pattern and this appeared to be present in cells in which the onset of infection was delayed, and therefore I did not concentrate on those cells. Some of the images I will be discussing contain cells with the delayed pattern and I will point them out.

One question I was interested in was whether VP16-EGFP from the incoming virus could be observed within the cell. At 2 hpi (Fig. 9A, B), I was unable to distinctly see VP16-EGFP from incoming virus. Within the cell, a small amount of background light was emitted and the vacuoles and granules reflect the laser. This excess light was only apparent through the oculars and is not picked up by the camera. EGFP fluorescence can also be seen through the oculars, though in very little specks of light, but this small amount is also not intense enough to be picked up by the camera.

At 4 hours post infection newly synthesized VP16-EGFP can be visualized. This expression was diffuse and very faint throughout the cytoplasm with more intensity within the nucleus. Figures 9C and E reveal the diffuse haze staining the nucleus. A very faint haze was also observed throughout the cytoplasm, but was difficult to capture without adding too much light noise to the camera. The VP16-EGFP began accumulating at more intense, discrete dots within the nucleus (Fig. 9F) with nucleolar exclusion in all of the expressing cells. Figure 9G shows a large cell nucleus with a haze of VP16-EGFP and small dots of increased intensity. This image is one of a digital series of optical sections taken through the cell every 0.5 μm (Appendix Figure A).

Figure 9. DG1 time course, VP16-EGFP localization at 2 hpi and 4 hpi. Live cell analysis of VP16-EGFP in cells infected with DG1 at an moi of 10. (A) Fluorescence at 2 hpi, (B) brightfield image of the same cell at 2 hpi. (C, E, F, G) Fluorescence at 4hpi, (D) brightfield image of the cell in (C).

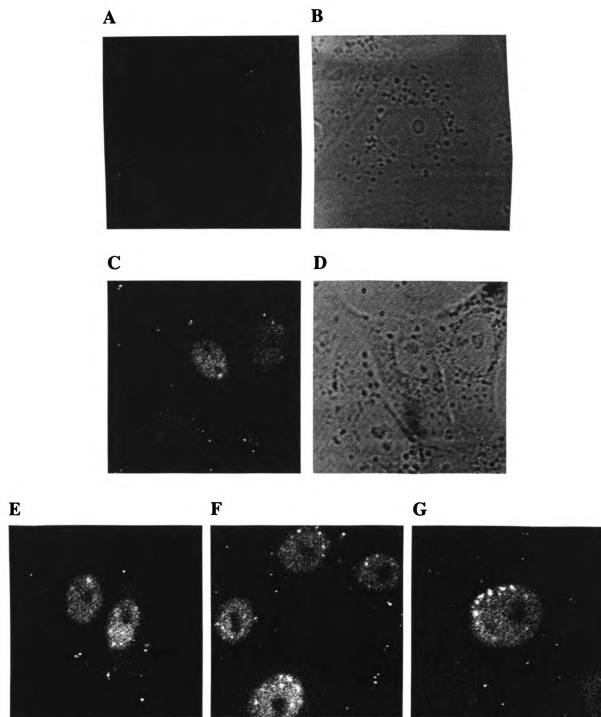


Figure 9

At 6 hours post infection, the cytoplasmic expression of VP16-EGFP was abundant and spread throughout the cell. The nuclear localization became much more pronounced within distinct nuclear dots in a uniform pattern throughout the nucleus. These dots are found in a range of four to ten throughout the infected cells. Figure 10A demonstrates the number and uniformity of the nuclear dots. There are eight dots within this nucleus spread evenly throughout. The bottom cell seen in this figure is one of the delayed patterns discussed above. This cell resembles a 4 h pattern of expression. Figures 10 B, C, and D also demonstrate the diffuse cytoplasmic expression as well as the nuclear localization of VP16-EGFP. These cells do not contain the completely distinct nuclear dots within the nucleus. Rather, in these cells the nuclear dots are beginning to coalesce and form larger nuclear blobs. Also observed in all cells of this time point was the nucleolar exclusion of VP16-EGFP (arrows in Fig. 10D and E). Figure 10F is an image of a cell that has just divided. A 0.5 μm series of images through this cell is shown in the Appendix Figure B. The two nuclei are symmetrically related in their patterns of VP16-EGFP localization. They both demonstrate nuclear dots and larger nuclear blobs, which are believed to be the original nuclear dots that have grown and coalesced. The two nuclei almost resemble mirror images of each other with three smaller nuclear dots on one side of the nucleus, and larger elongated connecting nuclear dots on the other side of the nucleus.

Cells infected with DG1 for 8 h display similar patterns as 6 h. These cells display large nuclear blobs within the infected cell nucleus as well as a bright and diffuse expression throughout the cytoplasm. Also observed is an increase in intensity of VP16-EGFP in the perinuclear region of the cell and intense cytoplasmic speckles. Figure 11A

Figure 10. DG1 time course, VP16-EGFP localization at 6 hpi. Live cell analysis of VP16-EGFP in cells infected with DG1 at an moi of 10. (A, B, C, D, F) Fluorescence at 6 hpi. (E) Brightfield image of cell in (D). Arrows in (D) and (E) point out the nucleolus.

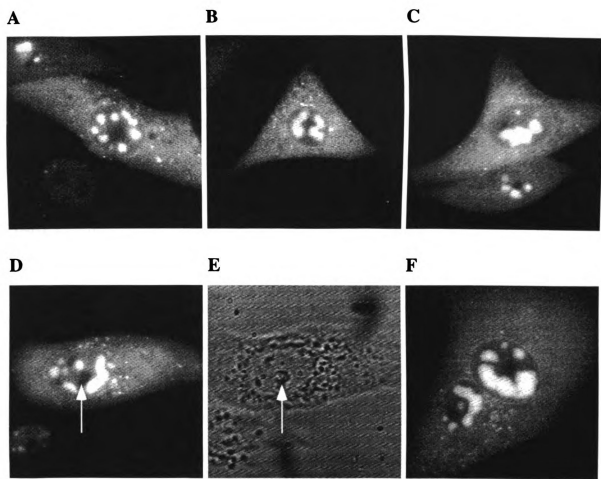


Figure 10

shows three cells with the perinuclear region clearly defined. The top cell also contains a small amount of the cytoplasmic speckles. Figures 11B and C are optical sections of the same cells, the first being at the surface of the cell and the second being 2 μm deeper into the cells. At the adherent surface of the cell an accumulation of VP16-EGFP fluorescence appears in its extremities. These accumulations I've termed surface patches. A deeper look into the cell reveals a nucleus with VP16-EGFP nuclear blobs, perinuclear accumulation, and some cytoplasmic speckles. These cytoplasmic speckles are round in shape but are not uniform in size. In figure 11D the diffuse expression of cytoplasmic VP16-EGFP is not as bright as in the other images. This revealed the cytoplasmic speckles throughout the cell. Figures 11E and F continue to demonstrate the bright cytoplasmic expression and nuclear localization of VP16-EGFP. In figure 11E, faint cells in the background with nuclear dots can be observed. Figure 11G also demonstrates these delayed patterns, presumably due to a slower initiation of viral infection. Figure 11I shows two cells, the top cell having brighter cytoplasmic expression than the bottom cell, and both containing VP16-EGFP blobs within the nucleus. A series of 0.5 μm optical sections of these cells is shown in Appendix figure C. Both cells demonstrate a perinuclear accumulation as well as cytoplasmic speckles throughout the cell.

After 10 hpi the VP16-EGFP blobs within the nucleus continued to grow, yet they remain non-nucleolar. An increased amount of cytoplasmic speckles was also observed. Figure 12A is a section through the cell and nucleus that demonstrates the increased number and intensity of the cytoplasmic speckles. Interestingly, the increase of fluorescent speckles corresponds to an increase of cytoplasmic vacuoles or granules observed in the cell by light microscopy (Fig. 12B). Figures 12C, D, and E also

Figure 11. DG1 time course, VP16-EGFP localization at 8 hpi. Live cell analysis of VP16-EGFP in cells infected with DG1 at an moi of 10. (A, D, F, G, I) Fluorescence at 8 hpi. (H) Brightfield image of cell in (G). (B) Fluorescence of the surface of cells, (C) fluorescence of same cells in (B) 2 μm deeper. Arrows in (A) point out the perinuclear accumulation of VP16-EGFP and (B) point out the surface patches.

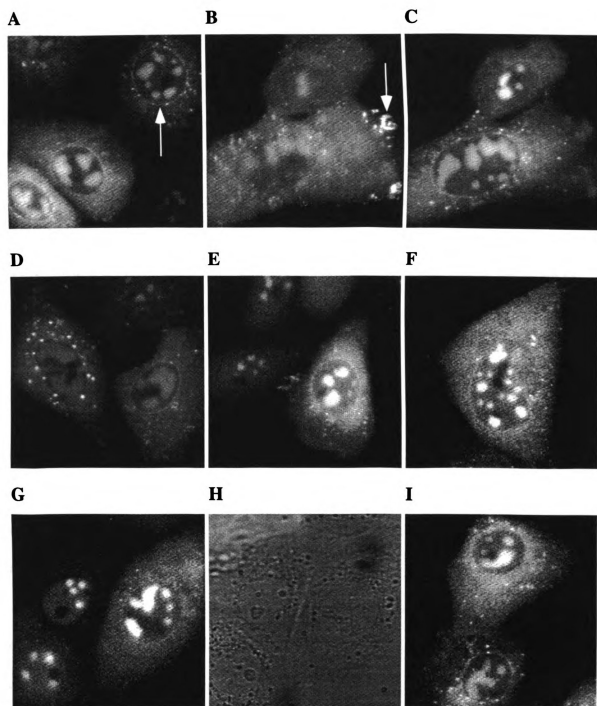


Figure 11

demonstrate the increase in the nuclear blob size and cytoplasmic speckles, as well as a continued perinuclear accumulation. Surface patches also continued to increase in size, number and intensity (Fig. 12G) and the fluorescence between two cells at cell-cell junctions increased (Fig. 12F). Figure 12I is one of a 0.5 μm series of images shown in Appendix figure D. This series demonstrates surface patches at the cells extremities as well as large nuclear blobs, perinuclear accumulation, and cytoplasmic speckles. The brightfield image of the same cell also demonstrates a large number of cytoplasmic vacuoles or granules.

12 hpi with DG1 some of the cells start to lose their flat, spread out shape, and begin to round up into a ball. This beginning of a cytopathic effect is demonstrated in figures 13 A and B. The brightfield image reveals the cytoplasm of the infected cells no longer taking up a lot of surface area, but is restricted and compacted around the nucleus.

Figures 13C and F continue to demonstrate the fluorescent pattern of cytoplasmic expression, nuclear blobs, perinuclear accumulation, and cytoplasmic speckles. Figures 13D and E demonstrate the accumulation of VP16-EGFP at surface patches and within nuclear blobs 3.2 μm deeper within the cell. Figures 13G and H are also images of the accumulation of fluorescence at cell-cell junctions not just at the surface of the cell (Fig. 13G) but all the way through the cell (Fig 13H - 3.2 μm deeper). Figure 13I is one image of a 0.5 μm series through three cells shown in Appendix figure E. The brighter centered cell displays surface patches, cell-cell junction accumulation, bright cytoplasmic expression, cytoplasmic speckles, perinuclear accumulation, and large nuclear blobs. The remaining two cells are delayed patterns that most likely represent virus that initiated

Figure 12. DG1 time course, VP16-EGFP localization at 10 hpi. Live cell analysis of VP16-EGFP in cells infected with DG1 at an moi of 10. (A, C, D, E, F, I) Fluorescence at 10 hpi. (B) Brightfield image of cell in (A). (G) Fluorescence at the surface of the cells, (H) fluorescence of same cells in (G) but 4 μm deeper. Arrows in (B) point out the cytoplasmic vacuole or granules, in (F) point out the accumulation at cell-cell contacts, and in (G) point out surface patches.

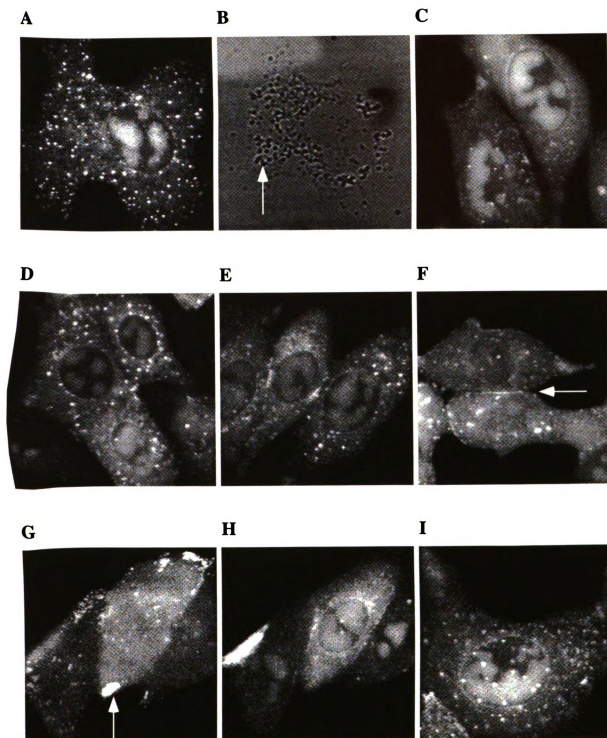


Figure 12

Figure 13. DG1 time course, VP16-EGFP localization at 12 hpi. Live cell analysis of VP 16-EGFP in cells infected with DG1 at an moi of 10. (A, C, F, I) Fluorescence at 12 hpi. (B) Brightfield image of cell in (A). (D) Fluorescence at the surface of the cells, (E) fluorescence of same cells in (D) but 3.2 μm deeper. (G) Fluorescence at surface of cells, (H) fluorescence of same cells in (H) but 3.2 μm deeper.

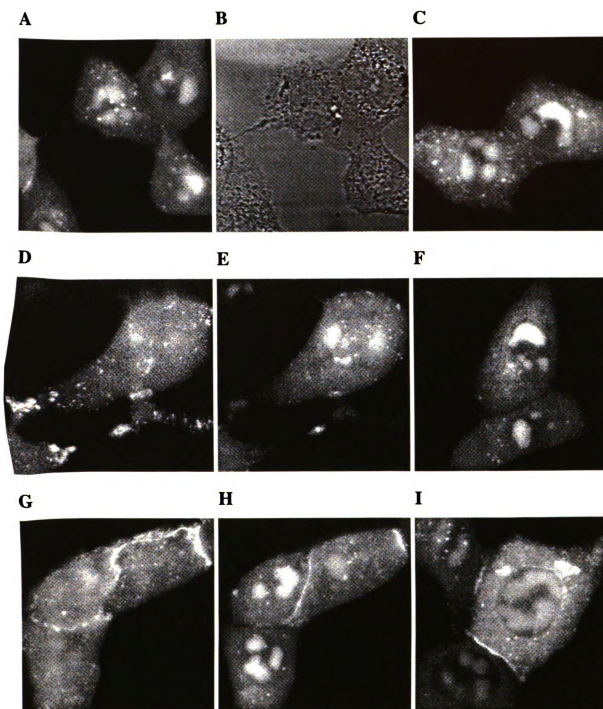


Figure 13

infection later than the majority of the cells. These two cells appear similar to cells at the 6 or 8 h time points.

At 14 hours post infection cells are beginning to clump and stick to each other. Figure 14A, B, and C, shows three optical sections of the same three cells at 0 μm , 1.5 μm , and 2.6 μm , respectively. The adherent surface of the cell displays numerous, intense surface patches (Fig. 14A). Deeper within the cell, accumulation of fluorescence is obvious at cell junctions and within the nucleus. The leftmost cell is very compact and cytoplasmic making it difficult to obtain an image of a defined nuclear structure. The bottom cell displays tiny intense speckles, similar to what has been observed in the cytoplasm, yet these are within the nucleus. The nuclear blob structures within this cell's nucleus no longer have any defined domains. Aside from the speckled localization, VP16-EGFP was diffuse and dense throughout the entire nucleus of this cell. The rightmost cell still displays defined nuclear blobs that have a very intense fluorescence. A small number of nuclear localized speckles can also be observed within this cell. More observations of these tiny nuclear speckles can be seen in figures 14 D, E, and F. These cells also display a loss of defined nuclear blobs with a more diffuse and dense nuclear staining. Figure 14G shows this nuclear diffusion and density in the absence of nuclear speckles. Figure 14H shows the adherent surface of the cells and the accumulation of fluorescence between cells. Figure 14I represents one of a 0.5 μm series of images shown in Appendix figure F. This series of images demonstrates the accumulation of fluorescence at cell-cell junctions, as well as the loss of defined blob structures in the nucleus (top cell).

Figure 14. DG1 time course, VP16-EGFP localization at 14 hpi. Live cell analysis of VP16-EGFP in cells infected with DG1 at an moi of 10. (D, E, F, G, H, I) Fluorescence at 14 hpi. (A) Fluorescence at the surface of the cells, (B) fluorescence of same cells in (A) but 1.5 μm deeper, and (C) fluorescence of same calls in (A) and (B) but 2.6 μm deeper (total 4.1 μm from (A)).

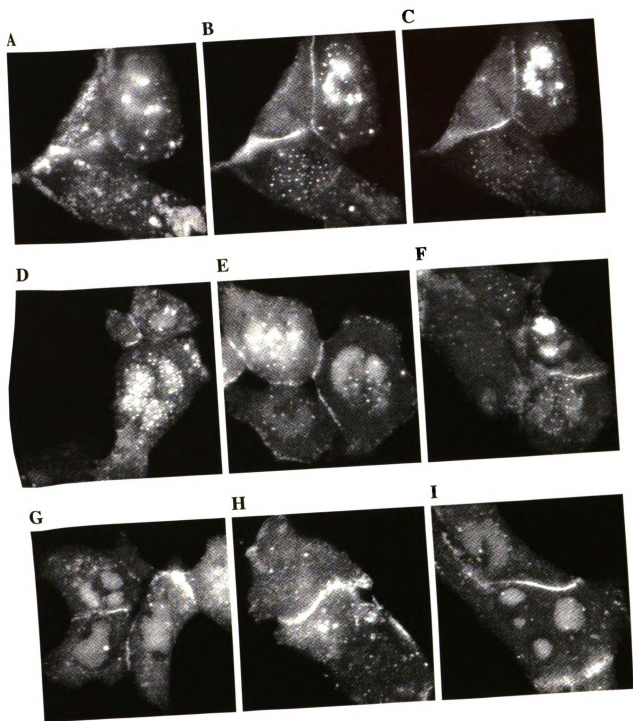


Figure 14

At 16 hours post infection the fluorescence within the cells is very intense. Cells only need to be exposed for a short time (0.5-1s in comparison to 3s for early times) for the camera to get a good image. Figures 15A, B, G, and H demonstrate the continued accumulation of surface patches on the adherent side of the infected cell, as well as large nuclear blobs and larger nuclear speckles deeper within the cells. Figure 15C also demonstrates larger nuclear speckles, while figure 15D represents the smaller nuclear speckles seen at earlier time points. The majority of the infected cell nuclei at this time point no longer contain distinct nuclear blobs, but instead have a diffuse and dense VP16-EGFP localization within the infected cell nucleus (Fig. 15D, E and F). This dense and diffuse localization still remains non-nucleolar (Fig. 15E arrow). Figure 15I shows an image of four cells with different VP16-EGFP localization patterns. This image is one of a 0.8 μm series of images shown in Appendix figure G. The two uppermost cells are representative of the majority of cells at this time after infection. The other two cells represent the population of cells that initiated infection later or more slowly due to a varying number of reasons. As seen in the brightfield image of the four cells, all of them are displaying cytopathic effect.

At late times after infection cells are displaying full cytopathic effect and are balling up in clumps. Figures 16A and B, and figures 17A through F, all demonstrate this balling and clumping effect. The cytopathic effects make it difficult to obtain good images of defined structures within the cell. Figures 16C and D show cells that are still semi-flat. These cells are very similar to what we have already observed at earlier times, believe that they represent cells that initiated infection slower or later than the rest. Figure 16E represents one image from a 0.5 μm series of images through balled up cells.

Figure 15. DG1 time course, VP16-EGFP localization at 16 hpi. Live cell analysis of VP16-EGFP in cells infected with DG1 at an moi of 10. (C, D, E, F, I) Fluorescence at 16 hpi. (A) Fluorescence at the surface of the cells, (B) fluorescence of same cells in (A) but 4 μm deeper. (G) Fluorescence at the surface of the cells, (H) fluorescence of the same cells in (G) but 4 μm deeper. Arrow in (F) points out the nucleolus.

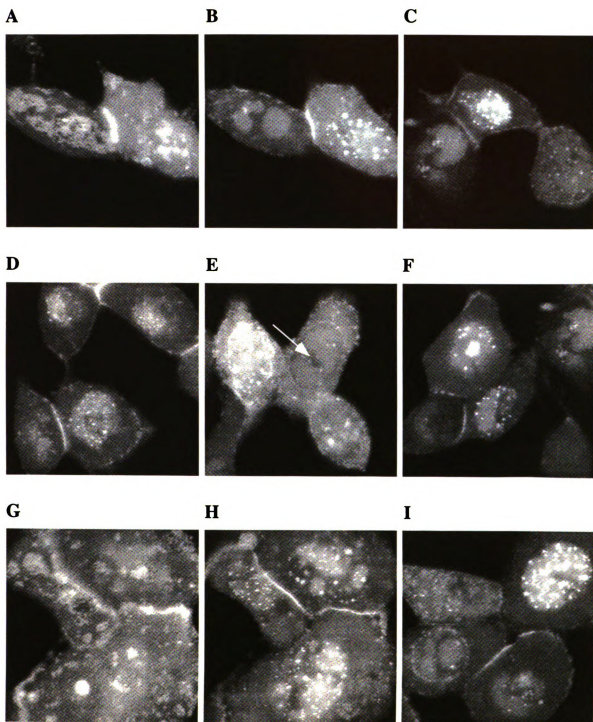


Figure 15

Figure 16. DG1 time course, VP16-EGFP localization at 20 hpi. Live cell analysis of VP16-EGFP in cells infected with DG1 at an moi of 10. (A, B, C, D, E) Fluorescence at 20 hpi.

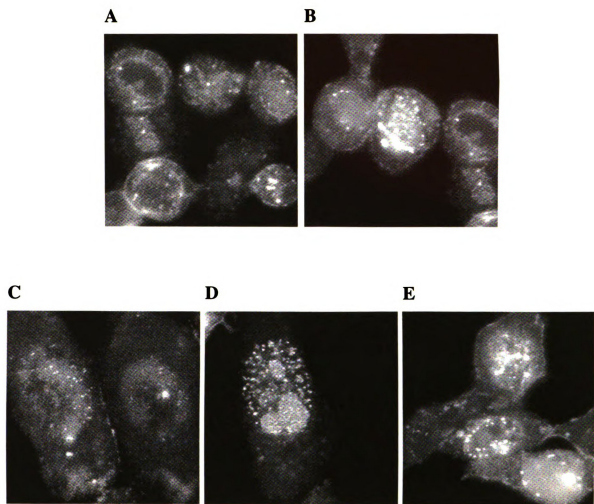


Figure 16

Figure 17. DG1 time course, VP16-EGFP localization at 24 hpi. Live cell analysis of VP16-EGFP in cells infected with DG1 at an moi of 10. (A) Fluorescence at 20 hpi. (B) Brightfield image of same cells in (A). (C, D, E, F) Fluorescence at 20 hpi.

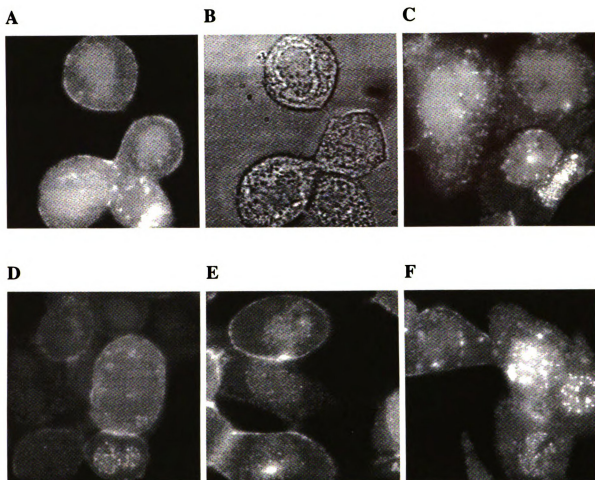


Figure 17

This whole series is shown in Appendix figure H. As you see in the brightfield image, the nucleus expands throughout the whole cell. Within three of the cells the nuclear dots are distributed not throughout the nucleus as we've seen earlier, but around the inner edges of the nucleus.

Time course analysis of VP16-EGFP during a viral infection

Low multiplicity infection

To determine if the localization patterns of VP16-EGFP during infection are different at a lower multiplicity of infection, I repeated the time course with a lower MOI. Vero cells were infected with DG1 at an MOI of 1 and images were collected as described above. In general, the patterns of localization were very similar to those observed at the higher multiplicity infection. The differences observed were that a smaller number of cells were infected after the first hour, and the timing of expression was slower than in the higher multiplicity infection. At later times a secondary infection of the uninfected cells occurred.

Until 4 hours post infection, little fluorescence was seen in the cells (Fig. 18A and C), yet some cells at 4 hours started showing a very faint cytoplasmic and nuclear haze (Fig. 18E, F, G). At 6 hours post infection, the infected cells began to display the same pattern of expression as seen in the higher multiplicity at 4 hours. Figures 19A and B demonstrate the nuclear haze and beginning accumulation of VP16-EGFP at distinct nuclear dots. Figures 19C, D, and E also demonstrate nuclear and cytoplasmic expression with the nuclear dots beginning to grow and coalesce into nuclear blobs.

Figure 18. DG1 time course, VP16-EGFP localization at 2 hpi and 4 hpi. Live cell analysis of VP16-EGFP in cells infected with DG1 at an moi of 1. (A) Fluorescence at 2 hpi, (B) brightfield image of the same cell at 2 hpi. (C, E, F, G) Fluorescence at 4hpi, (D) brightfield image of the cell in (C).

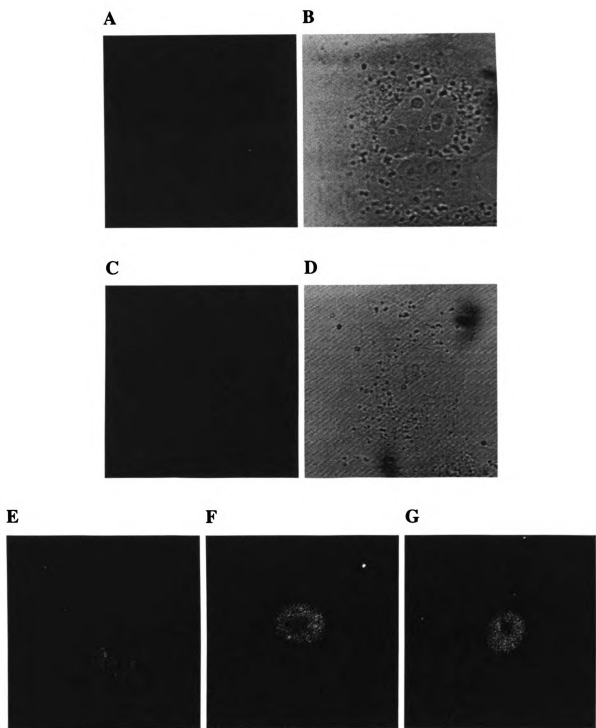


Figure 18

Figure 19. DG1 time course, VP16-EGFP localization at 6 hpi. Live cell analysis of VP16-EGFP in cells infected with DG1 at an moi of 1.

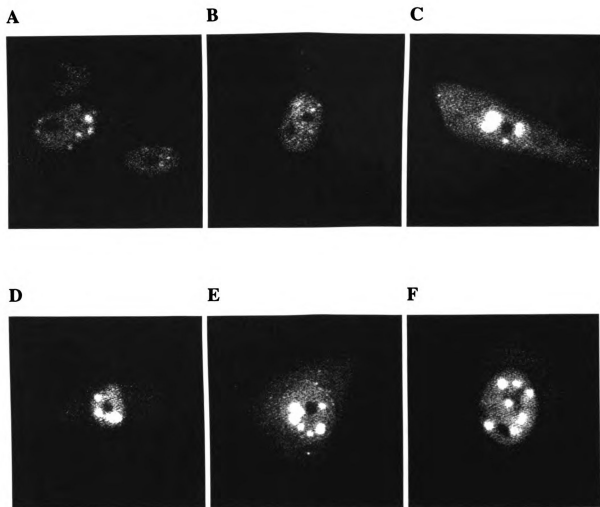


Figure 19

Figure 19F is one of a 0.5 μm series of images displayed in Appendix figure I. This image is a representation of the nuclear accumulation of VP16-EGFP in distinct, uniform nuclear dots within the infected cell nucleus.

Eight hours after low multiplicity infection with DG1, many cells continued to display a cytoplasmic and nuclear haze with the accumulation of fluorescence in nuclear dots and nuclear blobs (Fig. 20A, B, C, D, F). Also seen in a minor number of cells was a brighter and more advanced pattern of fluorescence in large nuclear blobs, with perinuclear accumulation and cytoplasmic speckles (Fig. 20G and H, 2 μm difference).

Figure 20I is a representative image of a 0.5 μm series shown in Appendix figure J. Three different cells displaying different patterns are shown in these images. The right cell displays cytoplasmic and nuclear haze, the left cell displays the accumulation of VP16-EGFP at distinct nuclear dots, and the center cell displays the growth and coalescence of the nuclear dots into nuclear blobs.

At 10 h the pattern of localization of VP16-EGFP in the early-infected cells is very similar to the pattern seen in the higher multiplicity infection. Many cells show patterns believed to be from a late starting infection. These cells display nuclear and cytoplasmic haze with the formation of nuclear dots and blobs (Fig. 21A). The cells showing a more advanced infection display an increase in brightness in both the cytoplasm and nucleus. The nuclear blobs have grown to take up much of the nucleus. Fluorescence was accumulating at the perinuclear region of the cell as well as in cytoplasmic speckles. All of these localization patterns are seen in figures 21B through F. At this time some cells are also beginning to accumulate intense fluorescence in

Figure 20. DG1 time course, VP16-EGFP localization at 8 hpi. Live cell analysis of VP16-EGFP in cells infected with DG1 at an moi of 1. (A, B, C, D, F, I) Fluorescence at 8 hpi. (E) brightfield image of cell in (D). (G) Fluorescence at surface of cell, (H) fluorescence of same cell in (G) but 2 μm deeper.

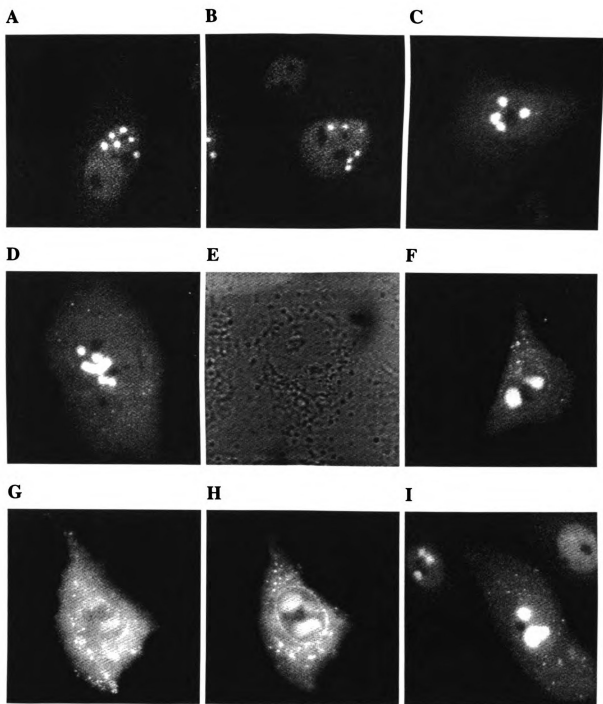


Figure 20

Figure 21. DG1 time course, VP16-EGFP localization at 10 hpi. Live cell analysis of VP16-EGFP in cells infected with DG1 at an moi of 1. (A, B, C, D, E, F, I) Fluorescence at 10 hpi. (G) Fluorescence at surface of cell, (H) fluorescence of same cell in (G) but 2 μm deeper.

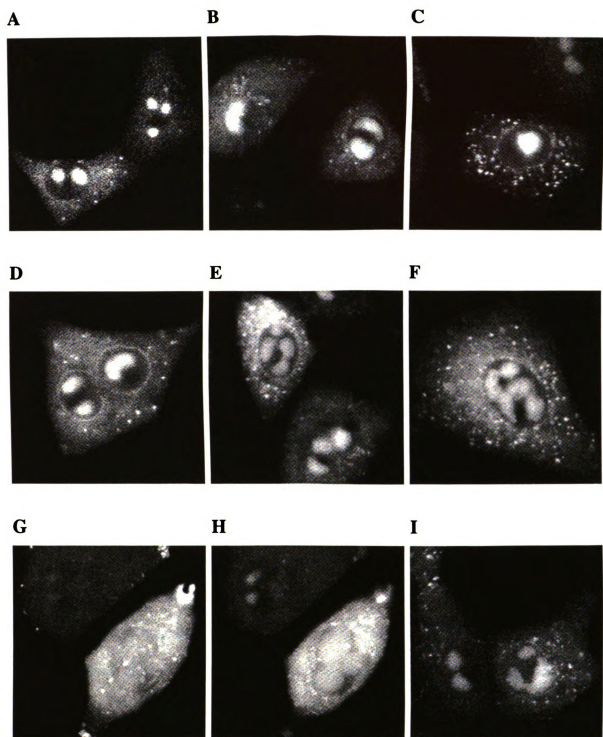


Figure 21

surface patches at the cells extremities (Figure 21G and H – 2 μm difference). Figure 21I is a representative image from a series of 0.5 μm images shown in Appendix figure K.

14 hours after infection the expression pattern remains very similar (Fig. 22A, C, F). Figure 22B displays a cell that has just divided. The pattern of localization between the two cell nuclei is almost a mirror image with one large nuclear blob on the far side of each nucleus. Figure 22D demonstrates the accumulation of fluorescence at cell-cell contacts. A number of cells at this time point were beginning to accumulate fluorescence in nuclear speckles, as seen in figures 22G and H. The image shown in figure 22I is one of a 0.5 μm series of images displayed in Appendix figure L. The three cells in this series show intense cytoplasmic expression, nuclear dots, larger nuclear blobs, perinuclear accumulation, as well as cytoplasmic speckles.

16 hours post infection with DG1, the infected cells are beginning to display cytopathic effect by beginning to ball up and clump. Figures 23A, B and H demonstrate the dense accumulation of VP16-EGFP within the nucleus. Loss of defined blob structures was beginning to occur. Also seen was the continuance of the perinuclear accumulation and cytoplasmic speckles. Figures 23D, E, and F demonstrate the increase accumulation and intensity of fluorescence at cell-cell contacts. These images as well as figure 23G, also demonstrate the accumulation of fluorescence in nuclear speckles within the infected cell nucleus. Figure 23I is another representation of a 0.5 μm series of images displayed in Appendix figure M.

At 20 hours post infection the Vero cells are displaying near full cytopathic effect making it difficult to obtain detailed images. At this stage in infection the cells are displaying intense cytoplasmic as well as nuclear fluorescence. Accumulations at surface

Figure 22. DG1 time course, VP16-EGFP localization at 14 hpi. Live cell analysis of VP16-EGFP in cells infected with DG1 at an moi of 1. (A, B, C, D, E, F, G, H, I) Fluorescence at 14 hpi. (E) Brightfield image of cells in (D).

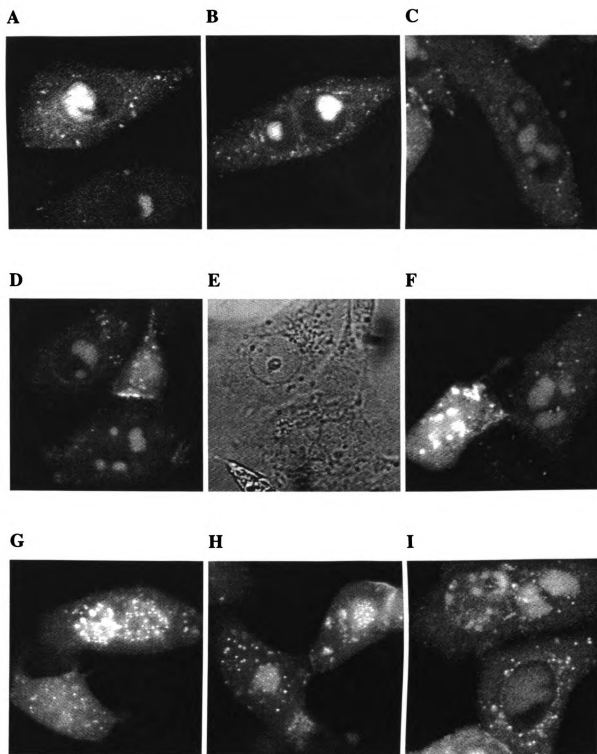


Figure 22

Figure 23. DG1 time course, VP16-EGFP localization at 16 hpi. Live cell analysis of VP16-EGFP in cells infected with DG1 at an moi of 1. (A, B, D, G, H, I) Fluorescence at 16 hpi. (C) Brightfield image of cells in (B). (E) Fluorescence at surface of cells, (F) fluorescence of same cells in (E) but 4 μm deeper.

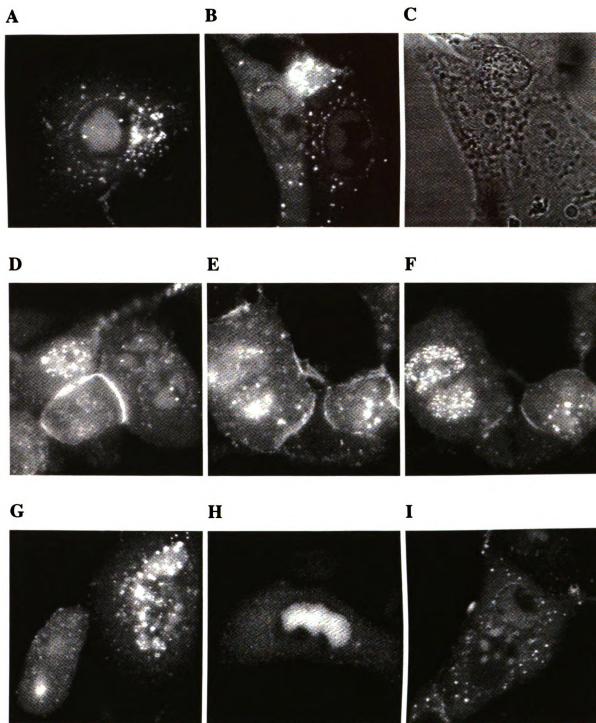


Figure 23

patches, cell-cell contacts (Fig. 24A, E, G), as well as a complete loss of defining nuclear structures with a dense nuclear expression of VP16-EGFP throughout (Fig. 24D, F), and accumulations of intense nuclear speckles (Fig. 24B, C, H, I) began to occur. Figure 24I is one of a 0.8 μm series of images shown in Appendix figure N. This series of images demonstrates the localization of the nuclear speckles around the inner space of the nucleus. This localization pattern for the nuclear speckles is also demonstrated at 24 hours in figures 25A through F.

A summary of the pattern of localization of VP16-EGFP throughout a full course of DG1 lytic replication is shown in figure 26. At 2 hpi the input fluorescence is not visible. New synthesis of VP16-EGFP begins between 2 and 4 hpi and localizes into the nucleus in a nuclear haze with the beginning of the accumulation into nuclear dots. As infection progresses, the nuclear dots of VP16-EGFP fluorescence continue to grow and coalesce into nuclear blobs. At 6 hpi VP16-EGFP begins to accumulate in the cytoplasm as well as in the nucleus, and at 8 hpi this cytoplasmic accumulation is also seen in the perinuclear region of the infected cell. Between 8 and 10 hpi VP16-EGFP accumulates into cytoplasmic speckles located throughout the infected cell as well as in surface patches and at cell-cell junctions. At 12 hpi the nuclear blobs have grown to take up most of the nuclear space and the cell is beginning to display cytopathic effect. At 14 hpi VP16-EGFP fluorescence accumulates in nuclear speckles and this corresponds with the disappearance of the cytoplasmic speckles. At 20 hpi there is intense fluorescence in both the nucleus and cytoplasm and the cells are displaying full cytopathic effect.

Time course analysis of VP26-GFP during a viral infection

Another virus, K26GFP, containing a VP26-GFP fusion gene, was obtained from P. Desai [111]. I was interested in comparing the localization of the capsid protein VP26 with the tegument protein VP16. Vero cells were infected with K26GFP at an MOI of 10 and live cell analysis of infection was carried out as described above. Due to the difference in the types of expression and localization of VP16-EGFP and VP26-GFP, the images for the K26GFP virus were more difficult to analyze. The accumulation of VP26-GFP in small punctate dots on different planes throughout the nucleus resulted in out of focus light from above or below the confocal plane of view still present in the image. I tried to reduce this problem by taking images where the majority of fluorescence was in focus.

Since the K26GFP virus carries a GFP fusion in the capsid of the virion, I again tried to visualize incoming virus. As seen in Figure 26A and B, small points of light were seen in the vicinity of the nucleus, but these were difficult to distinguish from the background within the cell and exposures above three seconds resulted in too much light noise for the camera. Figures 26C and D are images from 4 hours post infection. In these images small points of light in the vicinity of the cell nuclei is again demonstrated. Figures 26E and F demonstrate a large cell nucleus surrounded with fluorescent dots. This was an unusual cell and not many others were seen to have this intense accumulation.

Figures 27A, B, and C display images for infected cells at six hours post infection with K26GFP. Infected cells at this time displayed a light diffuse expression of VP26-

Figure 24. DG1 time course, VP16-EGFP localization at 20 hpi. Live cell analysis of VP16-EGFP in cells infected with DG1 at an moi of 1. (A) Fluorescence at surface of cells, (B) fluorescence of same cells in (A) but 4 μm deeper. (C, D, E, I) Fluorescence at 20 hpi. (G) fluorescence at surface of cells, (H) fluorescence of same cells in (G) but 5.3 μm deeper.

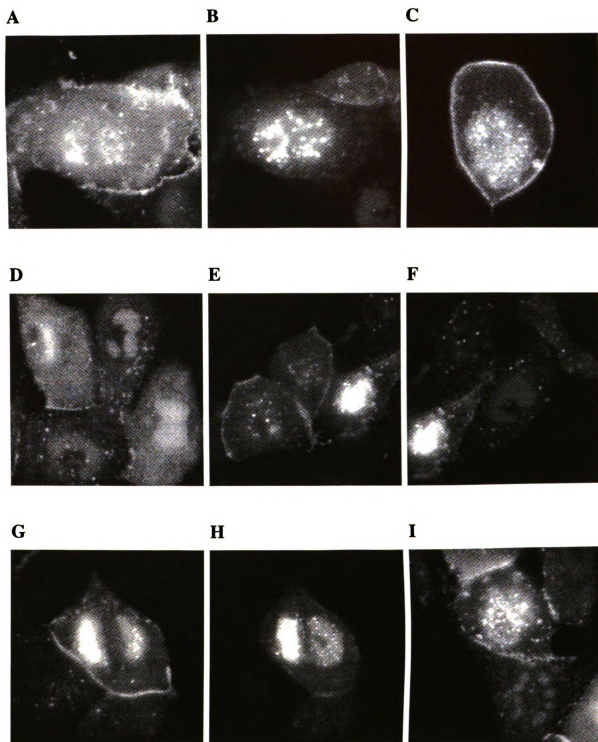


Figure 24

Figure 25. DG1 time course, VP16-EGFP localization at 24 hpi. Live cell analysis of VP16-EGFP in cells infected with DG1 at an moi of 1. (A) Fluorescence at 24 hpi, (B) brightfield image of cell in (A). (C, F) Fluorescence at 24 hpi. (D) Fluorescence at surface of cells, (E) fluorescence of same cells in (D) but 2.7 μm deeper.

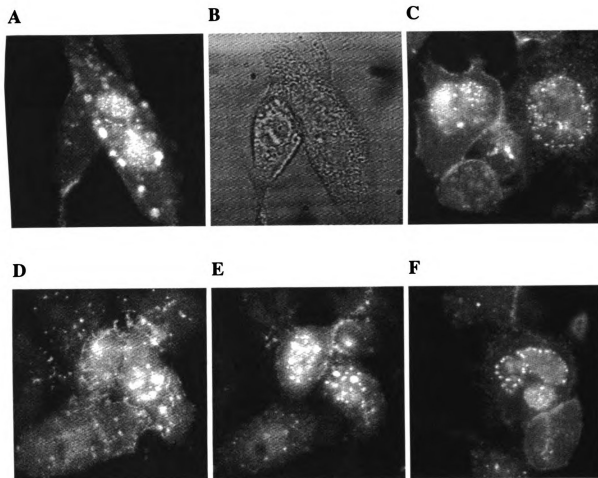


Figure 25

Figure 26. Summary of VP16-EGFP localization during a complete time course of infection with DG1. Fluorescence at (A) 2 hpi, (B) 4 hpi, (C) 6 hpi, (D) 8 hpi, (E) 10 hpi, (F) 12 hpi, (G) 14 hpi, (H) 16 hpi, (I) 20 hpi.

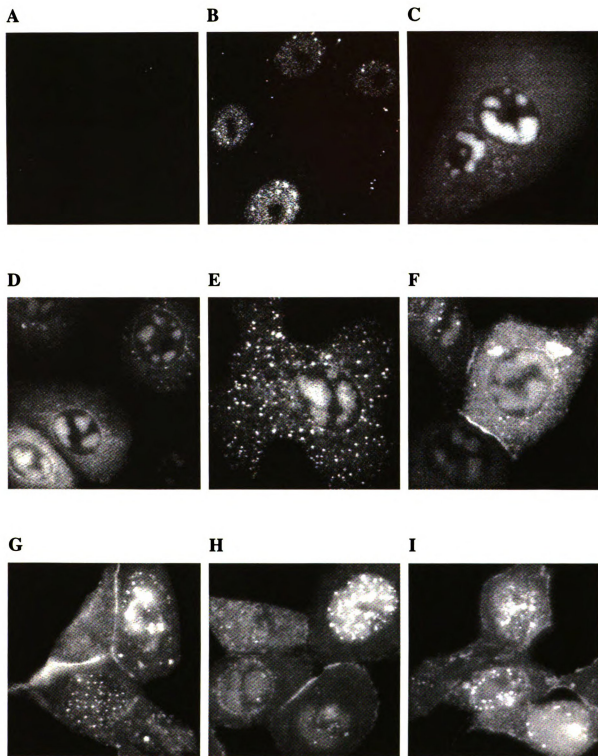


Figure 26

GFP, which does not get picked up by the camera. These cells also displayed a number of punctate dots within the nuclear area, if this is from the incoming virus or newly expressed VP26-GFP is unknown. Figure 27C is one of a series of 0.5 μm images, shown in Appendix figure O, that demonstrates the outer nuclear localization of the punctate dots. At eight hours post infection some cells are observed with a diffuse but nonuniform haze throughout the nucleus with nucleolar exclusion (Fig. 27D). Also observed was the increase in number and size of the punctate accumulations of VP26-GFP (Fig. 27E). Figure 27F is a representative of a 0.5 μm series displayed in Appendix figure P. This series of images displays two cells, one with punctate nuclear dots, the other with both nonuniform nuclear haze and nuclear dots.

10 hours post infection, cells were showing cytoplasmic localization of fluorescence, especially at surface patches (Fig. 27G), as well as punctate nuclear dots of different sizes (Fig. 27H, I). Figure 27I is one of a 0.5 μm series of images shown in Appendix figure Q. This series demonstrates three cells with intense fluorescent punctate dots within the nucleus. At 12 hours, the fluorescence within the cytoplasm and at the cells extremities continued to increase. Figures 28A and B are overexposures (1.5s and 3s respectively) of the infected cells to demonstrate the cytoplasmic fluorescence. Figure 28C is a representative of a 0.5 μm series of images shown in Appendix figure R that again demonstrates the punctate nuclear accumulations of VP26-GFP.

16 hours after a high multiplicity infection with K26GFP, fluorescence was visualized at cell-cell contacts (Fig. 28D) as well as spread throughout the cytoplasm

Figure 27. K26GFP time course, VP26-GFP localization at 2 hpi and 4 hpi. Live cell analysis of VP26-GFP in cells infected with K26GFP at an moi of 10. (A) Fluorescence at 2 hpi, (B) brightfield image of cell in (A). (C, D, E) Fluorescence at 4 hpi. (F) Brightfield image of cell in (E). Arrow in (D) points out a point of fluorescence in the vicinity of the nucleus.

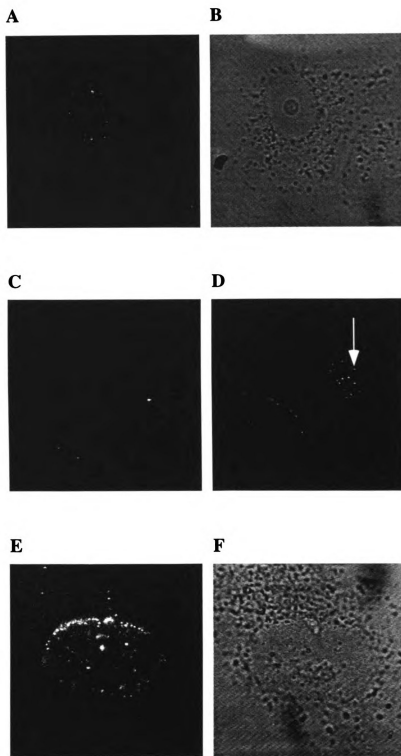


Figure 27

Figure 28. K26GFP time course, VP26-GFP localization at 6 hpi, 8 hpi and 10 hpi. Live cell analysis of VP26-GFP in cells infected with K26GFP at an moi of 10. (A, B, C) Fluorescence at 6 hpi. (D, E, F) Fluorescence at 8 hpi. (G) Fluorescence at 10 hpi at surface of cell, (H) fluorescence of same cell in (G) but 2.3 μm deeper. (I) Fluorescence at 10 hpi.

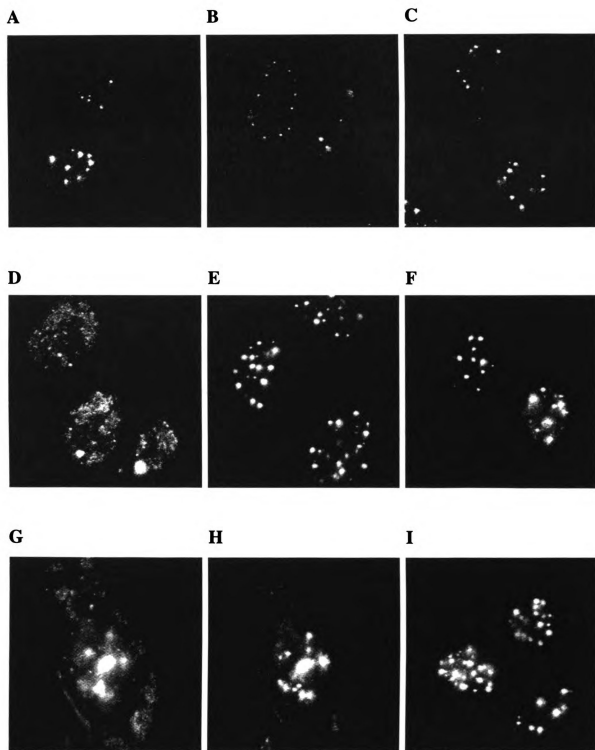


Figure 28

(Fig. 28E, F). Also at this time the perinuclear accumulation of the fluorescence was observed. This is demonstrated in figures 28G, H, and I. Figure 28I is also one of a 0.5 μm series of images shown in Appendix figure S. This series of images demonstrates the perinuclear fluorescence as well as intense punctate nuclear dots localized to the inner side of the nucleus. 20 hours after infection the cells were demonstrating cytopathic effect and clumping together. An intense fluorescence was seen throughout all infected cells. Figures 29A, B and C demonstrate the cytoplasmic fluorescence as well as the perinuclear accumulation and punctate nuclear dots located to the inner side of the nucleus. Figures 29D, E and F also demonstrate nuclear dots as well as the surface patches of VP26-GFP fluorescence.

A summary of the pattern of localization of VP26-GFP throughout a full course of K26GFP lytic replication is shown in figure 31. At 2 hpi I was able to visualize the input fluorescence from the viral capsids in a high multiplicity infection. Synthesis of new VP26-GFP begins between 4 and 6 hpi and the fluorescence in the nucleus near the periphery as intense punctate dots. As infection progresses these punctate nuclear dots of VP26-GFP fluorescence continue to grow in size, number and intensity. Between 10 and 12 hpi, VP26-GFP accumulates in the cytoplasm as tiny points of fluorescence. At 16 hpi there is a perinuclear accumulation of the tiny points of fluorescence, which continues throughout the remainder of the infection course. At 20 hpi there is fluorescence in both the nucleus and cytoplasm and the cells are displaying full cytopathic effect.

Discussion

VP16-EGFP localization

VP16 is an essential HSV protein that plays known roles in two parts of the viral replicative cycle. It is a powerful transcriptional activator, responsible for initiating the cascade of gene expression, as well as a structural component of the viral tegument [1]. To perform these roles as an essential viral protein, VP16 must be present at specific locations in the cell at certain times throughout infection. At early times, input VP16 from the infecting virion localizes in the nucleus to activate transcription of the IE genes. The VP16 gene itself is categorized as a leaky late gene, therefore the expression of the VP16 product occurs at later times after expression of IE and DE genes. The site of the actual formation of the complete virion particle is controversial, therefore it is not known if newly expressed VP16 should return to the nucleus, or should remain in the cytoplasm for packaging. To attempt to gain a better understanding of herpes virus maturation and egress, I wanted to determine the localization of VP16 throughout a viral replicative cycle.

When trying to study the localization of viral proteins, transfection is not comparable to infection. The viral proteins are going to interact with many other cellular and viral factors that will determine its location within the cell. It is important for the actual study of the pathology of the virus that protein localization is looked at in the context of live viral infection.

Figure 29. K26GFP time course, VP26-GFP localization at 12 hpi and 16 hpi. Live cell analysis of VP26-GFP in cells infected with K26GFP at an moi of 10. (A, B, C) Fluorescence at 12 hpi. (D, E, F, G, I) Fluorescence at 16 hpi. (H) Brightfield image of cells in (G). Arrow in (G) points out the perinuclear accumulation of VP26-GFP.

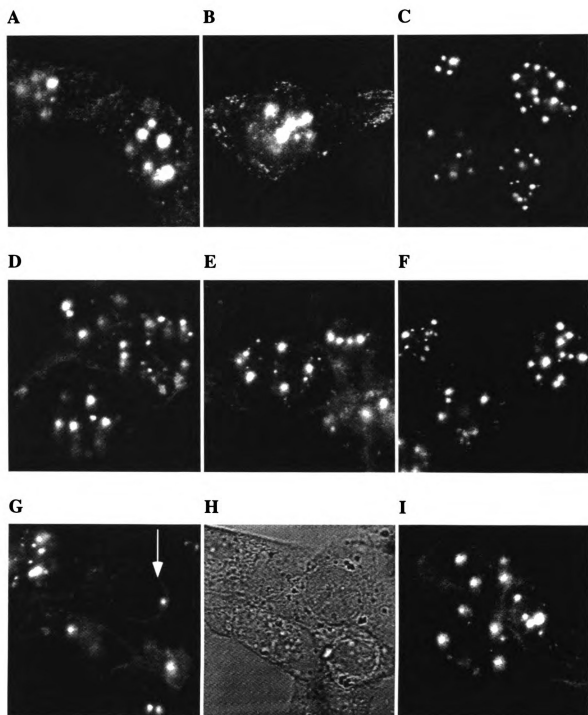


Figure 29

Figure 30. K26GFP time course, VP26-GFP localization at 20 hpi. Live cell analysis of VP26-GFP in cells infected with K26GFP at an moi of 10. (A, B, F) Fluorescence at 20 hpi. (C) Brightfield image of cells in (B). (D) Fluorescence at surface of cells, (E) fluorescence of same cells in (D) but 5 μm deeper.

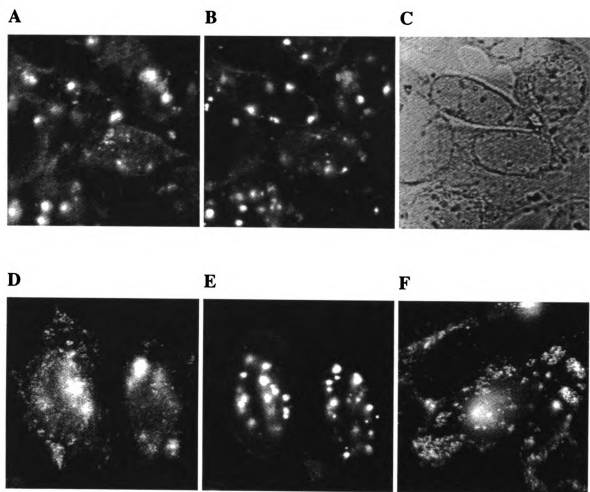


Figure 30

Figure 31. Summary of VP26-GFP localization during a complete time course of infection with K26GFP. Fluorescence at (A) 2 hpi, (B) 4 hpi, (C) 6 hpi, (D) 8 hpi, (E) 10 hpi, (F) 12 hpi, (G) 14 hpi, (H) 16 hpi, (I) 20 hpi.

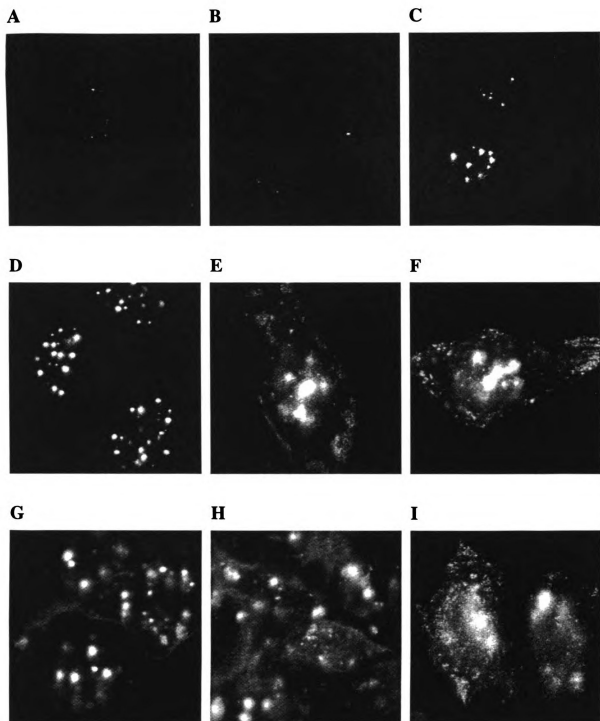


Figure 31

I wanted to utilize the power of the green fluorescent protein as a useful tag to monitor the fate and localization of my protein of interest, VP16. I constructed a recombinant virus, DG1, which contains a VP16-EGFP fusion gene and expresses a VP16-EGFP fusion protein that is packaged into the virion tegument. The addition of the EGFP onto the activation domain of VP16 had no effect on the ability of DG1 to infect, or form infectious progeny virus. The addition of the 27 KDa EGFP to VP16 also increased the size of the protein to be packaged into the tegument, yet this fusion protein was still packaged into the virion.

Transfection experiments can be misleading or incomplete when it comes to the study of the localization of viral proteins. To stress this point I compared the localization patterns of a plasmid expressing EGFP, a plasmid expressing VP16-EGFP, and the pattern of localization of VP16-EGFP in a cell that was infected with DG1. The diffuse localization of VP16-EGFP in the transient transfection highly resembled the localization of the unfused EGFP. In contrast, the localization of VP16-EGFP in the context of a live viral infection was drastically different. VP16-EGFP was extensively nuclear in accumulations resembling dots.

To study the localization of VP16-EGFP in more detail, I performed a time course of analysis, examining the cells every two hours after infection. One question I was interested in was if it was possible to visualize incoming virions. At two hours post infection I was unable to visualize any VP16-EGFP fluorescence within the cells. This lack of fluorescence may be due to the dissociation of the tegument after the viral envelope fuses with the plasma membrane of a cell. There have been electron microscopy images that demonstrate that after fusion of the viral envelope with the cell

membrane, naked capsids appear in the cytoplasm and the electron dense tegument disperses while some remains at the plasma membrane [26] [25].

In a study carried out by Morrison et al., immunochemical analysis of tegument proteins at early times in infection demonstrated that VP1/2, accumulated in the perinuclear region, whereas VP13/14, and VP16, both displayed weak cytoplasmic staining accompanied by strong nuclear immunofluorescence. This nuclear staining pattern was not homogeneous, with distinct areas (most likely representing the nucleoli) free of staining [12]. This observation of the nuclear localization of VP16 was obtained by infecting the cells at a very high multiplicity of infection. In the time course performed with DG1, cells were infected at MOIs of 10 or 1, which more closely resembles a physiological infection. VP16 is packaged into the viral tegument at approximately 1000 copies per virion [65]. If the tegument was remaining structurally associated with the capsid as it is being transported to the NPC, it should be visible. On the other hand, if the tegument were dispersing upon entry of the virus into the cell, it would not be possible to visualize one molecule of VP16-EGFP.

Newly synthesized VP16-EGFP is observed in the infected cells by 4 hours in the high multiplicity infection. The localization pattern of the VP16-EGFP molecules is faintly diffuse through out the cytoplasm with a more intense expression in the nucleus. In my experiments, like in other reports, this nuclear localization is not seen in the nucleolus structures of the cell. Also seen in a number of infected cells is the beginning of intense accumulation of VP16-EGFP at certain domains within the nucleus. At 6 hpi the nuclear accumulations become more obvious, and the VP16-EGFP is seen localized

in what I've termed "nuclear dots". These nuclear dots are uniform throughout the infected cells, averaging in numbers from 4-10 per nucleus.

This VP16-EGFP localization into nuclear dots is consistent with the immunolocalization studies of VP16 performed by other labs [12]. The localization of VP16-EGFP also parallels what is known about the localization of the proteins that make up the ND10 nuclear domain structures that are found within the nuclei of uninfected cells. Upon infection with HSV-1, ND10s undergo modification, dispersal, and degradation of certain proteins. This drastic modification of the nuclear domain structures is due to the expression of the IE gene product ICP0 [60]. In cells that are infected with an ICP0 mutant, the ND10 domains are not dispersed and all input viral genomes were found adjacent to the ND10s [61]. Similarly, another DNA virus, SV40, also disperses ND10s and localizes the viral DNA to the nonrandom ND10 sites within the nucleus (reviewed in [48]).

In the live cell images of DG1 infection a distinct number of VP16-EGFP nuclear dots is observed within each nucleus. I believe these dots could be newly synthesized VP16-EGFP colocalizing with the viral DNA at sites of the ND10 domains. In figures 10F, 21D, 22B, as well as Appendix figure B, images of cells that have just undergone division, demonstrate nuclei with symmetrical patterns of VP16-EGFP localization. ND10s are reported to have a nonrandom distribution within the nucleus. Therefore, it is possible that the nonrandom and symmetrical accumulation of VP16-EGFP within these nuclei represent the localization at ND10 sites.

The observation that newly synthesized VP16-EGFP is targeted and transported into the nucleus to these putative ND10 sites is an interesting idea. At this point in the

infection cycle the IE genes have already been expressed by the initial input VP16 molecules and viral DNA replication has most likely begun. Is VP16-EGFP still activating transcription at this later time, or is it playing a role in viral DNA replication?

As time increases the VP16-EGFP nuclear dots increase in size and coalesce into larger nuclear blobs of fluorescence. As DNA replication proceeds, many more copies of the viral genome are being made and it is possible that this growth and condensation of the nuclear fluorescence is representing that increase in viral DNA. VP16 has been shown to colocalize with the virally encoded single stranded DNA binding protein, ICP8 [12]. This colocalization was pictured and described as large globular structures. Studies of ICP8 have also reported an initial accumulation at a few discrete foci within the nucleus, and that these foci appear to evolve into replication compartments that actively incorporate BrdU [64]. In addition, when cells were infected with an ICP0 mutant virus, ICP8 colocalized with Sp100. This demonstrates a correspondence between ICP8 localization and ND10 structures [62]. Another interesting observation was the symmetrical localization of ICP8 within the nuclei of two daughter cells [61] [115]. The data reported for ICP8 localization within replication domains, associated with ND10s, and in symmetrical nonrandom patterns throughout the infected cell nucleus, provides support for the localization of VP16-EGFP with ND10s at viral replication compartments.

As infection continues new patterns of VP16-EGFP localization are observed. Perinuclear accumulation of fluorescence is seen, as well as the appearance of intense “speckles” of fluorescence throughout the cytoplasm. These new patterns of localization

could

virus

pack

acqu

and

from

pote

sub

cyt

be

tra

ini

th

pe

te

c

:

could be indicative of the maturation and egress pathway(s) of newly formed progeny virus out of the cell.

Capsids form and package viral DNA within the nucleus. The newly formed and packed capsids then bud through the inner nuclear membrane into the perinuclear space acquiring an initial envelope [1]. One potential pathway of virus egress is through the ER and Golgi network. Through this secretory pathway the envelope glycoproteins obtained from the inner nuclear membrane are processed to their mature forms [82]. Another potential pathway is the initial envelopment through the inner nuclear membrane with subsequent deenvelopment of the capsid by budding through the outer membrane into the cytoplasm [83].

The patterns of localization of VP16-EGFP observed in infection with DG1 can be applied to either pathway. While some of the newly synthesized VP16-EGFP is transported back into the nucleus, the accumulation within the cytoplasm increases as infection progresses. If tegumentation of the viral capsid is occurring outside the nucleus this may be represented by the accumulation of VP16-EGFP in the cytoplasm and in the perinuclear region. Comparing the VP16-EGFP localization patterns with that of other tegument proteins at late times may provide support for this theory. Morrison et al. demonstrated the perinuclear accumulation of newly synthesized VP1/2 and VP13/14 late in infection [12]. In a study very similar to my VP16-EGFP localization study, Elliot et al. followed the localization of VP22-GFP throughout a live cell during infection. Their results demonstrate the diffuse cytoplasmic localization of the newly expressed VP22-GFP followed by the localization into a more distinctive pattern, with particles

concentrated to one side of the nucleus. This particulate material then traveled through an exclusively cytoplasmic pathway to the cell periphery [102].

In a separate study, the same group demonstrated the colocalization of VP16 and VP22 to the edge of the nucleus during infection, as well as the reorganization of both proteins in cotransfection into a novel assembly near the nucleus [19]. These demonstrations of VP22 remaining cytoplasmic and accumulating near the nucleus throughout infection provide additional evidence for the tegument assembly site being within the cytoplasm of the infected cell.

The other new pattern of VP16-EGFP localization at later times is the accumulation into punctate cytoplasmic speckles. The appearance of these speckles seems to correlate with the appearance of more vesicles or granules within the cytoplasm of the infected cell. It is possible that these speckles of fluorescence represent accumulations of viral tegument proteins at certain tegument assembly sites within the cytoplasm. They could also represent cytoplasmic Golgi derived vesicles into which the tegumented capsids bud to acquire a mature envelope. Electron microscopic evidence has shown a thick and electron-opaque region along the membrane regions involved in envelopment of the viral particle within the cytoplasm [101]. This cytoplasmic accumulation of tegument at Golgi derived membranes has also been reported for another α herpesvirus, VZV [91].

As discussed above, newly synthesized VP16-EGFP is transported back into the nucleus into nuclear dots structures which grow and fuse to engulf much of the nuclear space. It is possible that tegument assembly could be occurring within these nuclear blobs. The nuclear accumulation of other tegument proteins has not been well

documented, yet some evidence does exist. VP22-GFP was detected in patterns other than its predominant cytoplasmic pattern. The patterns observed were the colocalization of VP22-GFP with mitotic chromatin, as well as diffusely localized single cell nuclei and daughter cell nuclei [116]. In an ultrastructural study of the α herpesvirus, PrV, nucleocapsids were observed budding into the perinuclear space acquiring an initial tegument that was sharp bordered, homogenous, and very electron dense [26]. These results supply support for the accumulation and formation of the tegument within the nucleus.

As the infection with DG1 progresses and the intensity of the VP16-EGFP within the cell grows, accumulations of fluorescence at the adherent surface of the cell begin to occur. This accumulation is most likely due to newly formed infectious virus being transported out of the cell. When the vesicles carrying the mature virions reach the adherent surface the virus is not able to leave the cell so it remains there and forms what I have termed “surface patches”. This accumulation due to the trapping of mature virus may also explain the accumulations at cell-cell junctions. HSV-1 virions can not superinfect a cell that has already been infected, therefore newly formed virus accumulates at the surface of its host cell because it can not fuse into the neighboring infected cell.

At 14 hours after a high multiplicity infection of DG1, a new pattern fluorescence is present. In some of the infected cells the nuclear accumulation of VP16-EGFP has become very dense and the distinct structures of nuclear blobs can no longer be identified. The fluorescence fills up most of the enlarged nuclear space. Within some of these enlarged nuclei, the accumulation of intense, punctate “nuclear speckles” is visible.

Initially these speckles appear to be randomly localized throughout the nucleus, yet as the infection progresses into later times (20 and 24 hpi) the nuclear speckles appear to be localized along the inner nuclear membrane of the cells.

Interestingly, when these nuclear speckles appear, the cytoplasmic speckles disappear. The disappearance of the cytoplasmic speckles may be an artifact of the imaging, whereas the intense expression within the cytoplasm and nucleus may be overwhelming the image and the cytoplasmic speckles can not be seen. Another explanation of the loss of cytoplasmic speckles may be due to the necrosis of the infected cell.

Cells productively infected with herpesviruses do not survive. Almost from the beginning of the reproductive cycle, the infected cells undergo major structural alterations that ultimately result in their destruction [1]. The cytopathic effect displayed by the DG1 infected cells begins to become obvious at twelve hpi. The cells begin to lose their stretched out, flat shape and start to become compact and balled up. After a complete round of viral replication and formation of newly infectious viral progeny has occurred, the cells display complete cytopathic effect. At this point the cells are completely balled up, with the nucleus making up most of the cell volume. These cells clump together and begin to release from the adherent surface of the coverslip.

The observations of DG1 infection at both high and low multiplicity's demonstrate that the patterns of localization are very similar between the two infections. The observed differences between the two infections is a slower onset of VP16-EGFP expression in the cells infected with only 1 MOI, as well as an increased number of cells that were not infected in the first round of infection. These differences were expected

because a higher input of infectious virus will result in more cells being infected as well as an increase in the amount of input viral particles within the infected cells. This slower onset of viral infection resulted in an approximate two hour lag in VP16-EGFP localization pattern when compared to the higher multiplicity infection. At late times (20 and 24 hpi) the patterns of VP16-EGFP localization were very comparable between the two different infections.

VP26-GFP localization

Capsid assembly occurs within the nucleus of the infected cell. HSV-1 capsid shells contain four virally encoded proteins in major amounts, VP5, VP19, VP23, and VP26 [6] [7]. VP26 is the smallest capsid protein with a size of 12 KDa. This viral protein is expressed as a late gene after the onset of viral replication. VP26 is located on the outer surface of the capsid shell and is present at approximately 1000 copies per capsid [6].

Desai et al. constructed a recombinant virus, named K26GFP, that expressed a VP26-GFP fusion protein that was still capable of interacting with VP5 and was incorporated into the capsid shell. Cells infected with K26GFP exhibited a punctate nuclear fluorescence at early times in the replication cycle, whereas at later times a generalized cytoplasmic and nuclear fluorescence, including fluorescence at the cell membranes, was observed [111].

I obtained this recombinant virus and visualized VP26-GFP throughout a time course of infection to have a more detailed look at the localization of a capsid protein, as

well as to compare the localization patterns of a capsid protein with the tegument protein VP16. I was again interested in the possibility of visualizing incoming virion. Unlike in the infections with DG1, I was able to visualize very small points of fluorescence in the cells infected with K26GFP at 2 hpi. These points of fluorescence were usually found near the nucleus, mostly lining the outer edges. It is possible that this fluorescence is representing capsids that are associated with the nuclear pore complexes. Electron micrograph images have demonstrated that incoming capsids accumulate at the cytosolic face of the nuclear pore complexes (NPCs), oriented with a penton toward the nuclear pore [30] [26]. After association with the NPC the viral genome is then rapidly and efficiently released into the cell's nucleus where it will be transcribed and replicated. In contrast to DG1, I was able to visualize fluorescence at very early times with K26GFP. This suggests that as virus entry into the cell occurs the majority of the tegument structure disperses and VP16 travels to the nucleus either alone, or in amounts that are not detectable to the camera.

After expression of new VP26-GFP (6 and 8 hpi) the protein localized into distinct punctate dots within the nucleus. This punctate pattern is similar to what was observed by Desai et al. in their initial analysis of this recombinant virus [111]. By utilizing the ability of the confocal microscope to obtain images on different planes throughout the infected cell, I was able to observe that the punctate dots of VP26-GFP fluorescence were located along the inner nuclear membrane of the cell nucleus. This agrees with the electron microscopic evidence of capsid assembly occurring in crystalline arrays or clusters along the inner nuclear membrane of the infected cell nucleus [117] [118]. The punctate dots of localization for VP26-GFP are different than the nuclear dots

formed by VP16-EGFP. The VP26-GFP dots are smaller, more compact, and more intense than the VP16-EGFP dots and are distributed throughout the nucleus on different planes. These dots are also arranged along the inner membrane of the nucleus, whereas the VP16-EGFP nuclear dots are nonrandomly distributed throughout the inside of the nucleus.

As the infection progressed (10 and 12 hpi), the intensity of the punctate nuclear dots increased and cytoplasmic localization of VP26-GFP began to be observed. This cytoplasmic localization is most obvious at the adherent surface of the infected cells. This addition to the VP26-GFP fluorescent pattern correlates with the accumulation of cytoplasmic speckles and surface patches in cells infected with DG1 and is believed to be the accumulation of newly formed virus being released from the cell.

At late times in the infection cycle of K26GFP an increase in cytoplasmic fluorescence as well as a perinuclear accumulation occurs. The VP26-GFP localization outside the nucleus could possibly be newly formed capsids traversing through the nuclear membranes acquiring a tegument on the outside of the nucleus. If this is the case the localization of fluorescence at the perinuclear area is most likely occurring at earlier times but only becomes apparent at these late times. This is presumably due to an increase in the amounts of mature capsids budding out of the nucleus causing an increase in the intensity of fluorescence in the perinuclear area that is not concealed by the intensity of the nuclear fluorescence.

The results reported from my visualization of VP26-GFP localization within live, infected cells was an extension of the original, preliminary studies performed by Desai et al. The observations described by Desai et al. were generally similar to what I observed

in my time course, yet the additional time points and ability to construct a series of images through the cells allowed me to obtain and present more thorough results on the localization of VP26-GFP. The observations of incoming capsids are the first demonstrations of the entry of virions within live cells. The localization of newly synthesized VP26-GFP was observed to be solely nuclear at early times, with cytoplasmic accumulation becoming more intense at later times. The nuclear localization of VP26-GFP within punctate dots remained very similar throughout the whole course of infection, with slight increases in size as the infection progressed. This differs with the reported observations from Desai et al. for VP26-GFP localization at late times. In their experiments they report that the punctate nuclear fluorescence became less intense and was replaced with a more generalized nuclear fluorescence [111]. These differences in localization patterns may be due to the collection of images at a lower magnification. My images were collected using a 60X objective, whereas Desai et al. collected images with a 40X objective. At a higher magnification it was easier to obtain images with more in focus light within the nucleus than at a lower magnification.

Chapter 4

HCF-1 DEPENDENT NUCLEAR LOCALIZATION OF VP16

Introduction

VP16 plays a dual role in HSV-1 lytic infection. First it is a structural component of the virion tegument, and second it is a powerful transcriptional activator of the viral IE genes. After entry into the cell, VP16 localizes to the nucleus to activate transcription through two regulatory sequences, the TAATGARAT and GA-rich elements [66] [67] [68]. Transcriptional activation is initiated by the formation of VP16 and two cellular proteins, Oct-1 and HCF-1, into a VP16 induced complex (VIC) [71] [73]. The first step in assembly of this complex is the association of VP16 with HCF-1, which subsequently associates with Oct-1 already bound to the TAATGARAT motif [74], [75].

VP16 is a 490 amino acid protein that is composed of two different structural and functional domains. The first 400 amino acids contain regions of interaction with HCF-1 (residues 355-370), Oct-1 (residues 370-390), and vhs (residues 1-400) [79]. The C-terminal 80 amino acids (410-490) make up the transcriptional activation domain (AD) [80]. Without this domain VP16 can still interact with HCF-1 and Oct-1 at IE promoters, but can not activate transcription.

Oct-1 is a member of the POU domain family of transcription factors [69]. This protein provides the DNA binding specificity to the formation of the VIC.

The precise role of HCF-1 within the cell is unknown. HCF-1 has been suggested to play a role in cell-cycle progression. In a screen for temperature sensitive cell cycle mutants,

Goto et al. isolated a cell line, tsBN67 that arrested at the nonpermissive temperature after normal proliferation for 1-2 days. This temperature sensitive phenotype is reversible and results from a single amino acid substitution (proline to serine) at position 134 within the β propeller domain of HCF-1 [110]. This mutation does not affect the processing of the HCF-1 but does affect the ability of HCF-1 to form the VP16 induced complex. The only known cellular target of HCF-1 is the basic leucine zipper transcription factor LZIP [108] [107]. LZIP interacts with HCF-1 through a six amino acid sequence, REHAYS. This sequence is also found in the HCF-1 interaction domain of VP16 (amino acids 360 – 365) [108]. Mutations affecting the REHAYS motif of VP16 abolished its interaction with HCF-1 *in vitro* [105] [119].

Recently, LaBoissiere et al. demonstrated that in cells cotransfected with expression vectors for full length VP16 and full length HCF-1 or HCF-1 with just the N and C terminal domains, VP16 relocated from a diffuse to a mainly nuclear pattern. When the putative NLS of HCF-1 within the carboxy terminus was deleted, the ability of HCF-1 to form VIC *in vitro* was not affected, but the nuclear localization of VP16 was abolished. The candidate NLS was also fused to a reporter gene that is normally localized in both the cytoplasm and nucleus resulting in induced nuclear accumulation of that gene product [105].

This suggestion that HCF-1 is the factor responsible for the targeting and transport of VP16 into the nucleus became an interesting question. It is known that VP16 must interact with HCF-1 to form VIC with Oct-1. If this interaction occurs outside of the nucleus of the infected cell and is the sole mode of nuclear transport for VP16 is an interesting question. I utilized the temperature sensitive HCF-1 mutation in the tsBN67

cells and my recombinant DG1 virus to test the interaction and nuclear import of VP16-EGFP.

Experimental Results

To test if HCF-1 is the factor responsible for the transport of VP16-EGFP into the nucleus, I utilized the ts mutation of HCF-1 in tsBN67 cells. Parental BHK cells were also used as a control. Cells were seeded onto two-well chambered coverslips and grown for two days at either the permissive temperature, 33°C, or the nonpermissive temperature, 39°C. After two days, the tsBN67 cells were infected with DG1 at an MOI of 50. Parental BHK cells were infected with DG1 at an MOI of 10. The infections were performed at both the permissive temperature, 33°C, as well as the nonpermissive temperature, 39°C. Infection at this high MOI allowed me to detect the input VP16-EGFP. Images were collected as 6 s exposures. These long exposures resulted in excessive light noise, which I tried to avoid by imaging cells within the middle of the screen.

The parental BHK cells at both temperatures displayed the typical expression and localization pattern of VP16-EGFP as seen in the Vero cell experiments. The cells at 33°C displayed the expression and localization of VP16-EGFP slower than the cells at 39°C. At 33°C there was no expression of VP16-EGFP at 4 hpi (Fig. 30A), whereas at 39°C the cells were accumulating VP16-EGFP within the nucleus and beginning to form

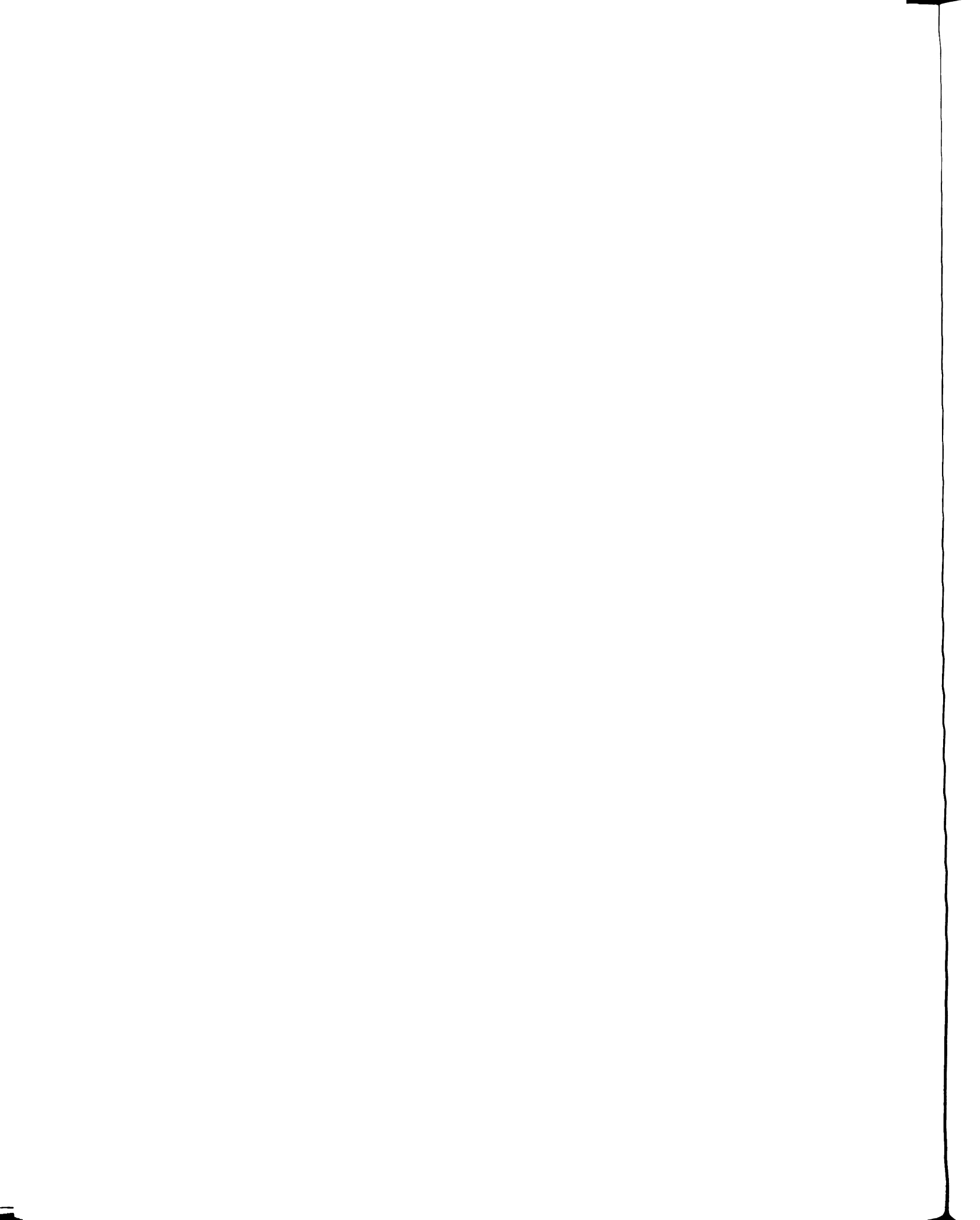


Figure 32. DG1 infection of BHK cells at 33°C and 39°C, localization of VP16-EGFP. Live cell analysis of VP16-EGFP in BHK cells infected with DG1 at an MOI of 10. (A, B, C) 33°C. (D, E, F) 39°C. (A, D) Fluorescence at 2 hpi, (B, E) 9 hpi, and (C, F) 24 hpi.

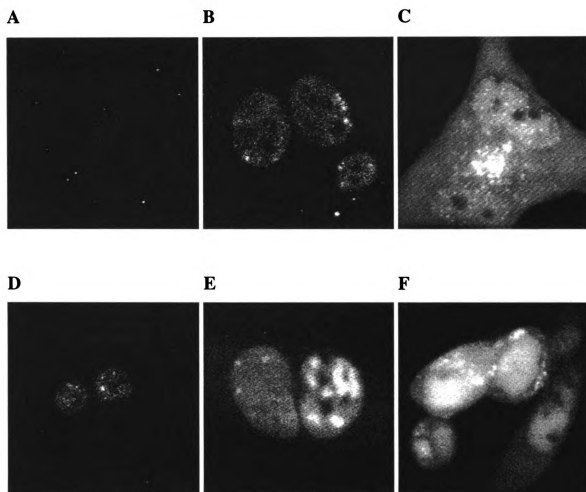


Figure 32

nuclear dots (Fig. 30D). At 9 hpi the cells at 33°C started displaying diffuse nuclear accumulation of VP16-EGFP (Fig. 30B) and the cells at 39°C continued accumulating fluorescence within nuclear dots and nuclear blobs (Fig. 30E). 24 hpi BHK cells at both temperatures were displaying intense expression of VP16-EGFP as well as cytopathic effect (Fig. 30C and F).

At 2 hpi in tsBN67 cells at 33°C, input VP16-EGFP was localized to the nucleus of the infected cells. Figures 31A and B show four cells with the nuclear localization of VP16-EGFP. A series of 1 μm images of these cells is shown in Appendix figure T. The observation of the tsBN67 cells at the nonpermissive temperature 39°C showed the nuclear exclusion of VP16-EGFP (Fig. 31C and D). A series of 1 μm images shown in Appendix figure U demonstrates this exclusion with VP16-EGFP fluorescence localized mainly in the cytoplasm with perinuclear accumulation.

At 6 hpi there was a more obvious accumulation of VP16-EGFP within the nuclei of tsBN67 cells at 33°C (Fig. 32A-D). Figure 32A is one representative image from a 1 μm series of images shown in Appendix figure V. These cells, with functional HCF-1 show an accumulation of VP16-EGFP within the nucleus as well as the expression of newly synthesized VP16-EGFP within the cytoplasm. The tsBN67 cells that were infected at the nonpermissive temperature continued to display the nuclear exclusion of VP16-EGFP. Figures 32E and F are images from a 1 μm series of images shown in Appendix figure W. These images demonstrate the cytoplasmic and perinuclear accumulation of VP16-EGFP for four cells. Figures 32G and H are representative images of a 1 μm series of images displayed in Appendix figure X. These images demonstrate the cytoplasmic and perinuclear accumulation of VP16-EGFP in two daughter cells.

Figure 33. DG1 infection of tsBN67 cells at 33°C and 39°C, localization of VP16-EGFP at 2 hpi. Live cell analysis of VP16-EGFP in cells infected at an MOI of 50. (A) Fluorescence in tsBN67 cells at 33°C at 2 hpi. (B) Brightfield image of cells in (A). (C) Fluorescence in tsBN67 cells at 39°C at 2 hpi. (D) Brightfield image of cells in (C).

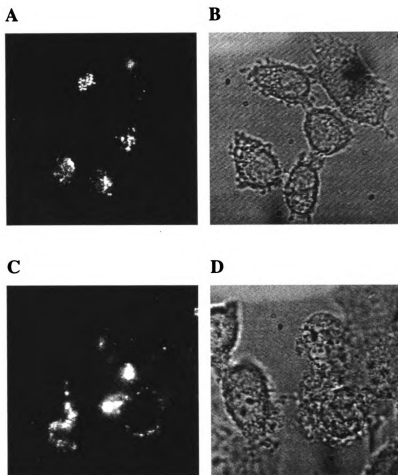


Figure 33

Figure 34. DG1 infection of tsBN67 cells at 33°C and 39°C, localization of VP16-EGFP at 6 hpi. Live cell analysis of VP16-EGFP in cells infected at an MOI of 50.
(A) Fluorescence in tsBN67 cells at 33°C at 6 hpi. (B) Brightfield image of cells in (A).
(C) Fluorescence in tsBN67 cells at 33°C at 6 hpi. (D) Brightfield image of cells in (C).
(E) Fluorescence in tsBN67 cells at 39°C at 6 hpi. (F) Brightfield image of cells in (E).
(G) Fluorescence in tsBN67 cells at 39°C at 6 hpi. (H) Brightfield image of cells in (G).

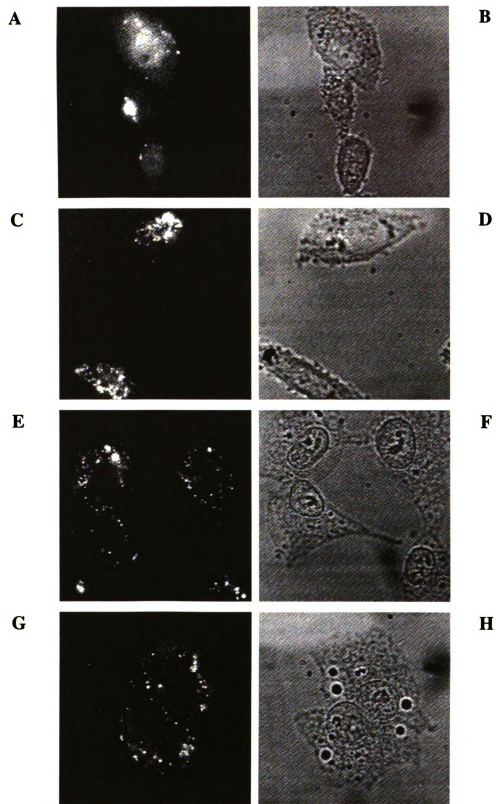


Figure 34

At 9 hpi the tsBN67 cells at 33°C resembled the VP16-EGFP expression and localization patterns of VP16-EGFP in the parental BHK cells (Figs. 33A, B, and C). The nuclear exclusion as well as the cytoplasmic and perinuclear accumulation of VP16-EGFP continued in the tsBN67 cells at nonpermissive temperature (Figure 33D through G). 24 hpi the cells at 33°C displayed cytopathic effect as well as an intense expression of fluorescence throughout the entire cell (Figs. 34A and B). In contrast, the cells at the nonpermissive temperature continued to display nuclear exclusion of VP16-EGFP. Figures 34C and D are representative images from a 1 μm series of images displayed in Appendix figure Y. These images display the continued accumulation of VP16-EGFP within the cytoplasm and perinuclear region of the infected cell.

Discussion

The isolation and characterization of a temperature sensitive cell line with a mutation in the putative cell cycle factor HCF-1 has been very useful in the study of HSV-1 infection. HCF-1 contains an NLS sequence within its carboxy terminus and has been shown to transport VP16 into the nucleus when both are coexpressed [105]. To look at the nuclear transport of VP16 in the context of a viral infection within live cells, I obtained the tsBN67 cell line and visualized the nuclear import of VP16-EGFP after infection with DG1.

As discovered in the DG1 time course of infection, input VP16-EGFP is not visible when cells are infected at low MOIs of 1 or 10. To observe the input VP16-EGFP, I infected the tsBN67 cells at an MOI of 50. This high MOI is not representative

Figure 35. DG1 infection of tsBN67 cells at 33°C and 39°C, localization of VP16-EGFP at 9 hpi. Live cell analysis of VP16-EGFP in cells infected at an MOI of 50. (A, B, C) Fluorescence in tsBN67 cells at 33°C at 9 hpi. (D) Fluorescence in tsBN67 cells at 39°C at 9 hpi. (E) Brightfield image of cells in (D). (F) Fluorescence in tsBN67 cells at 39°C at 9 hpi. (G) Brightfield image of cells in (F).

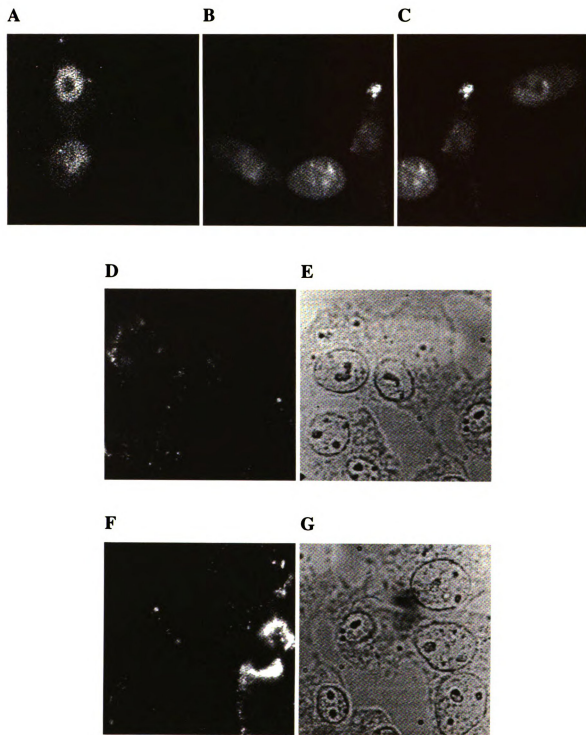


Figure 35

Figure 36. DG1 infection of tsBN67 cells at 33°C and 39°C, localization of VP16-EGFP at 24 hpi. Live cell analysis of VP16-EGFP in cells infected at an MOI of 50. (A, B) Fluorescence in tsBN67 cells at 33°C at 24 hpi. (C) Fluorescence in tsBN67 cells at 39°C at 24 hpi. (D) Brightfield image of cells in (C).

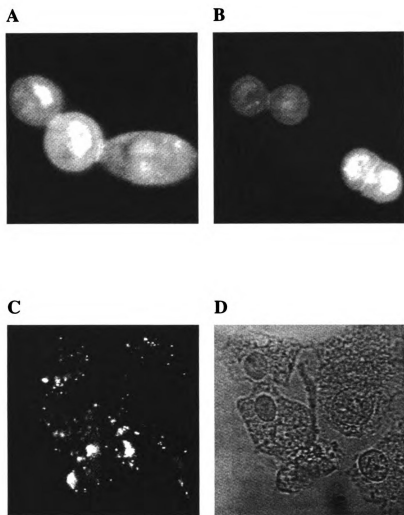


Figure 36

of a physiological infection and resulted in early onset of cytopathic effect. Nevertheless, with this high input of DG1, I was able to observe the fate of the input VP16-EGFP.

At the permissive temperature, tsBN67 cells infected with DG1 displayed VP16-EGFP nuclear localization at 2 hpi. As infection proceeded newly synthesized VP16-EGFP was observed. This VP16-EGFP began accumulating in patterns comparable to those seen in the DG1 time course, yet with a slower onset of infection. This slower infection is most likely due to the lower temperature of incubation (33°C vs. 37°C), and perhaps species specific factors. DG1 was originally assayed in Vero cells (derived from the African green monkey kidney), and tsBN67 cells are derived from baby hamster kidney cells.

In contrast to the cells at the permissive temperature, the tsBN67 cells at the nonpermissive temperature show no localization of VP16-EGFP into the nucleus. The temperature sensitive mutation within HCF-1 has been shown to disrupt its interaction with VP16 [110]. At 2 hpi with DG1, VP16-EGFP localizes in the cytoplasm as well as perinuclear. No VP16-EGFP was observed in any of the infected cell nuclei. This pattern of perinuclear accumulation and cytoplasmic localization continued until 24 hpi.

These results suggest that HCF-1 is the factor responsible for the nuclear import of input VP16 during HSV-1 infection. Recently LaBoissiere et al. reported that the intracellular distribution of HCF and newly synthesized VP16 in tsBN67 cells was similar to that observed in Vero cells, suggesting that late in infection the trafficking of both proteins was not dependent on their association [120]. This is somewhat contrasting with my results of VP16-EGFP nuclear import within tsBN67 cells. I report that the input VP16 requires the interaction with HCF-1 to localize to the nucleus, and without

this interaction it remains cytoplasmic and no new expression of VP16 occurs.

LaBoissiere et al. demonstrated biochemically that VP16 binding to HCF was defective in tsBN67 cells at the nonpermissive temperature, yet in an indirect immunofluorescence study newly synthesized VP16 was detected within nuclear replication compartments [120].

The main discrepancy between these two reports is the fact that there was no new expression of VP16-EGFP within the tsBN67 cells in my experiments. Therefore I could not observe the localization of newly synthesized VP16-EGFP and the effect of the HCF-1 mutation. Despite the apparent contradiction with the new data from LaBoissiere et al. my results still support the original model proposed by the same group that HCF-1 is the nuclear import factor [105]. In fact, their new results are slightly contradictory because their new model proposes that immediately after infection input VP16 translocates to the nucleus via an HCF-dependent pathway, whereas newly synthesized VP16 nuclear trafficking is HCF-independent [120]. This hypothesis fails to explain how VP16 is being expressed in the tsBN67 cells at nonpermissive temperature at a time point comparable to wild type.

It is still possible that data from both groups are correct, but that the observed differences are due to the use of different strains of HSV-1. I used the KOS strain in my experiments whereas they used the strain 17. To address these differences all the above experiments would need to be performed in the HSV-1 strain 17.

Chapter 5

CONCLUSIONS AND FUTURE DIRECTIONS

Until now most of evidence for the localization of viral proteins has been obtained by visualizing the viral protein of interest within a transiently transfected cell. When a viral protein is expressed alone, the protein will not be performing its usual function, and therefore its localization within the cell may not be applicable to the actual viral infection. Studies of the localization of viral proteins in the context of an infection have also been performed, but these studies involve immunochemical analysis of the cells. These analyses require the fixing and permeabilization of the cells, which may result in artifacts that interfere with the interpretation of the data.

The results described in the previous chapters demonstrate the localization of VP16 throughout a viral infection cycle. What makes this study different from other localization studies is the observation of VP16 in its natural environment within a live, infected cell. Important for the debate concerning herpesvirus maturation and egress is the identification of the tegument assembly site within the cell. If the viral particle is acquiring its envelope from the inner nuclear membrane, tegument assembly must occur within the nucleus. If the viral particle is acquiring its envelope in the cytoplasm, tegument assembly can be occurring either within the nucleus or within the cytoplasm.

The model I propose, based on my observations and published reports, is as follows. HSV-1 infects a cell by fusing with the plasma membrane. Once inside the cell the tegument disassembles and VP16 is transported to the nucleus in a complex with HCF-1. The capsid is also transported to the nucleus, possibly by interacting with the

microtubules. Viral DNA is translocated into the nucleus and associates with cellular ND10 domains. VP16 and HCF-1 form a transcriptionally active complex with Oct-1 on the promoters of the IE genes. Expression of the IE gene products initiates expression of the DE genes and causes dispersion of the ND10 proteins. Prior to the initiation of viral DNA replication, expression of the leaky late genes, including VP16, begins. The DE gene products activate viral DNA replication and subsequently the expression of the late genes. The newly synthesized VP16 localizes to the nucleus to the domains of vDNA replication. VP16 plays a role in the activation of transcription as well as a putative role in viral DNA replication. As more viral genomes accumulate within the nucleus, more VP16 accumulates with the viral DNA. As capsids form and are packaging vDNA in crystalline arrays along the inner membrane of the nucleus, VP16 begins associating with other tegument proteins in the cytoplasm and accumulates on the outside of the nucleus. Packaged and assembled capsids first bud through the inner nuclear membrane acquiring an initial envelope. These enveloped capsids then deenvelope by budding through the outer nuclear membrane. While the capsid is near the outside surface of the nucleus it acquires either some or all of the tegument. These full or partially tegumented capsids then bud into a Golgi derived vacuole acquiring the remaining tegument proteins and a mature viral envelope.

Further studies will be required for additional support of this proposed maturation and egress pathway. I have demonstrated that the recombinant fusion virus DG1 displays wild type growth characteristics as well as the packaging of the VP16-EGFP fusion protein into the viral tegument. The activation of the IE genes should also be tested to determine if the VP16-EGFP fusion can activate transcription as well as wild type VP16.

This can be demonstrated by transiently transfecting reporter plasmids with IE gene promoters followed by infection with either wild type KOS or DG1, and assaying for chloramphenicol acetyltransferase activity.

The results obtained from the localization studies using the recombinant DG1 and K26GFP viruses were accumulated in a cell population in logarithmic growth. A continued look at the localization and colocalization of viral proteins within the cell during infection should be performed in cells that are synchronized to discount any artifactual data from cells in different stages of the cell cycle. Vero cells can be synchronized by isoleucine deprivation [121]. The infection process itself should also be synchronized to minimize the patterns of localization that are representative of a delayed infection. This synchronization can be performed by inoculating cells with virus at 4°C to allow virus binding to the plasma membrane, and subsequently shifting cells to 37°C to initiate viral infection [25]. Along with synchronous infection, a more stringent acid wash of the cells can be performed to remove any nonbound virions from the cells [R. Pichyangkura 1996].

Input VP16 localizes to the nucleus for transcriptional activation of the IE genes. I was not able to visualize the input VP16-EGFP when cells were infected at a lower MOI presumably because the tegument disassembles upon entry into the cell. In contrast to the tegument protein, I was able to visualize the input capsids from the K26GFP virus presumably because the capsids contain approximately 1000 copies of VP26-GFP in close proximity. To determine if the tegument is indeed dispersing, immunogold labeling of VP16 as well as VP26 or another capsid protein, such as VP5, could be observed using electron microscopy immediately after entry of the virus into the cell.

In the tsBN67 cells, infections with a very high MOI of DG1 allowed the visualization of input VP16-EGFP. These cells also demonstrated the nuclear localization of VP16 at the permissive temperature with functional HCF-1, but not at the nonpermissive temperature with a nonfunctional HCF-1. At the nonpermissive temperature the interaction of HCF-1 with VP16 is inhibited [110]. The nuclear exclusion of VP16-EGFP at this temperature suggests that HCF-1 plays a role as a nuclear transport carrier for VP16. The ts mutation within HCF-1 at the nonpermissive temperature disrupts the protein's interaction with VP16 and therefore it can not transport VP16 into the infected cell nucleus. At the nonpermissive temperature the mutation in HCF-1 also results in the cells being quiescent in G₀ [110]. It is possible that it is the cell cycle block that is blocking the nuclear localization of VP16 and not the ts mutation in HCF-1. The possibility of VP16 nuclear localization being affected by the quiescence of the cells must be ruled out. This can be done experimentally in two ways. First, Vero cells can be induced to go into G₀ by isoleucine deprivation [121], or by serum starvation (data not shown). These cells would therefore contain a functional HCF-1 but be in a quiescent state. After infection of these cells at a high MOI the nuclear localization of VP16-EGFP could be assessed. It is hypothesized that in these cells VP16-EGFP should localize in the nucleus similar to what is observed in tsBN67 cells at the permissive temperature. This would demonstrate that a cell cycle block does not affect the nuclear localization of VP16. Second, Mahajan et al. produced a truncated recombinant HCF-1 protein containing a single point mutation that retained the ability to form VIC, but could not rescue the tsBN67 phenotype [122]. Transient expression of this "mini" HCF-1 in tsBN67 cells at the nonpermissive temperature followed by infection with DG1, would

demonstrate the HCF-1 dependent nuclear localization of VP16-EGFP while the tsBN67 cells remain in G₀.

The knowledge of viral DNA localization to ND10 domains within the nucleus and the observation of VP16-EGFP localization in nonrandom, uniform dots within the infected cell nucleus leads to questions of VP16 localization to ND10 domains. To determine if these VP16-EGFP “nuclear dots” are representative of previous sites of ND10s, colocalization studies should be performed. Viruses with mutations in ICP0 have been shown to be deficient in the dispersal of the ND10 proteins [57]. If the VP16-EGFP fusion gene can be transferred into this virus, visualization of VP16 localization without the dispersal of the ND10 proteins can be obtained. At the same time, the infected cells can be immunostained with antibodies specific to PML or Sp100, and the colocalization of VP16-EGFP to ND10 domains can be determined.

A look at viral replication and transcription can also be performed during infection with DG1 to determine if the VP16-EGFP “nuclear dots” are active sites of transcription or replication. Infected cells can be labeled with bromodeoxyuridine (Br-UTP) to visualize transcription sites, or biotin-11-dUTP to visualize replication centers and these labels can be detected with a rhodamine-conjugated antibody, whereas the localization of VP16 will be demonstrated by the EGFP tag.

To look at the process of tegumentation of the virion, it would be useful to observe more than one tegument protein simultaneously. If a recombinant virus were to encode a second tegument protein fusion, such as VP22 tagged with a red fluorescent protein, the localization of both proteins could be visualized within a live cell during the process of viral assembly. This could also be performed by co-infecting with two

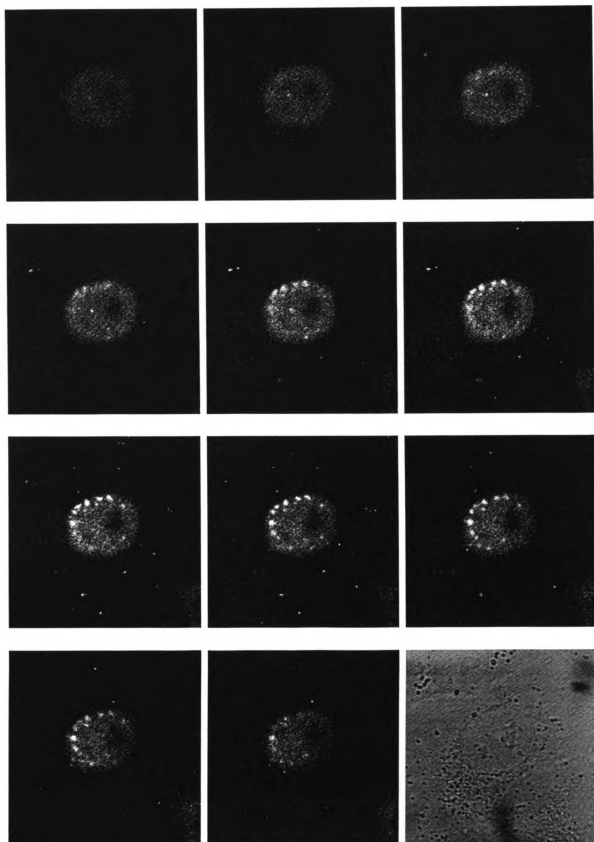
different viruses expressing tagged proteins. The major site of colocalization would give a better understanding to where the virion acquires its tegument.

In addition to the experiments laid out above it would be very useful to visualize the localization and trafficking patterns of a fluorescently tagged protein, or proteins, over a course of time within the same cell. The technology I had available to me did not allow me to look within the same cell more than once. Time-lapse analysis of the infected cells would give a more detailed look at the viral entry, assembly, trafficking, and egress pathways.

The construction of an EGFP-labeled herpesvirus has demonstrated that the incorporation of EGFP into the viral particle is not harmful to the production of infectious progeny virus. This new technology has allowed us to visualize protein localization and trafficking throughout course of viral infection within live infected cells. This is therefore a useful practice for the continued study of HSV-1 virology.

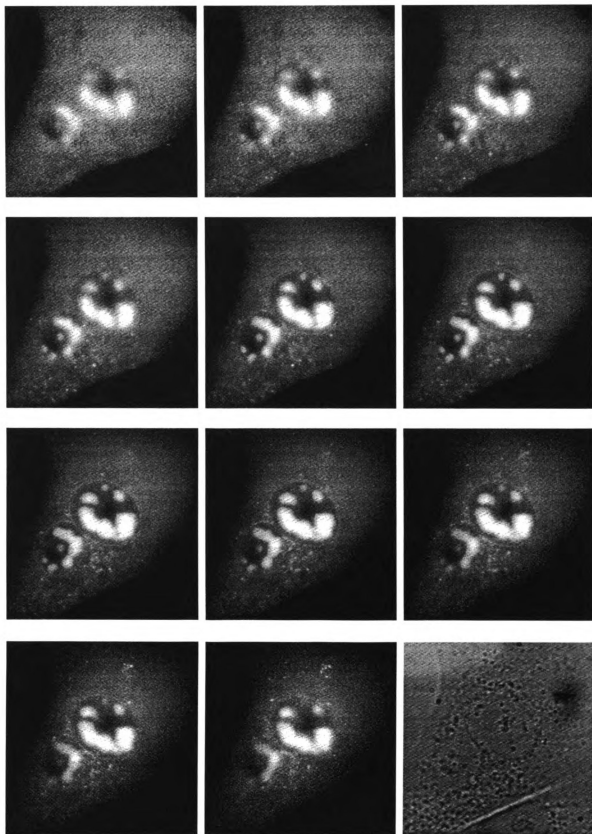
APPENDICES

Appendix Figure A. DG1 infection at 10 MOI, localization at 4 hpi.
Series of images with a 0.5 μm step size (3 s exposure)



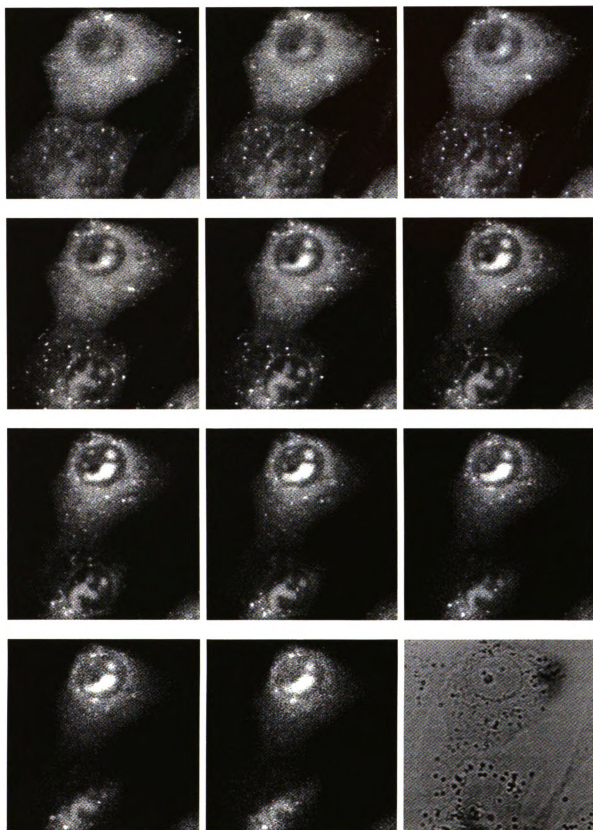
Appendix Figure A.

Appendix Figure B. DG1 infection at 10 MOI, localization at 6 hpi.
Series of images with a 0.5 μm step size (2.5 s exposure)



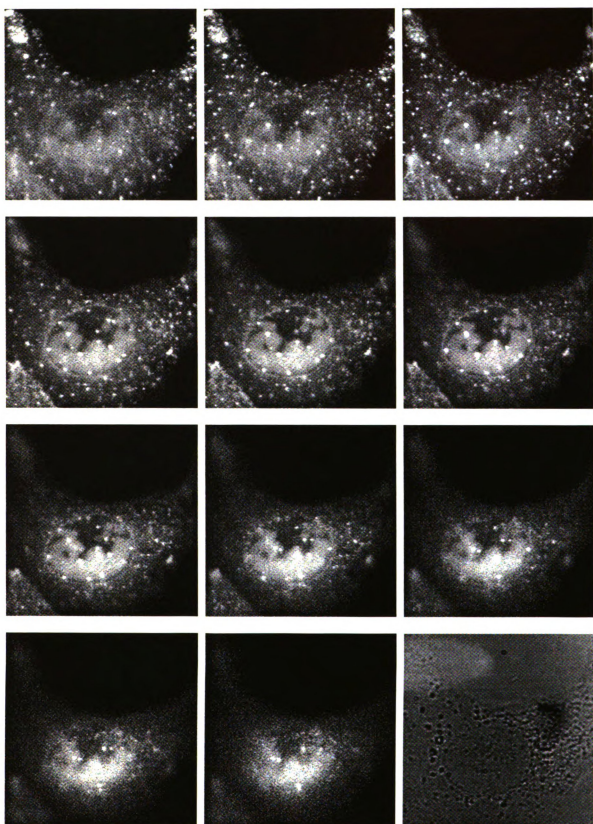
Appendix Figure B

Appendix Figure C. DG1 infection at 10 MOI, localization at 8 hpi.
Series of images with a 0.5 μm step size (2 s exposure)



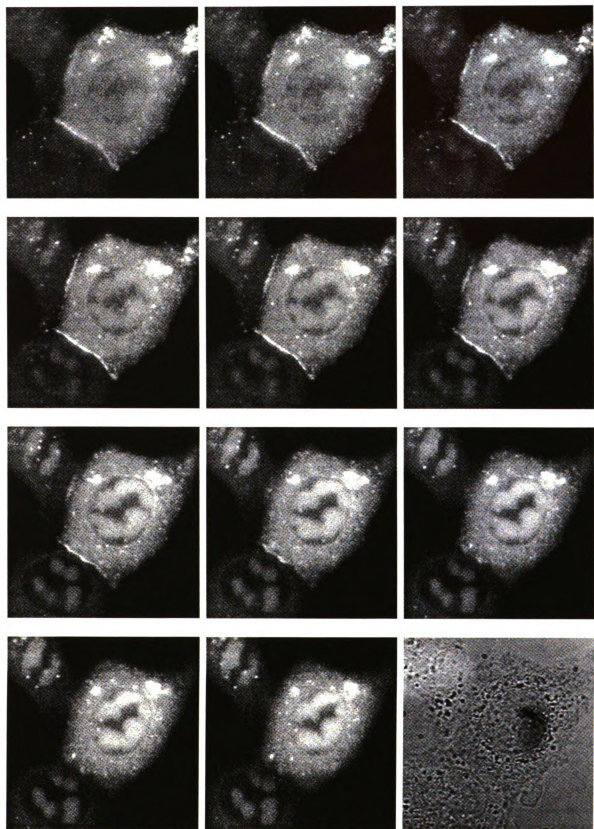
Appendix Figure C

Appendix Figure D. DG1 infection at 10 MOI, localization at 10 hpi.
Series of images with a 0.5 μm step size (1 s exposure)



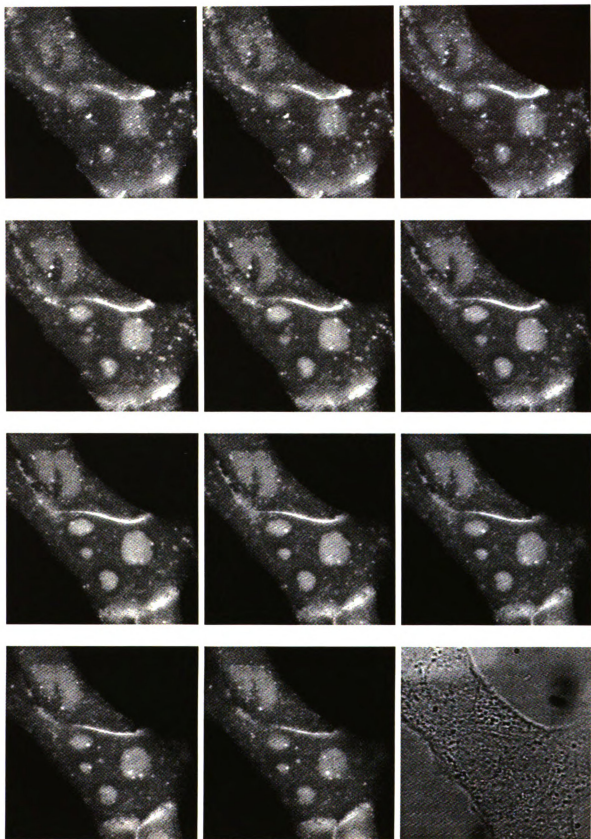
Appendix Figure D

**Appendix Figure E. DG1 infection at 10 MOI, localization at 12 hpi.
Series of images with a 0.5 μm step size (1 s exposure)**



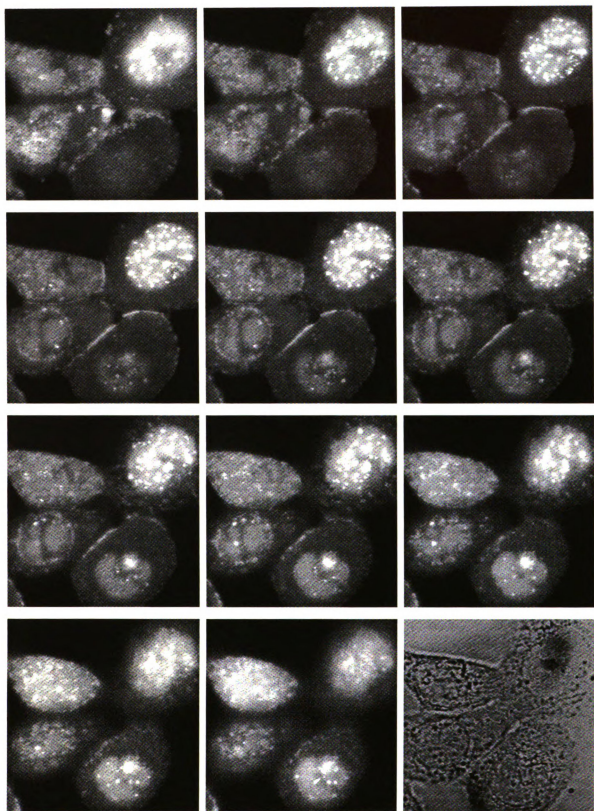
Appendix Figure E

Appendix Figure F. DG1 infection at 10 MOI, localization at 14 hpi.
Series of images with a 0.5 μm step size (1 s exposure)



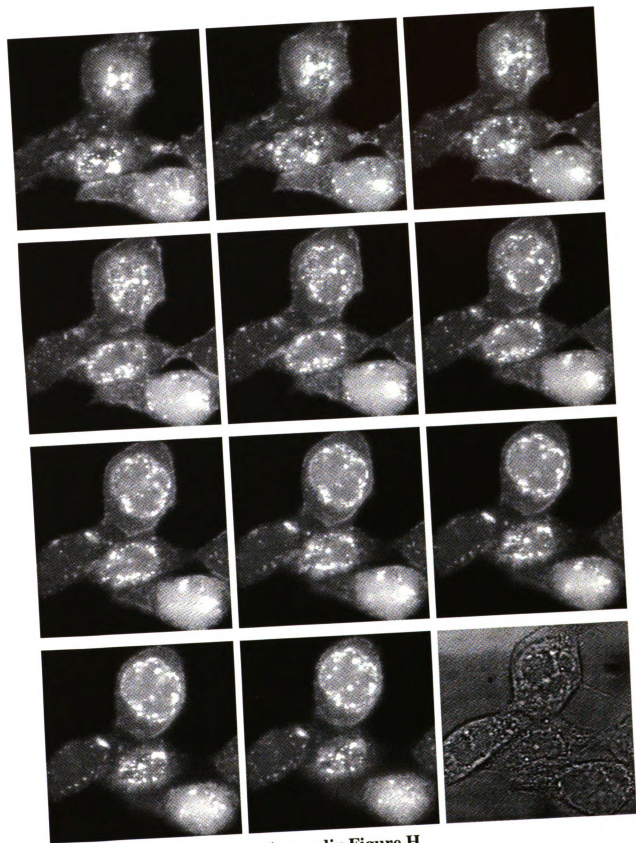
Appendix Figure F

Appendix Figure G. DG1 infection at 10 MOI, localization at 16 hpi.
Series of images with a 0.8 μm step size (1 s exposure)



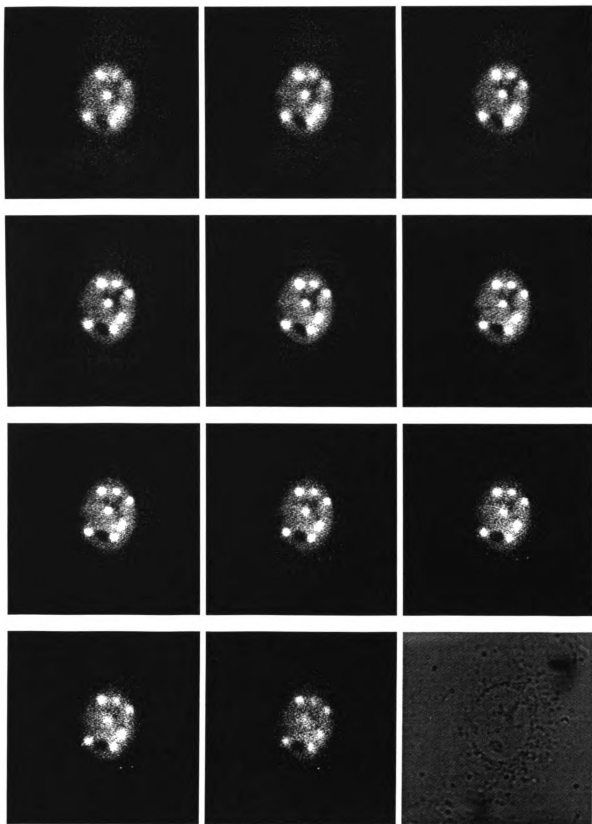
Appendix Figure G

Appendix Figure H. DG1 infection at 10 MOI, localization at 20 hpi.
Series of images with a 0.5 μm step size (1 s exposure)



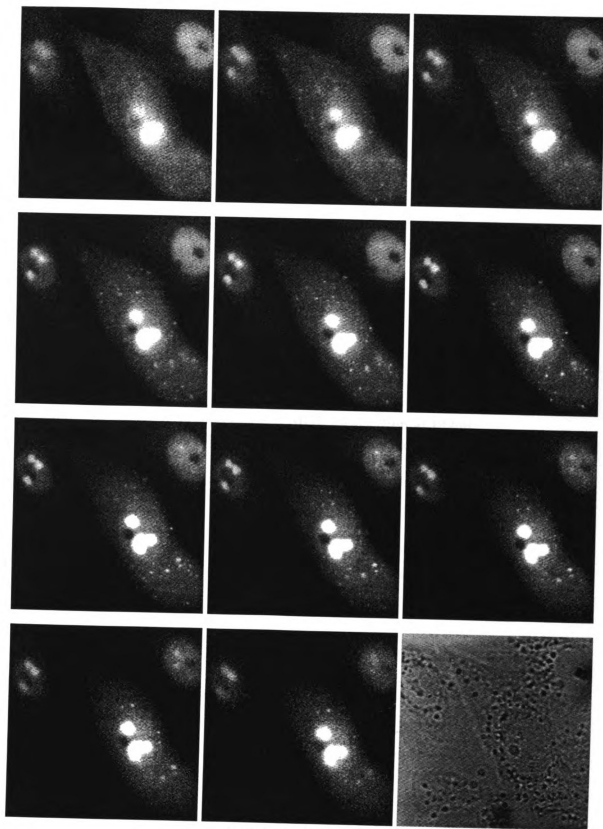
Appendix Figure H

**Appendix Figure I. DG1 infection at 1 MOI, localization at 6 hpi.
Series of images with a 0.5 μm step size (2.5 s exposure)**



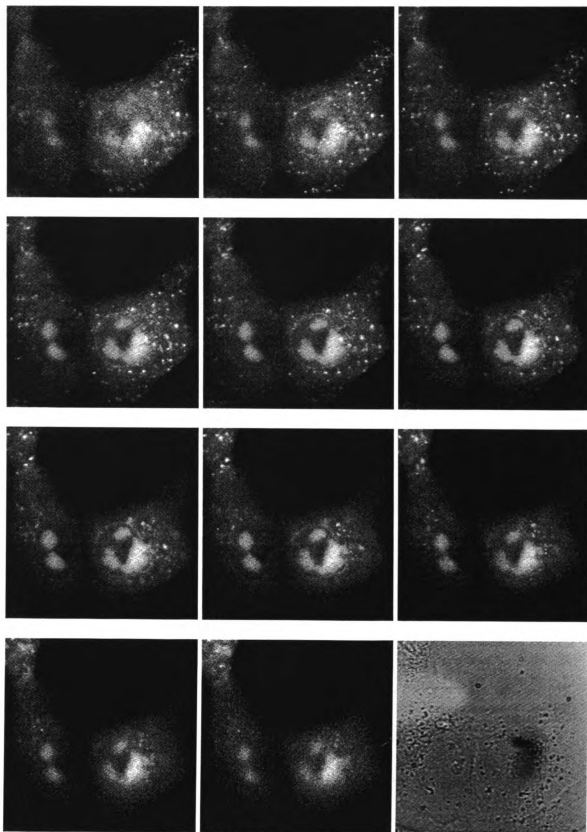
Appendix Figure I

Appendix Figure J. DG1 infection at 1 MOI, localization at 8 hpi.
Series of images with a 0.5 μm step size (3 s exposure)



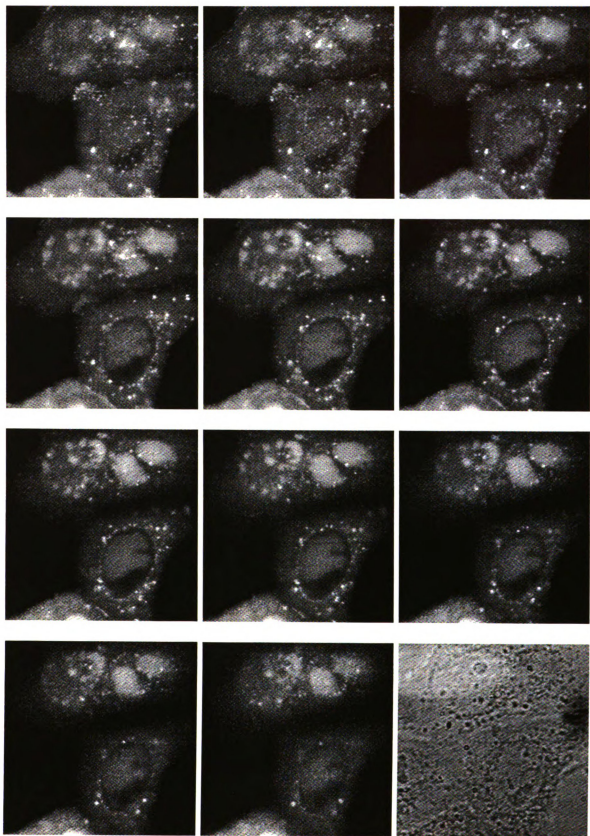
Appendix Figure J

**Appendix Figure K. DG1 infection at 1 MOI, localization at 10 hpi.
Series of images with a 0.5 μm step size (1.5 s exposure)**



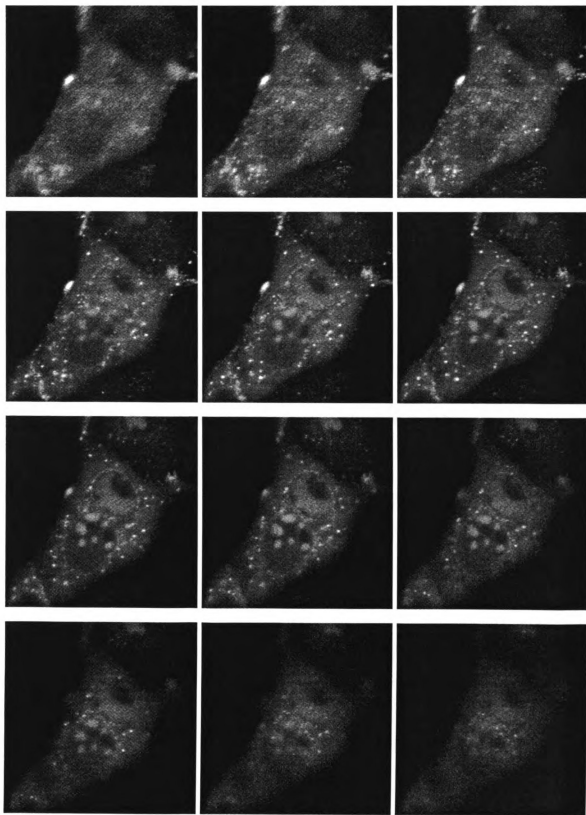
Appendix Figure K

Appendix Figure L. DG1 infection at 1 MOI, localization at 14 hpi.
Series of images with a 0.5 μm step size (1 s exposure)



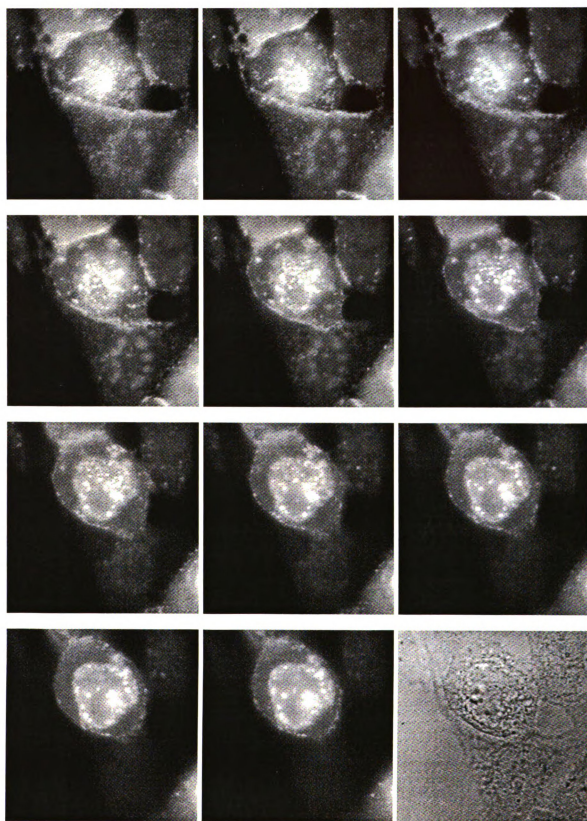
Appendix Figure L

**Appendix Figure M. DG1 infection at 1 MOI, localization at 16 hpi.
Series of images with a 0.5 μm step size (1.5 s exposure)**



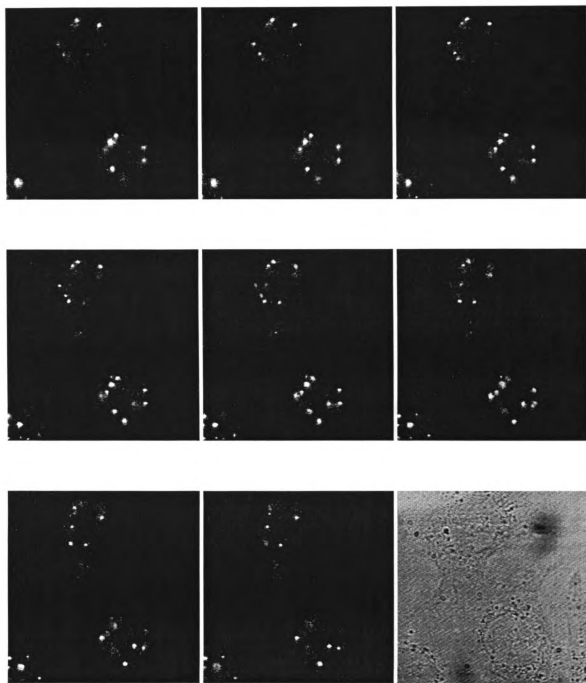
Appendix Figure M

Appendix Figure N. DG1 infection at 1 MOI, localization at 20 hpi.
Series of images with a 0.8 μm step size (1 s exposure)



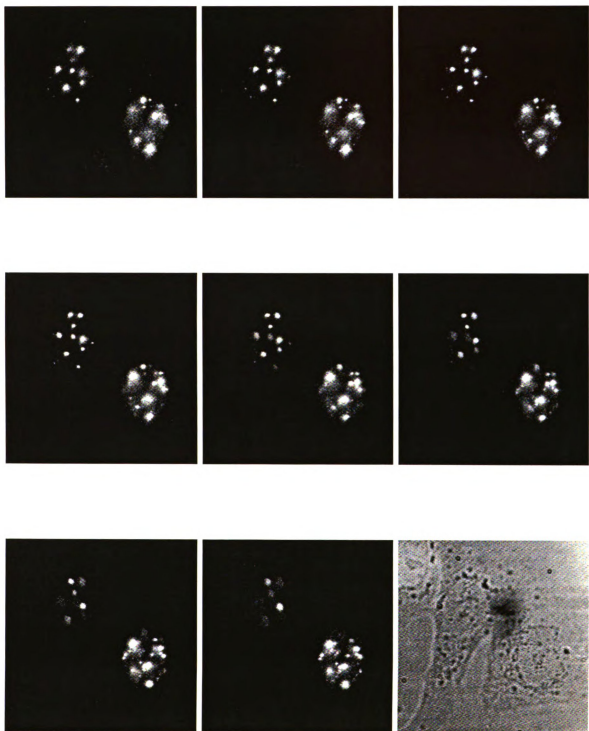
Appendix Figure N

Appendix Figure O. K26GFP infection at 10 MOI, localization at 6 hpi.
Series of images with a 0.5 μm step size (1 s exposure)



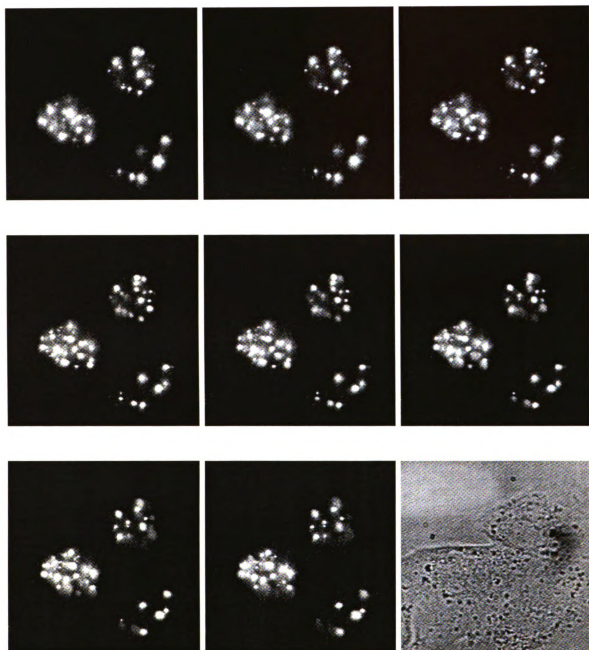
Appendix Figure O

Appendix Figure P. K26GFP infection at 10 MOI, localization at 8 hpi.
Series of images with a 0.5 μm step size (1 s exposure)



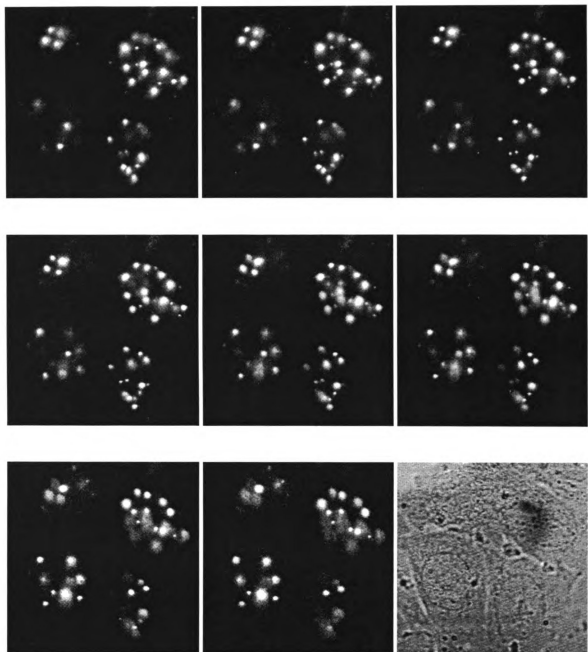
Appendix Figure P

**Appendix Figure Q. K26GFP infection at 10 MOI, localization at 10 hpi.
Series of images with a 0.5 μm step size (1 s exposure)**



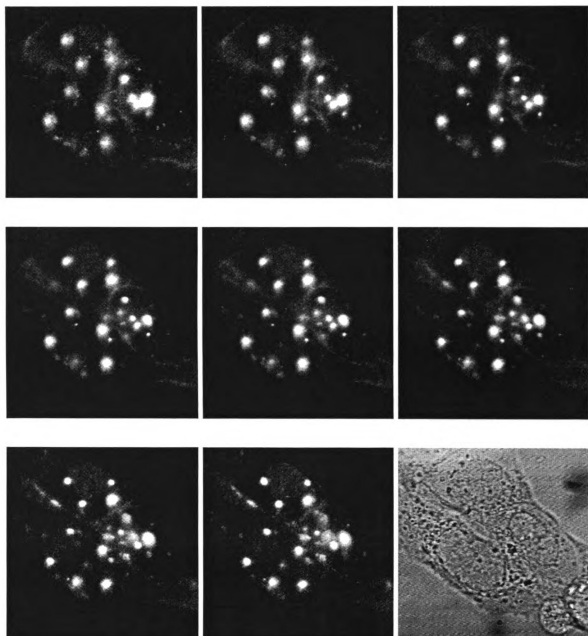
Appendix Figure Q

Appendix Figure R. K26GFP infection at 10 MOI, localization at 12 hpi.
Series of images with a 0.5 μm step size (1 s exposure)



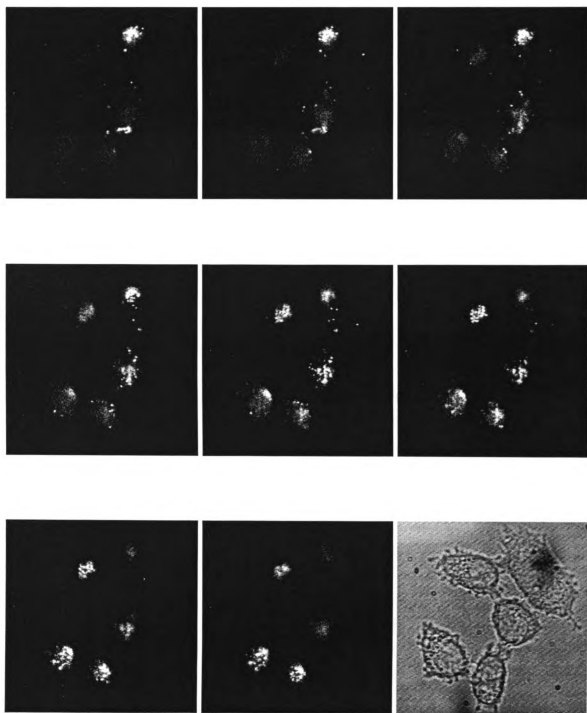
Appendix Figure R

Appendix Figure S. K26GFP infection at 10 MOI, localization at 16 hpi.
Series of images with a 0.5 μm step size (1 s exposure)



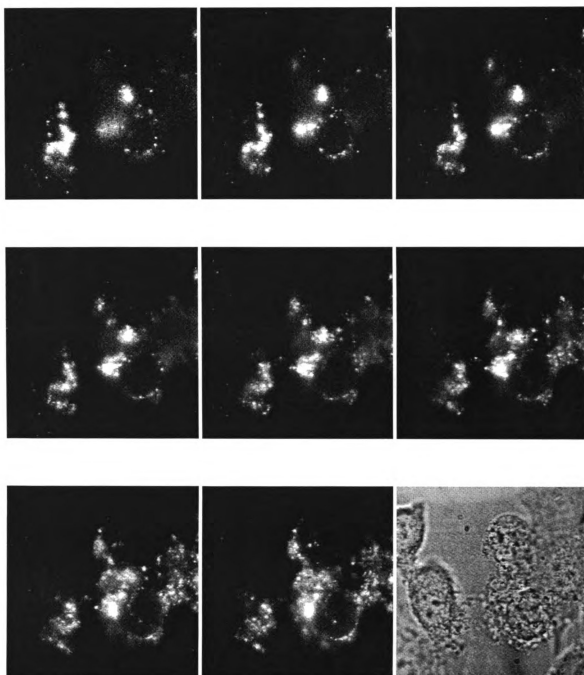
Appendix Figure S

Appendix Figure T. DG1 infection of tsBN67 cells at 33°C, localization at 2 hpi.
Series of images with a 1 μm step size (6 s exposure)



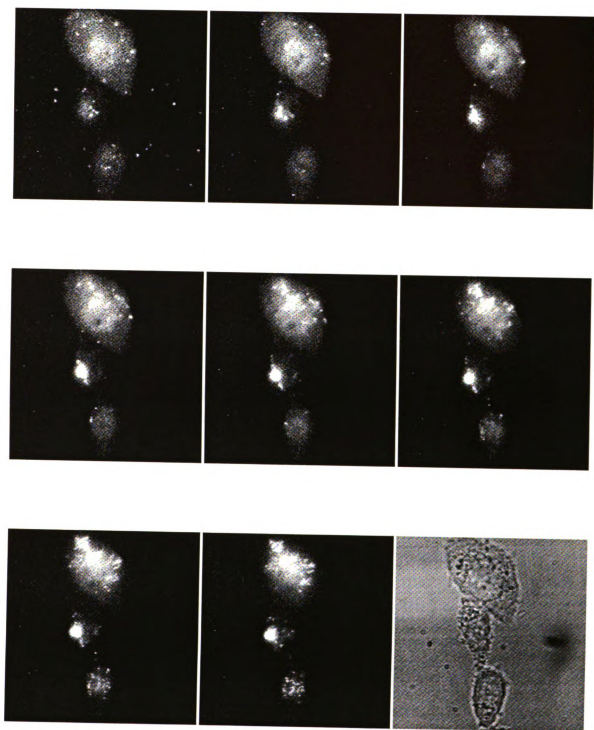
Appendix Figure T

Appendix Figure U. DG1 infection of tsBN67 cells at 39°C, localization at 2 hpi.
Series of images with a 1 μm step size (6 s exposure)



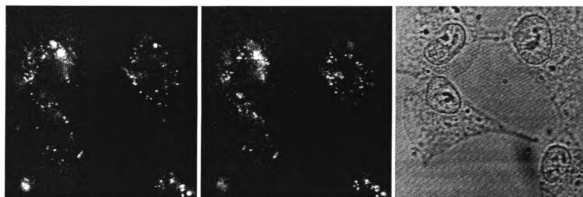
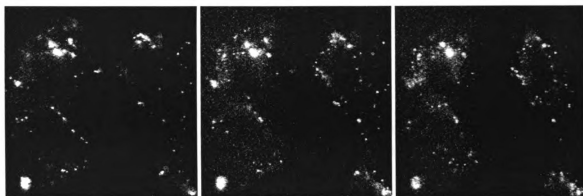
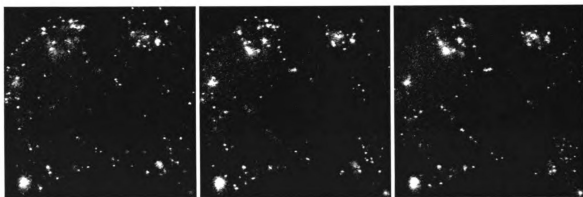
Appendix Figure U

Appendix Figure V. DG1 infection of tsBN67 cells at 33°C, localization at 6 hpi.
Series of images with a 1 μm step size (6 s exposure)



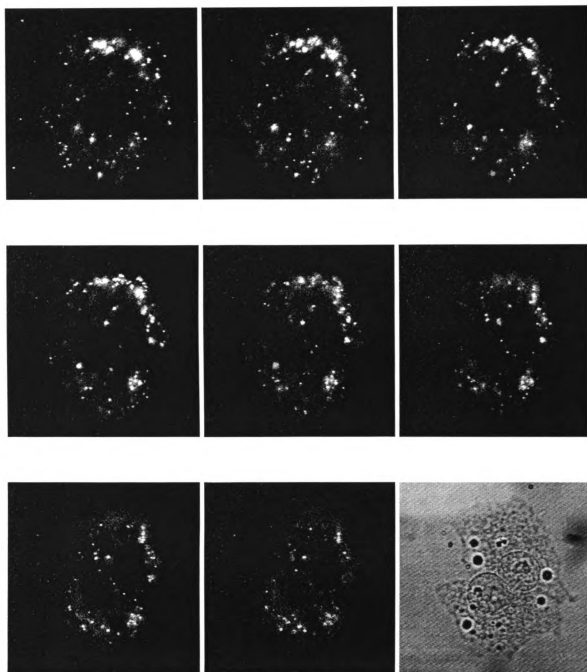
Appendix Figure V

Appendix Figure W. DG1 infection of tsBN67 cells at 39°C, localization at 6 hpi.
Series of images with a 1 μm step size (6 s exposure)



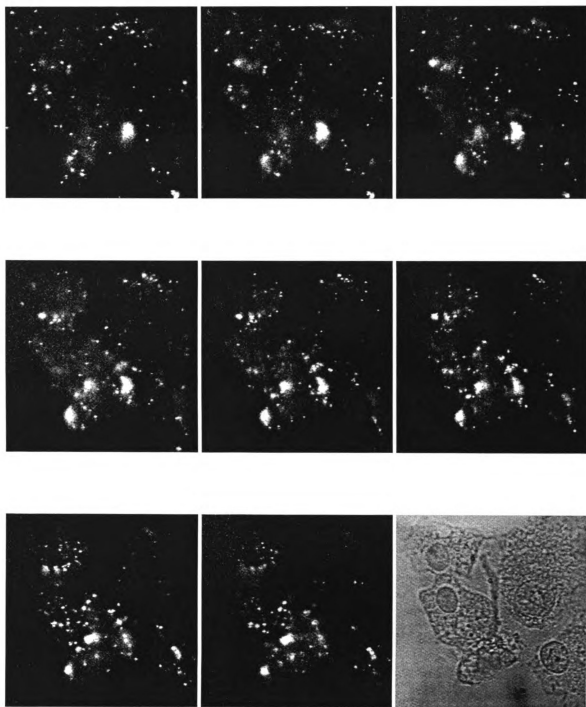
Appendix Figure W

Appendix Figure X. DG1 infection of tsBN67 cells at 39°C, localization at 6 hpi.
Series of images with a 1 μm step size (6 s exposure)



Appendix Figure X

Appendix Figure Y. DG1 infection of tsBN67 cells at 39°C, localization at 24 hpi.
Series of images with a 1 μm step size (6 s exposure)



Appendix Figure Y

BIBLIOGRAPHY

Bibliography

1. Roizman, B., R.J. Whitley, and C. Lopez, *The human herpesviruses*. 1993, New York: Raven Press.
2. Roizman, B. (1990). *Herpesviridae: A brief introduction*. Virology (ed. B. Fields) **2** (Chapter 64): 1787-1794.
3. Booy, F.P., W.W. Newcomb, B.L. Trus, J.C. Brown, T.S. Baker, and A.C. Steven (1991). *Liquid-crystalline, phage-like packing of encapsidated DNA in Herpes Simplex Virus*. Cell **64**: 1007-1015.
4. Zhou, Z.H., D.H. Chen, J. Jakana, F.J. Rixon, and W. Chiu (1999). *Visualization of tegument-capsid interactions and DNA in intact herpes simplex virus type 1 virions*. J Virol **73**: 3210-8.
5. Homa, F.L. and J.C. Brown (1997). *Capsid assembly and DNA packaging in herpes simplex virus*. Rev Med Virol **7**: 107-122.
6. Booy, F.P., B.L. Trus, W.W. Newcomb, J.C. Brown, J.F. Conway, and A.C. Steven (1994). *Finding a needle in a haystack: detection of a small protein (the 12- kDa VP26) in a large complex (the 200-MDa capsid of herpes simplex virus)*. Proc Natl Acad Sci U S A **91**: 5652-6.
7. Cohen, G.H., M. Ponce de Leon, H. Diggelmann, W.C. Lawrence, S.K. Vernon, and R.J. Eisenberg (1980). *Structural analysis of the capsid polypeptides of herpes simplex virus types 1 and 2*. J Virol **34**: 521-31.
8. Newcomb, W.W., B.L. Trus, F.P. Booy, A.C. Steven, J.S. Wall, and J.C. Brown (1993). *Structure of the herpes simplex virus capsid. Molecular composition of the pentons and the triplexes*. J Mol Biol **232**: 499-511.
9. Schrag, J.D., B.V. Prasad, F.J. Rixon, and W. Chiu (1989). *Three-dimensional structure of the HSV1 nucleocapsid*. Cell **56**: 651-60.
10. Newcomb, W.W., F.L. Homa, D.R. Thomsen, F.P. Booy, B.L. Trus, A.C. Steven, J.V. Spencer, and J.C. Brown (1996). *Assembly of the herpes simplex virus*

capsid: characterization of intermediates observed during cell-free capsid formation. J Mol Biol **263**: 432-46.

11. Chi, J.H. and D.W. Wilson (2000). *ATP-Dependent localization of the herpes simplex virus capsid protein VP26 to sites of procapsid maturation.* J Virol **74**: 1468-76.
12. Morrison, E.E., A.J. Stevenson, Y.F. Wang, and D.M. Meredith (1998). *Differences in the intracellular localization and fate of herpes simplex virus tegument proteins early in the infection of Vero cells.* J Gen Virol **79**: 2517-28.
13. Batterson, W., D. Furlong, and B. Roizman (1983). *Molecular genetics of herpes simplex virus. VIII. further characterization of a temperature-sensitive mutant defective in release of viral DNA and in other stages of the viral reproductive cycle.* J Virol **45**: 397-407.
14. Campbell, E.N., J.W. Palfreyman, and C.M. Preston (1984). *Identification of herpes simplex virus DNA sequences which encode a trans-acting polypeptide responsible for stimulation of immediate early transcription.* J. Mol. Biol. **180**: 1-19.
15. Weinheimer, S.P., B.A. Boyd, S.K. Durham, J.L. Resnick, and D.R. O'Boyle (1992). *Deletion of the VP16 open reading frame of herpes simplex virus type 1.* J. Virol. **66**: 258-269.
16. Zhang, Y., D.A. Sirko, and J.L.C. McKnight (1991). *Role of herpes simplex virus type-1 ULA6 and ULA7 in alphaTIF-mediated transcriptional induction - characterization of three viral deletion mutants.* J. Virol. **65**: 829-841.
17. Elliott, G., D. O'Reilly, and P. O'Hare (1996). *Phosphorylation of the herpes simplex virus type 1 tegument protein VP22.* Virology **226**: 140-5.
18. Meredith, D.M., J.A. Lindsay, I.W. Halliburton, and G.R. Whittaker (1991). *Post-translational modification of the tegument proteins (VP13 and VP14) of herpes simplex virus type 1 by glycosylation and phosphorylation.* J. Virol. **72**: 2771-2775.
19. Elliott, G., G. Mouzakis, and P. O'Hare (1995). *VP16 interacts via its activation domain with VP22, a tegument protein of herpes simplex virus, and is relocated to a novel macromolecular assembly in coexpressing cells.* J. Virol. **69**: 7932-7941.

20. Zelus, B.D., R.S. Stewart, and J. Ross (1996). *The virion host shutoff protein of herpes simplex virus type 1: messenger ribonucleolytic activity in vitro*. J. Virol. **70**: 2411-2419.
21. Smibert, C.A., B. Popova, P. Xiao, J.P. Capone, and J.R. Smiley (1994). *Herpes simplex virus VP16 forms a complex with the virion host shutoff protein vhs*. J. Virol. **68**: 2339-2346.
22. Szilagyi, J.F. and C. Cunningham (1991). *Identification and characterization of a novel non-infectious herpes simplex virus-related particle*. J Gen Virol **72**: 661-8.
23. McLauchlan, J. and F.J. Rixon (1992). *Characterization of enveloped tegument structures (L particles) produced by alphaherpesviruses: integrity of the tegument does not depend on the presence of capsid or envelope*. J Gen Virol **73**: 269-76.
24. Rajcani, J. and A. Vojvodova (1998). *The role of herpes simplex virus glycoproteins in the virus replication cycle*. Acta Virol **42**: 103-18.
25. Sodeik, B., M.W. Ebersold, and A. Helenius (1997). *Microtubule-mediated transport of incoming herpes simplex virus 1 capsids to the nucleus*. J. Cell. Biol. **136**: 1007-1021.
26. Granzow, H., F. Weiland, A. Jons, B.G. Klupp, A. Karger, and T.C. Mettenleiter (1997). *Ultrastructural analysis of the replication cycle of pseudorabies virus in cell culture: a reassessment*. J Virol **71**: 2072-82.
27. Penfold, M.E.T., P. Armati, and A.L. Cunningham (1994). *Axonal transport of herpes simplex virions to epidermal cells: evidence for a specialized mode of virus transport and assembly*. Proc. Natl. Acad. Sci. USA **91**: 6529-6533.
28. Holland, D.J., M. Miranda-Saksena, R.A. Boadle, P. Armati, and A.L.f. Cunningham (1999). *Anterograde transport of herpes simplex virus proteins in axons of peripheral human fetal neurons: an immunoelectron microscopy study*. J Virol **73**: 8503-8511.
29. Miranda-Saksena, M., P. Armati, R.A. Boadle, D.J. Holland, and A.L. Cunningham (2000). *Anterograde transport of herpes simplex virus type 1 in cultured, dissociated human and rat dorsal root ganglion neurons*. J Virol **74**: 1827-39.

30. Ojala, P.M., B. Sodeik, M.W. Ebersold, U. Kutay, and A. Helenius (2000). *Herpes Simplex Virus Type 1 Entry into Host Cells: Reconstitution of Capsid Binding and Uncoating at the Nuclear Pore Complex In Vitro*. *Mol Cell Biol* **20**: 4922-4931.
31. Knipe, D.M. (1989). *The role of viral and cellular nuclear proteins in herpes simplex virus replication*. *Adv Virus Res* **37**: 85-123.
32. Jackson, D.A., F.J. Iborra, E.M. Manders, and P.R. Cook (1998). *Numbers and organization of RNA polymerases, nascent transcripts, and transcription units in HeLa nuclei [published erratum appears in Mol Biol Cell 1998 Sep;9(9):2698]*. *Mol Biol Cell* **9**: 1523-36.
33. Pombo, A., E. Jones, F.J. Iborra, H. Kimura, K. Sugaya, P.R. Cook, and D.A. Jackson (2000). *Specialized transcription factories within mammalian nuclei [In Process Citation]*. *Crit Rev Eukaryot Gene Expr* **10**: 21-9.
34. Iborra, F.J., A. Pombo, D.A. Jackson, and P.R. Cook (1996). *Active RNA polymerases are localized within discrete transcription "factories" in human nuclei*. *J Cell Sci* **109**: 1427-36.
35. Jackson, D.A., A.B. Hassan, R.J. Errington, and P.R. Cook (1993). *Visualization of focal sites of transcription within human nuclei*. *Embo J* **12**: 1059-65.
36. Wansink, D.G., W. Schul, I. van der Kraan, B. van Steensel, R. van Driel, and L. de Jong (1993). *Fluorescent labeling of nascent RNA reveals transcription by RNA polymerase II in domains scattered throughout the nucleus*. *J Cell Biol* **122**: 283-93.
37. Bregman, D.B., L. Du, S. van der Zee, and S.L. Warren (1995). *Transcription-dependent redistribution of the large subunit of RNA polymerase II to discrete nuclear domains*. *J Cell Biol* **129**: 287-98.
38. Fakan, S., G. Leser, and T.E. Martin (1984). *Ultrastructural distribution of nuclear ribonucleoproteins as visualized by immunocytochemistry on thin sections*. *J Cell Biol* **98**: 358-63.
39. Zeng, C., E. Kim, S.L. Warren, and S.M. Berget (1997). *Dynamic relocation of transcription and splicing factors dependent upon transcriptional activity*. *Embo J* **16**: 1401-12.

40. Mintz, P.J. and D.L. Spector (2000). *Compartmentalization of RNA processing factors within nuclear speckles*. J Struct Biol **129**: 241-51.
41. Rice, S., A., M.C. Long, V. Lam, and C. Spencer, A. (1994). *RNA polymerase II is aberrantly phosphorylated and localized to viral replication of compartments following herpes simplex virus infection*. J. Virol. **68**: 988-1001.
42. Phelan, A., J. Dunlop, A.H. Patel, N.D. Stow, and J.B. Clements (1997). *Nuclear sites of herpes simplex virus type 1 DNA replication and transcription colocalize at early times postinfection and are largely distinct from RNA processing factors*. J Virol **71**: 1124-32.
43. Phelan, A., M. Carmo-Fonseca, J. McLaughlan, A.I. Lamond, and J.B. Clements (1993). *A herpes simplex virus type 1 immediate-early gene product, IE63, regulates small nuclear ribonucleoprotein distribution*. Proc Natl Acad Sci U S A **90**: 9056-60.
44. Martin, T.E., S.C. Barghusen, G.P. Leser, and P.G. Spear (1987). *Redistribution of nuclear ribonucleoprotein antigens during herpes simplex virus infection*. J Cell Biol **105**: 2069-82.
45. Zhang, X., S. Efstathiou, and A. Simmons (1994). *Identification of novel herpes simplex virus replicative intermediates by field inversion gel electrophoresis: implications for viral DNA amplification strategies*. Virology **202**: 530-9.
46. Ascoli, C.A. and G.G. Maul (1991). *Identification of a novel nuclear domain*. J Cell Biol **112**: 785-95.
47. Szostecki, C., H.H. Guldner, H.J. Netter, and H. Will (1990). *Isolation and characterization of cDNA encoding a human nuclear antigen predominantly recognized by autoantibodies from patients with primary biliary cirrhosis*. J Immunol **145**: 4338-47.
48. Maul, G.G. (1998). *Nuclear domain 10, the site of DNA virus transcription and replication*. Bioessays **20**: 660-7.
49. Dyck, J.A., G.G. Maul, W.H. Miller, Jr., J.D. Chen, A. Kakizuka, and R.M. Evans (1994). *A novel macromolecular structure is a target of the promyelocyte-retinoic acid receptor oncoprotein*. Cell **76**: 333-43.

50. Gongora, C., G. David, L. Pintard, C. Tissot, T.D. Hua, A. Dejean, and N. Mechti (1997). *Molecular cloning of a new interferon-induced PML nuclear body-associated protein*. J Biol Chem **272**: 19457-63.
51. Everett, R.D., M. Meredith, A. Orr, A. Cross, M. Kathoria, and J. Parkinson (1997). *A novel ubiquitin-specific protease is dynamically associated with the PML nuclear domain and binds to a herpesvirus regulatory protein [corrected and republished article originally printed in EMBO J 1997 Feb 3;16(3):566-77]*. Embo J **16**: 1519-30.
52. Boddy, M.N., K. Howe, L.D. Etkin, E. Solomon, and P.S. Freemont (1996). *PIC 1, a novel ubiquitin-like protein which interacts with the PML component of a multiprotein complex that is disrupted in acute promyelocytic leukaemia*. Oncogene **13**: 971-82.
53. Stadler, M., M.K. Chelbi-Alix, M.H. Koken, L. Venturini, C. Lee, A. Saib, F. Quignon, L. Pelicano, M.C. Guillemain, C. Schindler, and et al. (1995). *Transcriptional induction of the PML growth suppressor gene by interferons is mediated through an ISRE and a GAS element*. Oncogene **11**: 2565-73.
54. Chelbi-Alix, M.K., L. Pelicano, F. Quignon, M.H. Koken, L. Venturini, M. Stadler, J. Pavlovic, L. Degos, and H. de The (1995). *Induction of the PML protein by interferons in normal and APL cells*. Leukemia **9**: 2027-33.
55. Sternsdorf, T., T. Grotzinger, K. Jensen, and H. Will (1997). *Nuclear dots: actors on many stages*. Immunobiology **198**: 307-31.
56. Maul, G.G., H.H. Guldner, and J.G. Spivack (1993). *Modification of discrete nuclear domains induced by herpes simplex virus type 1 immediate early gene 1 product (ICP0)*. J Gen Virol **74**: 2679-90.
57. Everett, R.D. and G.G. Maul (1994). *HSV-1 IE protein Vmw110 causes redistribution of PML*. Embo J **13**: 5062-9.
58. Everett, R.D., M. Meredith, and A. Orr (1999). *The ability of herpes simplex virus type 1 immediate-early protein Vmw110 to bind to a ubiquitin-specific protease contributes to its roles in the activation of gene expression and stimulation of virus replication*. J Virol **73**: 417-26.

59. Muller, S., M.J. Matunis, and A. Dejean (1998). *Conjugation with the ubiquitin-related modifier SUMO-1 regulates the partitioning of PML within the nucleus.* *Embo J* **17**: 61-70.
60. Everett, R.D., P. Freemont, H. Saitoh, M. Dasso, A. Orr, M. Kathoria, and J. Parkinson (1998). *The disruption of ND10 during herpes simplex virus infection correlates with the Vmw110- and proteasome-dependent loss of several PML isoforms.* *J Virol* **72**: 6581-91.
61. Maul, G.G., A.M. Ishov, and R.D. Everett (1996). *Nuclear domain 10 as preexisting potential replication start sites of herpes simplex virus type-1.* *Virology* **217**: 67-75.
62. Uprichard, S.L. and D.M. Knipe (1997). *Assembly of herpes simplex virus replication proteins at two distinct intranuclear sites.* *Virology* **229**: 113-25.
63. Quinlan, M.P., L.B. Chen, and D.M. Knipe (1984). *The intranuclear location of a herpes simplex virus DNA-binding protein is determined by the status of viral DNA replication.* *Cell* **36**: 857-68.
64. de Bruyn Kops, A. and D.M. Knipe (1988). *Formation of DNA replication structures in herpes virus-infected cells requires a viral DNA binding protein.* *Cell* **55**: 857-68.
65. Heine, J.W., R.W. Honess, E.N. Cassain, and B. Roizman (1974). *Proteins specified by herpes simplex virus. XII. The virion polypeptides of type 1 strains.* *J. Virol.* **14**: 640-651.
66. Kristie, T.M. and B. Roizman (1984). *Separation of sequences defining basal expression from those conferring alpha gene recognition within the regulatory domains of herpes simplex virus 1 alpha genes.* *Proc. Natl. Acad. Sci. USA* **81**: 4065-4069.
67. Triezenberg, S.J., K.L. LaMarco, and S.L. McKnight (1988). *Evidence of DNA:protein interactions that mediate HSV-1 immediate early gene activation by VP16.* *Genes Dev.* **2**: 730-743.
68. LaMarco, K.L. and S.L. McKnight (1989). *Purification of a set of cellular polypeptides that bind to the purine-rich cis-regulatory element of herpes simplex virus immediate early genes.* *Genes Devel.* **3**: 1372-1383.

69. Sturm, R.A., G. Das, and W. Herr (1988). *The ubiquitous octamer binding protein Oct-1 contains a POU domain with a homeobox subdomain*. *Genes Dev.* **2**: 1582-1599.
70. O'Hare, P.O., C.R. Goding, and A. Haigh (1988). *Direct combinatorial interaction between a herpes simplex virus regulatory protein and a cellular octamer-binding factor mediates specific induction of virus immediate-early gene expression*. *EMBO J.* **7**: 4231-4238.
71. Kristie, T.M., J.H. LeBowitz, and P.A. Sharp (1989). *The octamer-binding proteins form multi-protein - DNA complexes with the HSV alpha TIF regulatory protein*. *EMBO J.* **8**: 4229-4238.
72. Goding, C.R. and P. O'Hare (1989). *Herpes simplex virus Vmw65-octamer binding protein interaction: a paradigm for combinatorial control of transcription*. *Virology* **173**: 363-7.
73. Xiao, P. and J.P. Capone (1990). *A cellular factor binds to the herpes simplex virus type-1 transactivator Vmw65 and is required for Vmw65-dependent protein-DNA complex assembly with Oct-1*. *Mol. Cell. Biol.* **10**: 4974-4977.
74. Katan, M., A. Haigh, C.P. Verrijzer, P.C. Vandervliet, and P. O'Hare (1990). *Characterization of a cellular factor which interacts functionally with Oct-1 in the assembly of a multicomponent transcription complex*. *Nucleic Acids Res.* **18**: 6871-6880.
75. Werstuck, G.H. and J.P. Capone (1993). *An unusual cellular factor potentiates protein-DNA complex assembly between oct-1 and Vmw65*. *J. Biol. Chem.* **268**: 1272-1278.
76. Wilson, A.C., K. LaMarco, M.G. Peterson, and W. Herr (1993). *The VP16 accessory protein HCF is a family of polypeptides processed from a large precursor protein*. *Cell* **74**: 115-25.
77. Wilson, A.C., R.N. Frieman, H. Goto, T. Nishimoto, and W. Herr (1997). *VP16 Targets an Amino-Terminal Domain of HCF Involved in Cell Cycle Progression*. *Mol. Cell. Biol.* : 6139-6146.
78. Simmen, K.A., A. Newell, M. Robinson, J.S. Mills, G. Canning, R. Handa, K. Parkes, N. Borkakoti, and R. Jupp (1997). *Protein interactions in the herpes*

- simplex virus type 1 VP16 induced complex: VP16 peptide inhibition and mutational analysis of the host cell factor requirements.* J. Virol. **71**: 3886-3894.
79. Lai, J.S. and W. Herr (1997). *Interdigitated residues within a small region of VP16 interact with Oct-1, HCF, and DNA.* Mol. Cell. Biol. **17**: 3947-3954.
80. Triezenberg, S.J., R.C. Kingsbury, and S.L. McKnight (1988). *Functional dissection of VP16, the trans-activator of herpes simplex virus immediate early gene expression.* Genes Dev. **2**: 718-729.
81. Lam, Q., C.A. Smibert, K.E. Koop, C. Lavery, J.P. Capone, S.P. Weinheimer, and J.R. Smiley (1996). *Herpes simplex virus VP16 rescues viral mRNA from destruction by the virion host shutoff function.* EMBO J. **15**: 2575-2581.
82. Johnson, D.C. and P.G. Spear (1982). *Monensin inhibits the processing of herpes simplex virus glycoproteins, their transport to the cell surface, and the egress of virions from infected cells.* J Virol **43**: 1102-12.
83. Stackpole, C.W. (1969). *Herpes-type virus of the frog renal adenocarcinoma. I. Virus development in tumor transplants maintained at low temperature.* J Virol **4**: 75-93.
84. Torrisi, M.R., C. Di Lazzaro, A. Pavan, L. Pereira, and G. Campadelli-Fiume (1992). *Herpes simplex virus envelopment and maturation studied by fracture label.* J Virol **66**: 554-61.
85. Stannard, L.M., S. Himmelhoch, and S. Wynchank (1996). *Intra-nuclear localization of two envelope proteins, gB and gD, of herpes simplex virus.* Arch Virol **141**: 505-24.
86. Jayachandra, S., A. Baghian, and K.G. Kousoulas (1997). *Herpes simplex virus type 1 glycoprotein K is not essential for infectious virus production in actively replicating cells but is required for efficient envelopment and translocation of infectious virions from the cytoplasm to the extracellular space.* J Virol **71**: 5012-24.
87. Foster, T.P. and K.G. Kousoulas (1999). *Genetic analysis of the role of herpes simplex virus type 1 glycoprotein K in infectious virus production and egress.* J Virol **73**: 8457-68.

88. Campadelli-Fiume, G., F. Farabegoli, S. Di Gaeta, and B. Roizman (1991). *Origin of unenveloped capsids in the cytoplasm of cells infected with herpes simplex virus 1*. J Virol **65**: 1589-95.
89. Campadelli-Fiume, G., S. Qi, E. Avitabile, L. Foa-Tomasi, R. Brandimarti, and B. Roizman (1990). *Glycoprotein D of herpes simplex virus encodes a domain which precludes penetration of cells expressing the glycoprotein by superinfecting herpes simplex virus*. J Virol **64**: 6070-9.
90. Lam, N. and G.J. Letchworth (2000). *Bovine herpesvirus 1 U(L)3.5 interacts with bovine herpesvirus 1 alpha- transinducing factor*. J Virol **74**: 2876-84.
91. Gershon, A.A., D.L. Sherman, Z. Zhu, C.A. Gabel, R.T. Ambron, and M.D. Gershon (1994). *Intracellular transport of newly synthesized varicella-zoster virus: final envelopment in the trans-Golgi network*. J Virol **68**: 6372-90.
92. Jones, F. and C. Grose (1988). *Role of cytoplasmic vacuoles in varicella-zoster virus glycoprotein trafficking and virion envelopment*. J Virol **62**: 2701-11.
93. Klussmann, J.P., E. Krueger, T. Sloots, Z. Berneman, G. Arnold, and G.R. Krueger (1997). *Ultrastructural study of human herpesvirus-7 replication in tissue culture*. Virchows Arch **430**: 417-26.
94. Roffman, E., J.P. Albert, J.P. Goff, and N. Frenkel (1990). *Putative site for the acquisition of human herpesvirus 6 virion tegument*. J Virol **64**: 6308-13.
95. Torrisi, M.R., M. Gentile, G. Cardinali, M. Cirone, C. Zompetta, L.V. Lotti, L. Frati, and A. Faggioni (1999). *Intracellular transport and maturation pathway of human herpesvirus 6*. Virology **257**: 460-71.
96. Papadimitriou, J.M., G.R. Shellam, and T.A. Robertson (1984). *An ultrastructural investigation of cytomegalovirus replication in murine hepatocytes*. J Gen Virol **65**: 1979-90.
97. Sanchez, V., K.D. Greis, E. Sztul, and W.J. Britt (2000). *Accumulation of virion tegument and envelope proteins in a stable cytoplasmic compartment during human cytomegalovirus replication: characterization of a potential site of virus assembly*. J Virol **74**: 975-86.

98. van Genderen, I.L., R. Brandimarti, M.R. Torrisi, G. Campadelli, and G. van Meer (1994). *The phospholipid composition of extracellular herpes simplex virions differs from that of host cell nuclei*. *Virology* **200**: 831-6.
99. Browne, H., S. Bell, T. Minson, and D.W. Wilson (1996). *An endoplasmic reticulum-retained herpes simplex virus glycoprotein H is absent from secreted virions: evidence for reenvelopment during egress*. *J Virol* **70**: 4311-6.
100. Whiteley, A., B. Bruun, T. Minson, and H. Browne (1999). *Effects of targeting herpes simplex virus type 1 gD to the endoplasmic reticulum and trans-Golgi network*. *J Virol* **73**: 9515-20.
101. Komuro, M., M. Tajima, and K. Kato (1989). *Transformation of Golgi membrane into the envelope of herpes simplex virus in rat anterior pituitary cells*. *Eur J Cell Biol* **50**: 398-406.
102. Elliott, G. and P. O'Hare (1999). *Live-cell analysis of a green fluorescent protein-tagged herpes simplex virus infection*. *J Virol* **73**: 4110-9.
103. Alberts, B., D. Bray, J. Lewis, M. Raff, K. Roberts, and J.D. Watson, *Molecular Biology of the Cell*. Third ed. 1994, New York: Garland Publishing, Inc. 1294.
104. Gorlich, D., F. Vogel, A.D. Mills, E. Hartmann, and R.A. Laskey (1995). *Distinct functions for the two importin subunits in nuclear protein import*. *Nature* **377**: 246-8.
105. LaBoissiere, S., T. Hughes, and P. O'Hare (1999). *HCF-dependent nuclear import of VP16*. *EMBO J.* **18**: 480-489.
106. Greaves, R.F. and P. O'Hare (1990). *Structural requirements in the herpes simplex virus type 1 transactivator Vmw65 for interaction with the cellular octamer-binding protein and target TAATGARAT sequences*. *J. Virol.* **64**: 2716-2724.
107. Lu, R., P. Yang, S. Padmakumar, and V. Misra (1998). *The herpesvirus transactivator VP16 mimics a human basic domain leucine zipper protein, human, in its interaction with HCF*. *J Virol* **72**: 6291-7.

108. Freiman, R.N. and W. Herr (1997). *Viral mimicry: common mode of association with HCF by VP16 and the cellular protein LZIP*. *Genes Dev* **11**: 3122-7.
109. Subak-Sharpe, J.H. and D.J. Dargan (1998). *HSV molecular biology: general aspects of herpes simplex virus molecular biology*. *Virus Genes* **16**: 239-51.
110. Goto, H., S. Motomura, A.C. Wilson, R.N. Freiman, Y. Nakabeppu, K. Fukushima, M. Fujishima, W. Herr, and T. Nishimoto (1997). *A single-point mutation in HCF causes temperature-sensitive cell-cycle arrest and disrupts VP16 function*. *Genes & Dev*. **11**: 23-29.
111. Desai, P. and S. Person (1998). *Incorporation of the green fluorescent protein into the herpes simplex virus type 1 capsid*. *J Virol* **72**: 7563-8.
112. Ausubel, F.M., R. Brent, R.E. Kingston, D.D. Moore, J.G. Seidman, J.A. Smith, and K. Struhl, eds. *Current Protocols in Molecular Biology*. Current Protocols, ed. V.B. Chanda. 1987-1994, John Wiley & Sons, Inc.
113. Day, R.N., S.K. Nordeen, and Y. Wan (1999). *Visualizing protein-protein interactions in the nucleus of the living cell*. *Mol Endocrinol* **13**: 517-26.
114. Cheng, L., J. Fu, A. Tsukamoto, and R.G. Hawley (1996). *Use of green fluorescent protein variants to monitor gene transfer and expression in mammalian cells*. *Nat Biotechnol* **14**: 606-9.
115. de Bruyn Kops, A. and D.M. Knipe (1994). *Preexisting nuclear architecture defines the intranuclear location of herpesvirus DNA replication structures*. *J Virol* **68**: 3512-26.
116. Elliott, G. and P. O'Hare (2000). *Cytoplasm-to-nucleus translocation of a herpesvirus tegument protein during cell division [In Process Citation]*. *J Virol* **74**: 2131-41.
117. Dasgupta, A. and D.W. Wilson (1999). *ATP depletion blocks herpes simplex virus DNA packaging and capsid maturation*. *J Virol* **73**: 2006-15.
118. Church, G.A. and D.W. Wilson (1997). *Study of herpes simplex virus maturation during a synchronous wave of assembly*. *J Virol* **71**: 3603-12.

119. Wu, T.-J., G. Monokian, D.F. Mark, and C.R. Wobbe (1994). *Transcriptional activation by herpes simplex virus type 1 VP16 in vitro and its inhibition by oligopeptides*. *Mol. Cell. Biol.* **14**: 3484-3493.
120. LaBoissiere, S. and P. O'Hare (2000). *Analysis of HCF, the cellular cofactor of VP16, in herpes simplex virus- infected cells*. *J Virol* **74**: 99-109.
121. Ralph, W.M., Jr., M.S. Cabatingan, and P.A. Schaffer (1994). *Induction of herpes simplex virus type 1 immediate-early gene expression by a cellular activity expressed in Vero and NB41A3 cells after growth arrest-release*. *J Virol* **68**: 6871-82.
122. Mahajan, S.S. and A.C. Wilson (2000). *Mutations in host cell factor 1 separate its role in cell proliferation from recruitment of VP16 and LZIP*. *Mol Cell Biol* **20**: 919-28.

MICHIGAN STATE UNIVERSITY LIBRARIES



3 1293 02334 2094